VIRUS SPREAD OVER NETWORKS: MODELING, ANALYSIS, AND CONTROL

BY

PHILIP E. PARÉ

DISSERTATION

Submitted in partial fulfillment of the requirements
for the degree of Doctor of Philosophy in Electrical and Computer Engineering
in the Graduate College of the
University of Illinois at Urbana-Champaign, 2018

Urbana, Illinois

Doctoral Committee:

Associate Professor Carolyn L. Beck, Chair
Professor Angelia Nedić
Professor Tamer Başar
Professor Rayadurgam Srikant

Abstract

The spread of viruses in biological networks, computer networks, and human contact networks can have devastating effects; developing and analyzing mathematical models of these systems can provide insights that lead to long-term societal benefits. Basic virus models have been studied for over three centuries; however, as the world continues to become connected and networked in more complex ways, previous models no longer are sufficient. Therefore virus spread over networks is a newer research topic, which provides a compelling modeling technique to capture real world behavior, and interest from the control field has provided an exciting new outlook on the area.

Prior research has focused mainly on network models with static graph structures; however, the systems being modeled typically have dynamic graph structures and have not been validated with real spread data over a network. In this dissertation, we consider virus spread models over networks with dynamic graph structures, and we investigate the behavior of these systems. We perform stability analyses of epidemic processes over time–varying networks, providing sufficient conditions for convergence to the disease-free equilibrium (the origin, or healthy state), in both the deterministic and stochastic cases. We also explore the scenario of multiple viruses, in the case of competing viruses, including human awareness, and coupled competing viruses. We analyze the healthy state and the endemic states of these models over static and dynamic graph structures. Various control techniques are also proposed to mitigate virus spread in networks. Illustrative figures and simulations are presented throughout. No previous work has explored identification and validation of network dependent virus spread models; model validation is considered herein using two datasets: 1) John Snow's fundamental 1854 cholera dataset and 2) a 2009-2012 USDA farm subsidy dataset. We conclude by discussing current work and future research directions.

To my wife, children, and family, for their love and support.
In memory of my late father, Philip E. Paré I.

Acknowledgments

This work was made possible by the love and support of my wonderful wife, Annette. Thanks to her efforts not only was I able to complete my degree requirements during a relatively normal workday and travel without worrying about the state of my family, but she also gave me lots of incentive to be efficient so I could also spend time at home with her and our wonderful children.

My advisors, Professors Carolyn L. Beck and Angelia Nedić, have provided me and my family amazing support, guidance, and advice, without which this dissertation would not have been possible. Their generosity in allowing me to travel to various conferences and workshops has enabled me to vitally expand my knowledge and network. Their guidance and advice have also prepared me to go forward and be successful in my career. The collaboration, guidance, and advice of my committee member Professor Tamer Başar has been an integral part of my success at the University of Illinois. My other committee member, Professor R. Srikant, who has also served as my academic advisor in the Department of Electrical and Computer Engineering (ECE), has provided essential guidance and advice for my navigation of the ECE Department as well as helping me prepare for my career after graduate school, and has been a great instructor for various courses I have taken. I would also like to thank Professors Geir Dullerud and Daniel Liberzon for their wonderful instruction and guidance.

I would like to thank all of my other collaborators in this work: Professor Ji Liu of Stony Brook University, Professor Barrett Kirwan of the Agricultural and Consumer Economics Department at UIUC, and Aditya Shivashankar, a master's student who I mentored and helped with the processing of the Snow dataset. Professor Ji Liu, in addition to being a great collaborator, has been a very good friend.

I acknowledge the support of the community of the Coordinated Science Lab (CSL), including my friends, other faculty, and the fantastic support staff, especially Thinh Doan and Angie Ellis. The sense of community that I enjoyed in CSL was a vital part of my doctoral work and I am grateful for all of the support, advice, and experience I gained through my research, collaborations, discussions with faculty, students, and staff, and through presenting at and organizing the CSL Student Conference (CSLSC). The experience I gained through serving on the organizing committee of the CSLSC was invaluable and I would like to acknowledge the support of my fellow 2017 General Co-Chair, Ravi Kiran Raman, and CSL Director, Klara Nahrstedt. I also want to acknowledge all of my friends and colleagues outside of CSL here at Illinois for their support and encouragement.

I would like to acknowledge my undergraduate and master's thesis advisor Professor Sean Warnick for teaching me how to do research, helping me get admitted to UIUC, and continuing to help and encourage me in my career path. I also want to acknowledge my friends from Dr. Warnick's Lab, IDeA Labs, for their friendship and all of their support: Anurag Rai, David Grimsman, Brigham Wilson, Enoch Yeung, Julius Adebayo, and Daniel Fullmer, to name only a few.

I have to acknowledge my family; in addition to my wonderful wife and children, my siblings and mother have been an invaluable source of love and support. My brother, Ryan Sheaparé, has always offered his advice and expertise when needed, including on several of the graphics in this dissertation. My sister, Monique Merilyn Paré Speirs, has been a wonderful example of diligence and hard work. My mother, DonnaMarie Paré, has always encouraged and supported me, including mostly funding a trip to present some of this work at *epiDAMIK: Epidemiology Meets Data Mining and Knowledge Discovery, ACM SIGKDD 2018* and partially funding a trip to present some of this work at the *54th IEEE Conference on Decision and Control*. Finally, I acknowledge my loving parents, both my mother and father, for raising me to always strive to be the best I can be. Their encouragement and examples have helped drive me to where I am today and will continue to help me excel.

Table of Contents

Chapter 1

Introduction

Mathematical models of epidemics have been studied for hundreds of years. Bernoulli developed one of the first known models inspired by the smallpox virus [1]. Of particular interest to the work discussed herein are the so-called susceptible-infected-susceptible (SIS) models, which have been developed for both continuous [2, 3, 4, 5, 6, 7, 8] and discrete time domains [8, 9, 10]. These are standard models commonly used to capture the evolution of virus infections in networks. In a basic SIS model, at each time step each individual node or agent is either *infected*, or *susceptible* to infection. A susceptible agent may be infected by neighboring agents with some given infection rate, β, where the network graph structure determines the connectivity between agents, and hence plays a direct role in facilitating or inhibiting the spread of infection. An infected agent may be cured with some given healing rate, δ, returning to the susceptible state. The first SIS model, developed by Kermack and McKendrick [2], is given by

$$\begin{aligned} \dot{S}(t) &= -\beta S(t)I(t) + \delta I(t) \\ \dot{I}(t) &= \beta S(t)I(t) - \delta I(t), \end{aligned} \tag{1.1}$$

where $S(t)$ is the group of susceptible agents and $I(t)$ is the group of infected agents. This behavior is depicted to Figure 1.1. This model considers the propagation of a virus over a trivial network, that is, it assumes complete connectivity, and models the infected and susceptible agents as two aggregated groups.

In [9], Wang *et al.* propose a discrete time model for virus spread over a nontrivial network and derive an epidemic threshold that guarantees convergence to the disease-free equilibrium (DFE) or healthy state; numerically this would be represented by the origin (for (1.1) this would be $I(t) = 0$). The authors give a convergence rate in terms of the largest eigenvalue of the adjacency matrix of the network, which is propor-

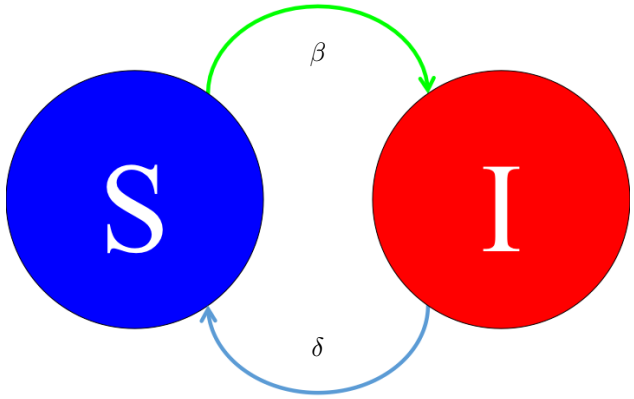

Figure 1.1: **SIS Model**–Each agent is either in the susceptible or infected group

tional to the ratio of the healing and infection rates. A necessary and sufficient condition for exponential stability of the DFE is provided, with several simulations and results for specific graph structures given. Peng *et al.*, in [10], provide a necessary and sufficient condition for stability of the DFE for an extension of the model from [9]. Peng *et al.* also discuss possible immunization techniques, and formulate a convex optimization problem for forming an optimal immunization strategy, based on a relaxation of the problem constraints. In [8], Ahn and Hassibi study both discrete and continuous time SIS models, where both the DFE and the non-disease-free equilibrium (NDFE), sometimes referred to as the endemic or epidemic equilibrium, are considered, and the existence, uniqueness and stability conditions for the NDFE are established. In [8], they only perform a local stability analysis of the endemic state of the model of interest; the analysis in Section 2.3 is global and for a more general model. In [3], Fall *et al.* analyze a continuous time SIS model, deriving sufficient conditions for global asymptotic stability for both the DFE and the NDFE. Van Mieghem *et al.*, in [6], expose some limitations of the model presented in [9], namely that it is only accurate if the infection rate is below the epidemic threshold, that is, the system is tending towards the DFE. The authors propose a 2^n-state Markov chain model and an n-intertwined Markov chain model as alternatives to the model in [9] and explore their stability properties by studying the limiting cases of the complete graph and the line graph. These two models will be explained in more detail in the following chapter of this dissertation. Preciado *et al.* use geometric programming ideas [11], in [12, 13], to develop optimal vaccination techniques for the continuous time model from [6]. Pasqualetti *et al.*, in [14], apply a network control technique to a discretized, linearized version of the model from [6]. In [15, 16], Khanafer *et al.* further explore the stability properties of the equilibria of the continuous time model from [6], and propose an antidote control technique. For reviews on epidemic processes see [17, 18].

The previous work in this area is mostly limited to static graph structures and limited to local analysis. However the main motivating applications have time–varying graph structures; therefore, to better understand and analyze virus spread, further study is required, which we carry out herein. The idea of competing viruses has been explored in previous work but the analysis has mainly been local and for only two viruses, and all of the previous work has been for static graph structures. We explore an arbitrary number of viruses over static and time–varying graph structures.

Preliminary control methods and analyses have also been developed and applied to infectious disease networks; we note a few recent works here, and provide a more in-depth review in Chapter 5. Various control techniques have been proposed for these virus models but the ability to implement them is questionable. We propose some novel techniques that are motivated by real epidemic treatment practices. No validation using real spread data has been done on these network dependent spread models; we present the first attempts using a 2009-2012 USDA farm subsidy dataset and John Snow's fundamental 1854 cholera dataset with quite good results herein. The background literature for each of these areas of interest is provided at the beginning of each relevant chapter.

1.1 Notation

Given a vector function of time $x(t)$, $\dot{x}(t)$ indicates the time-derivative. Given a vector $x \in \mathbb{R}^n$, the 2-norm is denoted by $\|x\|$ and the transpose by $x^\top$. Given two vectors $x_1, x_2 \in \mathbb{R}^n$, $x_1 \geq x_2$ indicates each element of x_1 is greater than or equal to the corresponding element of x_2, $x_1 > x_2$ indicates each element of x_1 is greater than or equal to the corresponding element of x_2 and $x_1 \neq x_2$, and $x_1 \gg x_2$ indicates that each

element of x_1 is strictly greater than the corresponding element of x_2. Given a matrix $A \in \mathbb{R}^{n\times n}$, the maximum eigenvalue is $\lambda_1(A)$ (if the spectrum is real), the largest real-valued part of the eigenvalues, or spectral abscissa, of A is denoted $s_1(A)$ (if the spectrum is possibly complex), and the spectral radius of A is $\rho(A)$. Also, a_{ij} indicates the i, j^{th} entry of A, and $\|A\|$ indicates the induced 2-norm of A (the maximum singular value of A). The notation $diag(\cdot)$ refers to a diagonal matrix with the argument on the diagonal. The notation $[n]$ refers to the set $\{1, \ldots, n\}$. We use $E[\cdot]$ to denote the expected value of the argument and $Pr[\cdot]$ to denote the probability of the argument.

1.2 Summary

In Chapter 2, we present the derivations for continuous- and discrete-time single-virus models. We provide some novel stability analysis for the discrete-time single-virus model introduced over static graph structures. In Chapter 3, we present novel stability analysis for the continuous-time single-virus model, including a compelling result that does not require the linearized system to be Hurwitz for all time. In Chapter 4, we propose a multi-virus model and perform analysis over both static and time–varying graph structures. In Chapter 5, we propose several control techniques: a quarantine heuristic and two antidote-administration approaches. In Chapter 6, we present the learning and validation results, showing how to estimate the spreading parameters of the system and then apply the results to the two datasets. In Chapter 7, we discuss ongoing work, future ideas, and additional ongoing research. We have completed several simulations to which we refer throughout the dissertation.

Chapter 2

Virus Models

In this chapter we introduce various different continuous- and discrete-time single-virus models.

2.1 Continuous-Time Single-Virus Model

In this section we carefully present the model derivation from a mean-field type approximation of a 2^n-state Markov chain, first discussed in [6]. We then evaluate the effectiveness of the approximation via an in-depth set of simulations. The majority of this material was originally published in [19] and is used here with permission.

2.1.1 Mean-Field Approximation Derivation

In [6], Van Mieghem *et al.* introduce a 2^n-state Markov chain, where each state of the chain, $Y_k(t)$, corresponds to a binary-valued string x of length n, where $x_i = 1$ or $x_i = 0$ indicates that the ith agent is either infected or susceptible, respectively, and the state transition matrix, $\bar{Q}$, is defined by

$$\bar{q}_{kl} = \begin{cases} \delta, & \text{if } x_i = 1, k = l + 2^{i-1} \\ \beta \sum_{j=1}^{n} a_{ij} x_j, & \text{if } x_i = 0, k = l - 2^{i-1} \\ -\sum_{j \neq l} \bar{q}_{jl}, & \text{if } k = l \\ 0, & \text{otherwise,} \end{cases} \tag{2.1}$$

for $i = 1, ..., n$. Here a virus is propagating over a network structure defined by a_{ij} (non-negative with $a_{jj} = 0, \ \forall j$), with n agents, β is the infection rate, δ is the healing rate, and, again, $x_i = 1$ or $x_i = 0$ indicates that the ith agent is either infected or susceptible, respectively.

The state vector $y(t)$ is defined as

$$y_k(t) = Pr[Y_k(t) = k], \tag{2.2}$$

with $\sum_{k=1}^{2^n} y_k(t) = 1$. The Markov chain evolves as

$$\frac{dy^\top(t)}{dt} = y^\top(t)\bar{Q}. \tag{2.3}$$

See Figure 2.1 for an example of this chain with $n = 3$. Let $v_i(t) = Pr[X_i(t) = 1]$, where $X_i(t)$ is the random variable representing whether the ith agent is infected (not to be confused with x_i, which is the ith entry of

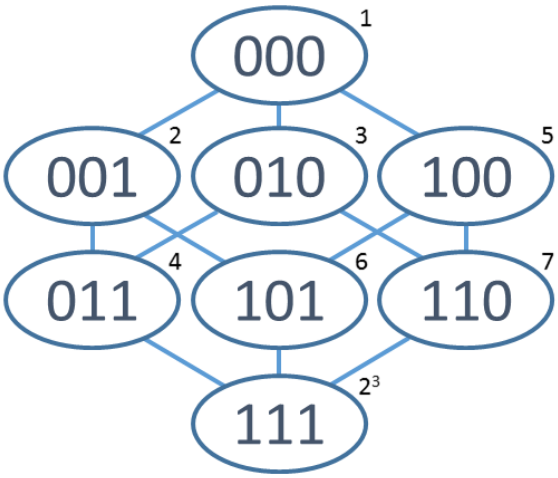

Figure 2.1: Example of 2^n-state model with $n = 3$: the superscripts indicate the ordering of the states, which correspond to the subscript of $y_k(t)$ in (2.2), and the internal strings indicate which agents are healthy (0) and which are infected (1), corresponding to x_i in (2.1).

the binary string associated with each state of the 2^n Markov chain). Then

$$v^\top(t) = y^\top(t)M, \tag{2.4}$$

where $M \in \mathbb{R}^{2^n \times n}$ with the rows being lexicographically-ordered binary numbers, bit reversed.[1] That is, $v_i(t)$ reflects the summation of all probabilities where $x_i = 1$, therefore giving the mean, $E[X_i]$, of the infection, X_i, of agent i. Note that the first chain state of the chain, which corresponds to $x = \mathbf{0}$, the vector of zeros, or the healthy state, for $\delta > 0$, is the absorbing, or sink, state of the chain. This means that the Markov chain will never escape the state once in it, and further, since it is the only absorbing state the system will converge to the healthy state with probability one [20].

A mean field approximation of this system is used to obtain an n-intertwined continuous Markov chain, where each node has two states: infected with probability $Pr[X_i(t) = 1]$ and healthy (susceptible) with probability $Pr[X_i(t) = 0]$. Taking the expected value of the infection transition rate, that is, the second case given in (2.1), and using $E[1_z] = Pr[z]$ gives

$$\begin{aligned} E[\bar{q}_{kl}|x_i = 0, k = l - 2^{i-1}] &= E\big[\beta \sum_{l=1}^{n} a_{ij} 1_{\{X_j(t)=1\}}\big] \\ &= \beta \sum_{l=1}^{n} a_{ij} Pr[X_j(t) = 1], \end{aligned} \tag{2.5}$$

where the second equality holds since the β and a_{ij} values are deterministic and known.

Denoting $p_i(t) = Pr[X_i(t) = 1]$ and noting that $Pr[X_i(t) = 0] = 1 - p_i(t)$, we can see that

$$\dot{p}_i(t) = (1 - p_i(t))\beta \sum_{j=1}^{n} a_{ij} p_j(t) - \delta p_i(t). \tag{2.6}$$

Applying the Central Limit Theorem, under the assumption of independent indicators, implies that large

[1] Matlab code: $M = fliplr(dec2bin(0 : (2^n) - 1) -' 0')$

deviations from the mean are unlikely; this is the motivation for the mean field approximation. However, it is clear that the indicators are not independent, by construction. The authors of [6] state

$$Pr[X_j(t) = 1 | X_i(t) = 1] \geq Pr[X_j(t) = 1],$$

which is true under the assumption $\beta \geq 0$, because if one node in the system is infected, it will have only a non-negative effect on the probability of infecting other nodes. That is, one agent being infected will never decrease the probability of another agent becoming infected. Therefore, the n-intertwined Markov chain model gives an *upper-bound* for the exact probability, $p_i(t)$, of infection [6].

Another way to derive the mean field approximation is to consider the probability that node i is healthy ($X_i = 0$) or infected ($X_i = 1$) at time $t + \Delta t$

$$\begin{aligned} Pr(X_i(t + \Delta t) = 0 | X_i(t) = 1, X(t)) &= \delta \Delta t + o(\Delta t) \\ Pr(X_i(t + \Delta t) = 1 | X_i(t) = 0, X(t)) &= \beta \sum_{j=1}^{n} a_{ij} X_j \Delta t + o(\Delta t), \\ &\vdots \end{aligned}$$

Letting Δt go to zero and taking expectations gives

$$\frac{dE(X_i(t))}{dt} = E\left((1 - X_i(t)) \beta \sum_{j=1}^{n} a_{ij} X_j(t) \right) - \delta E(X_i(t)). \tag{2.7}$$

Using the above equation, $Pr(z) = E(1_z)$, $p_i(t) = Pr(X_i(t) = 1)$, $(1 - p_i(t)) = Pr(X_i(t) = 0)$, and approximating $Pr(X_i(t) = 1, X_j(t) = 1) \approx p_i(t) p_j(t)$ (which again inaccurately assumes independence) gives

$$\frac{dp_i(t)}{dt} = (1 - p_i(t)) \beta \sum_{j=1}^{n} a_{ij} p_j(t) - \delta p_i(t),$$

the same as (2.6).

It has been shown that, under certain conditions, mean field approximations of SIS models may be inaccurate, leading to incorrect results [21]. However, as we have shown, the mean field approximation considered herein, while it is an approximation, is well constructed. The shortcomings of this mean field approximation are illustrated in Section 2.1.4.

Definition 1. *A virus model is* homogeneous *if β and δ are the same for all agents; otherwise it is a* heterogeneous *virus model.*

The model in (2.6) can be generalized to the heterogeneous virus, directed graph structure case:

$$\dot{p}_i(t) = (1 - p_i(t)) \beta_i \sum_{j=1}^{n} a_{ij} p_j(t) - \delta_i p_i(t), \tag{2.8}$$

where β_i is the non-negative susceptibility or infection rate of agent i; n is the number of agents; a_{ij} reflects the directed, non-negative, weighted, connection between agents, with $a_{ij} = 0$ if agents i and j are not neighbors; and δ_i is the non-negative healing rate of agent i. In matrix form, with $p(t)$ representing the

vector of the probabilities of infection of the agents, the model is

$$\dot{p}(t) = (BA - P(t)BA - D)p(t), \tag{2.9}$$

where $B = diag(\beta_1, \ldots, \beta_n)$, $A = [a_{ij}]$ represents the weighted network structure, $P(t) = diag(p_1(t), \ldots, p_n(t))$, and $D = diag(\delta_1, \ldots, \delta_n)$. Each node of the network can be interpreted as an individual agent [6], or as the centroid of a community, i.e., as a grouping of individuals [3]. While using the first interpretation, where p_i is the probability of infection of agent i, allowing a_{ii} to be nonzero can cause problems with the independent indicators assumption. Using the second interpretation, where p_i is the infected proportion of group i, makes nonzero a_{ii} permissible. Therefore for the analysis we allow this generalization.

For the single virus case we have the following result as Proposition 2 in [22] (Propositions 3 and 5 in [23]).

Proposition 1. *Suppose that $\delta_i \geq 0$ for all $i \in [n]$ and that matrix BA is nonnegative and irreducible. If $s(BA-D) \leq 0$, then $\mathbf{0}$ is the unique equilibrium of system (2.9), which is asymptotically stable with domain of attraction $[0,1]^n$. If $s(BA-D) > 0$, then system (2.9) has two equilibria, $\mathbf{0}$ and p^* which satisfies $p^* \gg \mathbf{0}$.*

For completeness the proof is included in Appendix A.

2.1.2 Connection to Reproduction Number

In the epidemiology literature the classical concept of the reproduction number R_0, which represents the number of people that get infected from a single infected person, is frequently used as one means of assessing spread. Clearly if $R_0 \leq 1$ the infection will not pervade the system. The condition given in Proposition 1, $s(BA - D) \leq 0$, is a generalization of the classical reproduction number R_0. Recall the well known result for the continuous time homogeneous virus model over a symmetric graph structure A (that is, where $a_{ij} = a_{ji}\ \forall i, j$), which appears in [6]:

Proposition 2. *The system in* (2.8) *with homogeneous virus spread converges exponentially fast to the healthy state if $\lambda_1(A) < \frac{\delta}{\beta}$.*

So for a homogeneous virus spreading on a fully-connected (normalized) graph, from Propositions 1 and 2,

$$\frac{\beta}{\delta} \leq 1 \iff s(BA - D) \leq 0,$$

and therefore

$$R_o = \frac{\beta}{\delta}.$$

2.1.3 Model Well-Posedness

To assure well-posedness of the model we include the following lemma.

Lemma 1. *If $p_i(0) \geq 0$, for all $i = 1, ..., n$, then $p_i(t) \geq 0$ for all $t \geq 0$, $i = 1, ..., n$.*

Proof. Assume $p_i(0) = 0$ and $p_j(0) \geq 0$ for all $j \neq i$. Then by (2.8), $\dot{p}_i(0) \geq 0$, driving $p_i(t) \geq 0$ for $t > 0$.

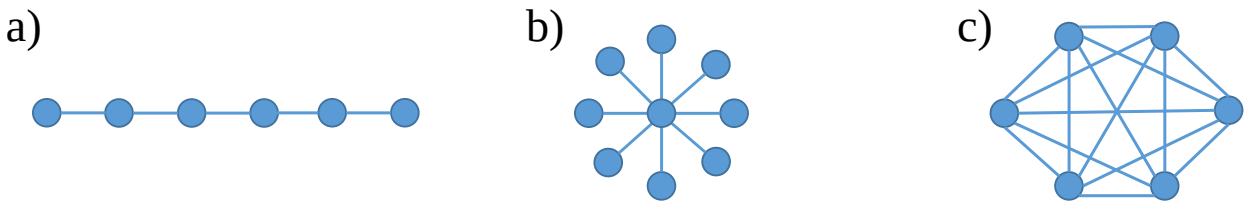

Figure 2.2: Graph structures: a) line b) star c) complete.

Assume $p_i(0) > 0$ and $p_j(0) \geq 0$ for all $j \neq i$. Since there exists a derivative by (3.1), $p_i(t)$ is continuous. Now suppose $\dot{p}_i(t) < 0$, for some interval $0 \leq \tau \leq t \leq T$, where, by the continuity of $p_i(t)$, at time T we have $p_i(T) = 0$. Then, similar to the first part of the proof, by (2.8), $\dot{p}_i(T) \geq 0$ and $p_i(t) \geq 0$ for $t > T$. $\square$

2.1.4 Effectiveness of the Approximate Model

In this section we first compare via simulations the 2^n state and n-intertwined Markov chain models in (2.3) and (2.6), respectively, over different graph structures, and then compare them for the complete, fully connected graph with the original model in (1.1).

An initial analysis has been completed in [6] to evaluate the accuracy of the mean field approximation used in the derivation of the n-intertwined model in (2.6). This analysis was performed only for the complete graph for $n = 11$ with three (β, δ) pairs. We further the analysis here by including additional graph structures (see Figure 2.2), values of n, (β, δ) combinations, and different initial conditions.

In [24], Li *et al.* compare the n-intertwined model and the Pastor-Satorras and Vespignani heterogeneous mean-field (HMF) approximation model from [25] using the $\epsilon-$SIS spreading model from Hill in [26] as the benchmark. For $\epsilon > 0$ an epidemic state exists, similar to Proposition 1 for (2.9), unlike the 2^n state model for which the disease-free equilibrium is an absorbing state; therefore the $\epsilon-$SIS spreading model is not a perfect substitute for the 2^n state model but is used because for $\epsilon = 0$ they are equivalent and it is more computationally tractable. Li *et al.* show via simulation that the n-intertwined model outperforms the HMF model for complete, star, bipartite, complete bipartite, Erdős-Rényi, Barabasi-Albert scale-free, and Watts-Strogatz small-world graphs, but not square lattice and path graphs when using the $\epsilon-$SIS spreading model as a baseline. In [27], Van Mieghem and van de Bovenkamp examine in more detail the expectation of the model in (2.3), similar to the idea in (2.7), using the definition of covariance, $cov(X_i, X_j) = E[X_i X_j] - E[X_i]E[X_j]$,

$$\begin{aligned}
\frac{dE[X_i]}{dt} &= E\left[\beta(1 - X_i)\sum_{j=1}^{n} a_{ij}X_j - \delta X_i\right] \\
&= \beta\sum_{j=1}^{n} a_{ij}E[X_j] - \beta\sum_{j=1}^{n} a_{ij}E[X_iX_j] - \delta E[X_i] \\
&= \beta(1 - E[X_i])\sum_{j=1}^{n} a_{ij}E[X_j] - \delta E[X_i] - \beta\sum_{j=1}^{n} a_{ij}cov(X_i, X_j) \\
&= \beta(1 - p_i)\sum_{j=1}^{n} a_{ij}p_j - \delta p_i - \underbrace{\beta\sum_{j=1}^{n} a_{ij}cov(X_i, X_j)}_{R_i},
\end{aligned}$$

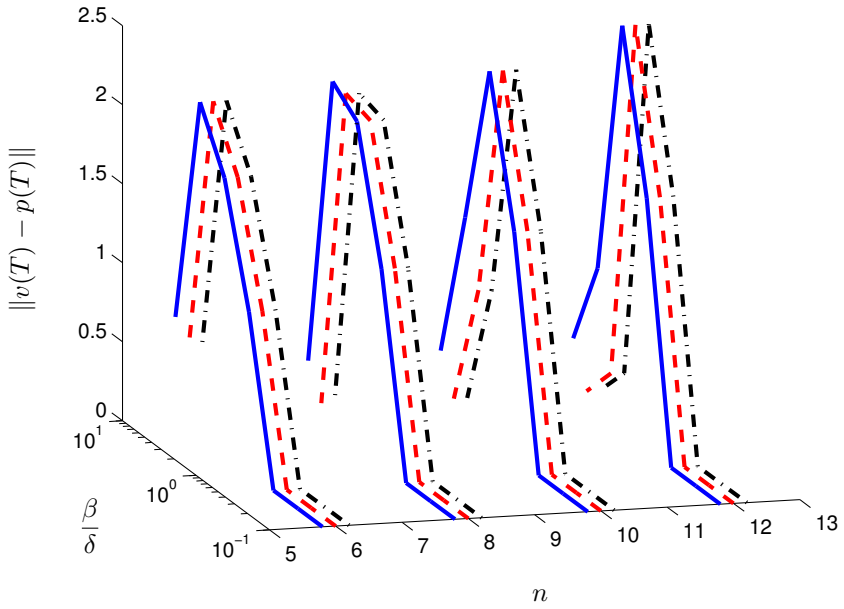

Figure 2.3: A plot of $\|v(T) - p(T)\|$ for the line graph, $T = 10000$. Results from using the different initial conditions $p^1(0)$, $p^2(0)$, $p^3(0)$ are depicted by the blue lines, red dashed lines, and black dash-dot lines, respectively. For a simulation of $n = 6$, $\frac{\beta}{\delta} = 1$, and $p(0) = p^3(0)$ see youtu.be/E49OTI4Pgh0.

calling R_i the mean field approximation correction term. The authors then develop three criteria for R_i and evaluate the criteria explicitly for the star graph and the complete graph using the different metrics. They also explored the effect of network size on one of the criteria for the complete, star, path, square lattice, and Erdős-Rényi graphs through simulation.

Static Graphs:

In this section we first compare via simulations the 2^n state and n-intertwined Markov chain models for line graphs, star (hub–spoke) graphs, and complete graphs; see Figure 2.2 for examples of each graph structure. All A matrices for these graphs are symmetric and binary-valued. In the star graph, the central node is the first agent. Each simulation was run for 10,000 time steps (final time $T = 10000$), with three initial conditions: 1) every agent infected, $p^1(0) = [1 \ \cdots \ 1]^\top$, 2) half the agents infected, $p^2(0) = [1 \ \cdots \ 1 \ 0 \ \cdots \ 0]^\top$, and 3) one agent infected, $p^3(0) = [1 \ 0 \ \cdots \ 0]^\top$. We explore the homogeneous virus model, (2.6), in these tests. The (β, δ) pairs used are $[(0.1, 1), (0.215, 1), (0.464, 1), (0.5, 0.5), (1, 0.464), (1, 0.215), (1, 0.1)]$, and the number of agents, $n = 6, 8, 10, 12$. We limited simulations to these n values since mean field approximations are typically worse for small values of n and there is a computational limitation due to the size of the 2^n model.

The results are given in Figures 2.3-2.5 in terms of the 2-norm of the difference between the state of the n-intertwined Markov chain model at the final time ($p(T)$), and the mean of the 2^n Markov model at the final time ($v(T)$ as defined by (2.4)). Since the n-intertwined Markov chain model is an upper bounding approximation, the results show that the two models converge to the DFE for most values of $\frac{\beta}{\delta}$ close to $1/10$, resulting in small errors. For most values of $\frac{\beta}{\delta}$ near 10 the n-intertwined Markov chain model again

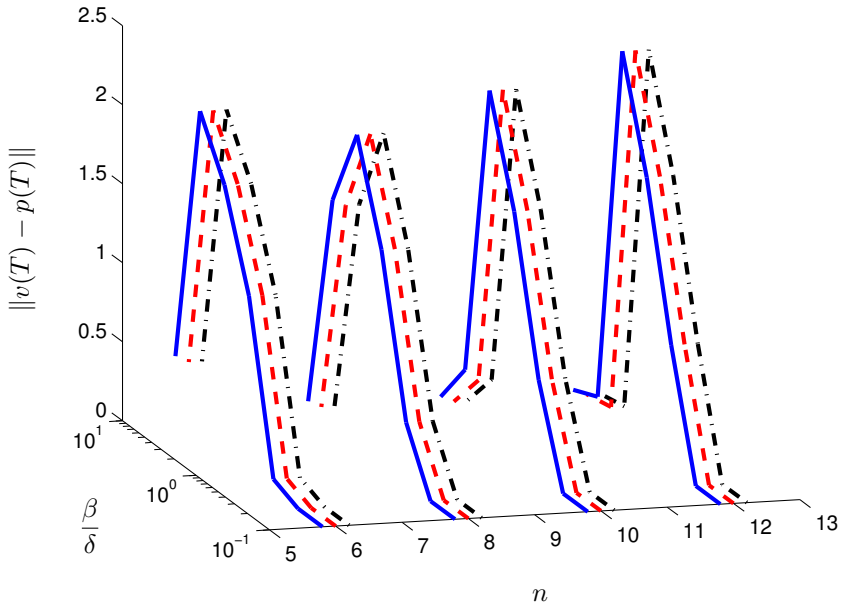

Figure 2.4: A plot of $\|v(T) - p(T)\|$ for the star graph, $T = 10000$. Results from using the different initial conditions $p^1(0)$, $p^2(0)$, $p^3(0)$ are depicted by the blue lines, red dashed lines, and black dash-dot lines, respectively. For a simulation of $n = 6$, $\frac{\beta}{\delta} = 1$, and $p(0) = p^3(0)$ see youtu.be/XOdNUDFngO4.

performs quite well since it is at a NDFE and the 2^n state model does not appear to reach the DFE in the finite time considered in the simulations ($T = 10000$). Therefore for certain time scales the n-intertwined model approximation could be sufficient. For values of $\frac{\beta}{\delta}$ that are not near $1/10$ or 10, the models differ quite drastically; the n-intertwined Markov chain model appears to be at a NDFE while the 2^n model appears, in most cases, to be at or close to the DFE, resulting in large errors.

Complete Graphs:

For completeness, we present a comparison of the results from the static complete graph to the results of simulating the original model in (1.1). Since (1.1) models the population as two groups, we take the average infection of the results of the n-intertwined model ($\frac{1}{n}\sum_{i=1}^{n} p_i(T)$) and the means of the 2^n model ($\frac{1}{n}\sum_{i=1}^{n} v_i(T)$, with $v(t)$ defined in (2.4)). These averages, with the scaled results of (1.1) ($\frac{1}{n}I(T)$), are compared in Figure 2.6. Note that the initial conditions $p^1(0)$, $p^2(0)$, $p^3(0)$, are analogous to $I^1(0) = n$, $I^2(0) = n/2$ and $I^3(0) = 1$, respectively. All three models behave similarly at the extremes and the original and n-intertwined models (in (1.1) and (2.6)) perform closely for all of the (β, δ) pairs. The 2^n model differs in most of the mid-valued ranges of $\frac{\beta}{\delta}$, which is consistent with the simulations summarized in Figure 2.5 and with the upper-bounding effect of the n-intertwined model.

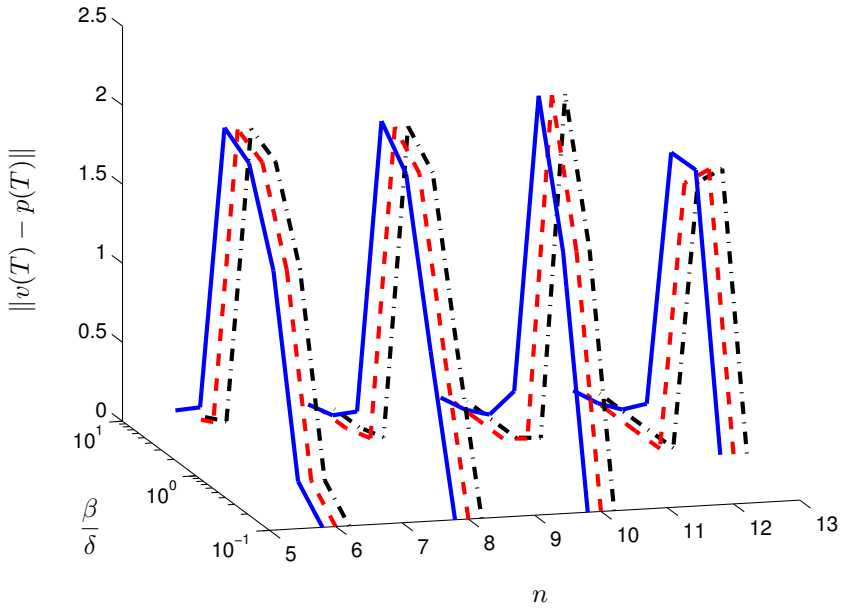

Figure 2.5: A plot of $\|v(T) - p(T)\|$ for the complete graph, $T = 10000$. Results from using the different initial conditions $p^1(0)$, $p^2(0)$, $p^3(0)$ are depicted by the blue lines, red dashed lines, and black dash-dot lines, respectively. For a simulation of $n = 6$, $\frac{\beta}{\delta} = 1$, and $p^3(0)$ see youtu.be/VTFZDdXsC6M.

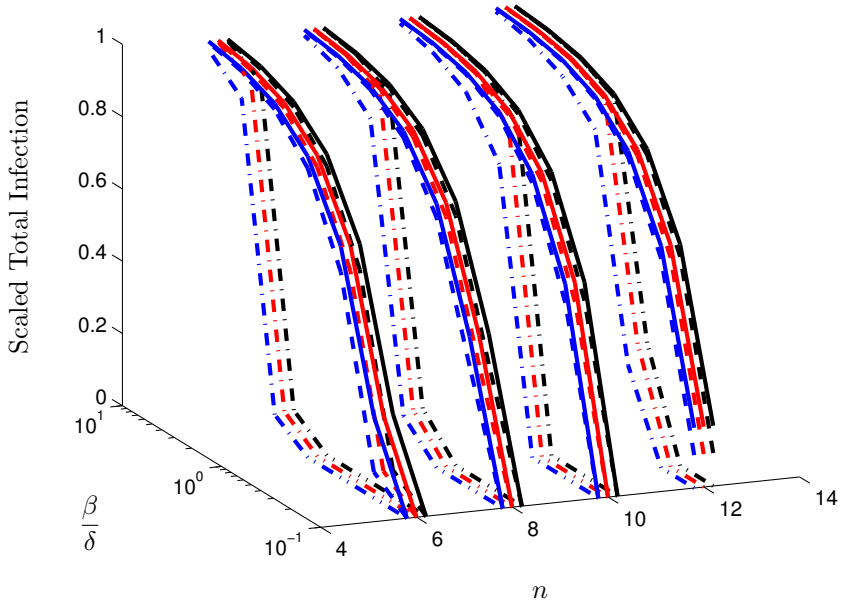

Figure 2.6: Comparison of complete graph models to (1.1): The plots of $\frac{1}{n}I(T)$, $\frac{1}{n}\sum_{i=1}^{n} p_i(T)$, $\frac{1}{n}\sum_{i=1}^{2^n} v_i(T)$ with $T = 10000$ are shown in solid, dashed, and dash-dot lines, respectively. Results from using the different initial conditions $p^1(0)$, $p^2(0)$, $p^3(0)$ are shown in blue, red, and black, respectively.

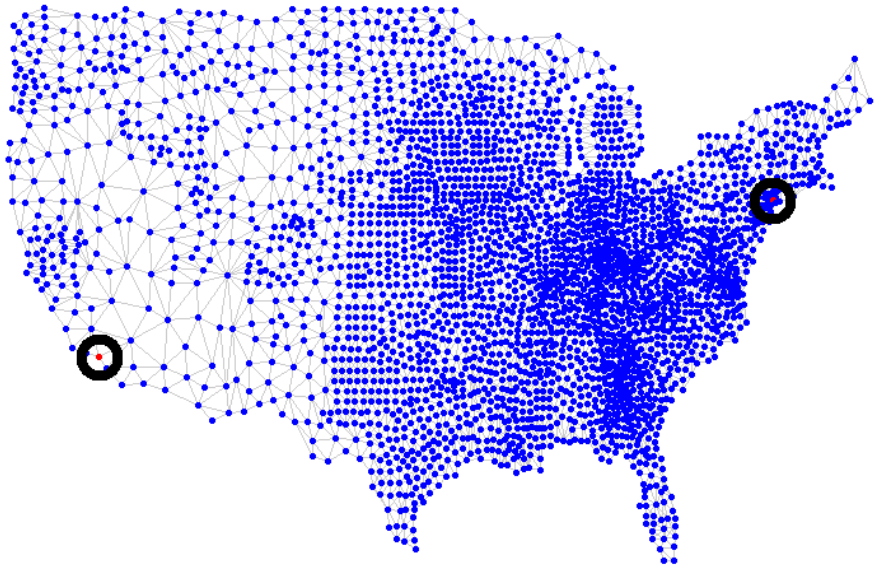

Figure 2.7: Initial condition with the virus originating from New York City and Los Angeles, indicated in red and circled to highlight their locations. The average infection proportion is $\frac{2}{3109}$.

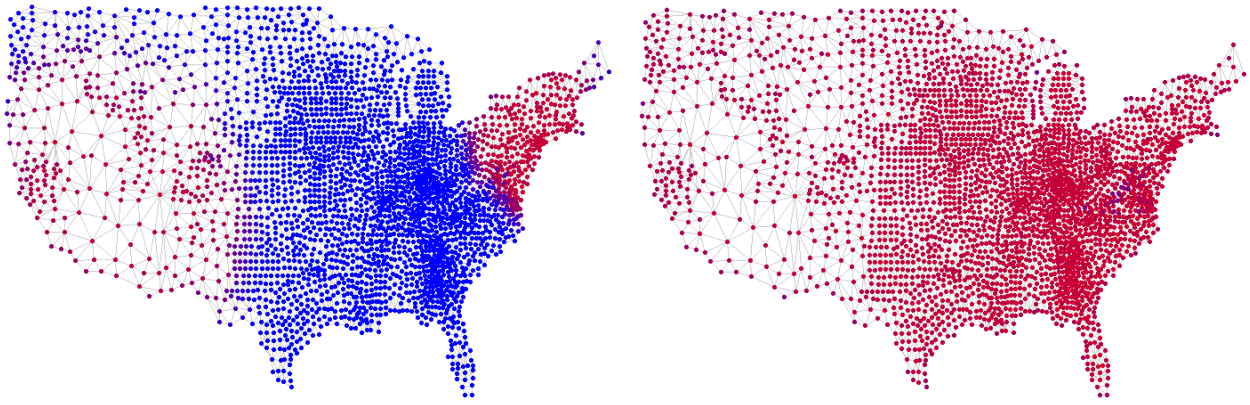

Figure 2.8: The virus $(\beta_1, \delta_1) = (0.1, 0.1)$: the infections after 45 time steps of propagating (left) with the average infection proportion of 0.1561, and the NDFE equilibrium (right) with average infection proportion of 0.7586.

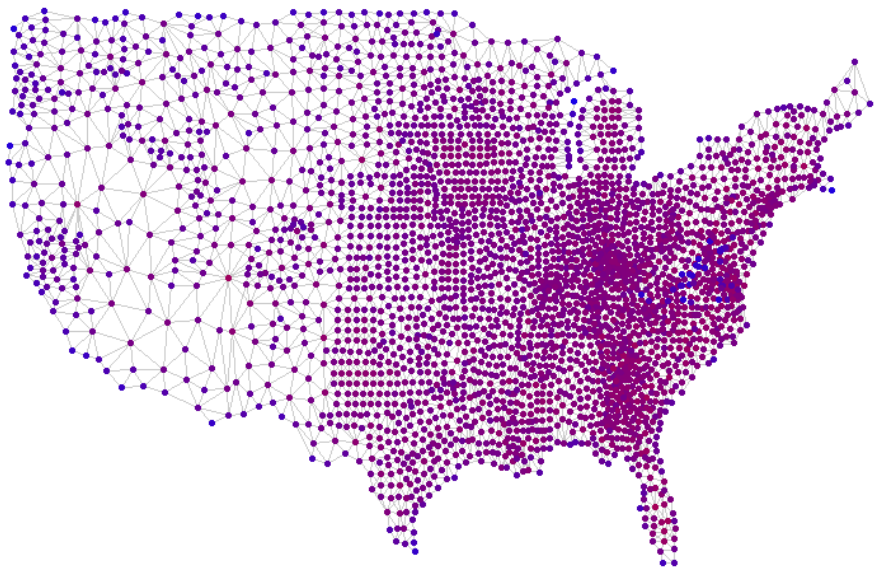

Figure 2.9: NDFE equilibrium of the virus $(\beta_2, \delta_2) = (0.1, 0.22)$. The average infection proportion is 0.6904.

2.1.5 Exploratory Large-Scale Data Simulation

To further illustrate the behavior of these systems we simulate the evolution of a virus process over a network representing the United States of America. We assume the virus starts in New York City and Los Angeles (Figure 2.7). The nodes of the graph correspond to counties in the domestic United States, and are placed in the centroid of each county. The edges denote that two counties are adjacent, with the corresponding A matrix being symmetric with ones on the diagonal. The off-diagonals of the A matrix are equal to one hundred times the inverse of the 2-norm distance between the centroids (given in latitude and longitude). We recognize that the homogeneity in the edge construction (opposed to heavier connections between more frequented edges) is probably not the most realistic, but it still provides an effective illustration. The infection rate corresponds to the percentage of the county infected, or alternatively, the probability the county is infected. We simulated two homogeneous viruses with $(\beta_1, \delta_1) = (0.1, 0.1)$ and $(\beta_2, \delta_2) = (0.1, 0.22)$. An intermediate state can be seen on the left side of Figure 2.8. The steady states of the two viruses can be seen in the right side of Figure 2.8 and Figure 2.9.

2.2 Discrete Time Single-Virus Model

In this section we introduce two discrete time SIS models and we discuss their relationship to each other and to the models in Section 2.1.1. The majority of this material was originally published in [28] and is used here with permission. Similar to the continuous-time case, there are two levels of granularity for modeling the system. The state p_i can correspond to a probability of infection of the ith agent [6] or to the percentage of infection of group i [3].

The first discrete time model is derived from the continuous time model in (2.8) where i indicates the ith agent or group i, p_i is the infection level, $\beta_i > 0$ is the infection rate, $\delta_i > 0$ is the healing rate, and a_{ij} are the non-negative, edge weights between the agents/groups. Note A is the matrix of a_{ij}'s and is not necessarily symmetric.

As discussed in Section 2.1.1, the model in (2.8) is derived using a mean-field approximation of the 2^n state Markov model in (2.3). Applying Euler's method [29] to (2.8) gives

$$p_i^{k+1} = p_i^k + h\left((1-p_i^k)\beta_i \sum_{j=1}^{n} a_{ij} p_j^k - \delta_i p_i^k\right), \tag{2.10}$$

where k is the time index and $h > 0$ is the sampling parameter. We can write (2.10) in matrix form

$$p^{k+1} = p^k + h((I - P^k)BA - D)p^k, \tag{2.11}$$

where $P^k = diag(p^k)$, $B = diag(\beta_i)$, and $D = diag(\delta_i)$.

Remark 1. *The model in* (2.8) *was derived from a mean field approximation of a* 2^n *state Markov chain model [6, 19]. Therefore* (2.10) *is an approximation of an approximation.*

Observation 1. *The disease-free state is an equilibrium of the model in* (2.10)*.*

Proof. Clearly $p^* = \mathbf{0}$ solves (2.10). □

Remark 2. *Consider a simple homogeneous example with* $\beta = 1$, $\delta = 0.1$, $n = 2$, *and*

$$A = \begin{bmatrix} 0 & 1 \\ 1 & 0 \end{bmatrix}.$$

Then $p^* = [.9 \quad .9]'$ *solves* (2.10)*:*

$$p_i^{k+1} = 0.9 + h\left((1-0.9)\beta \sum_{j=1}^{n} a_{ij}(0.9) - \delta(0.9)\right) = 0.9.$$

Therefore it is possible for (2.10) *to have an endemic state.*

An alternative discrete time model, studied in [8], is

$$p_i^{k+1} = p_i^k(1-\delta_i) + (1-p_i^k)\left(1 - \prod_{j=1}^{n}(1-\beta_i a_{ij} p_j^k)\right). \tag{2.12}$$

By expanding the model given in (2.12) we obtain

$$p_i^{k+1} = p_i^k - (1-p_i^k)\left[-\beta_i \sum_{j=1}^{n} a_{ij} p_j^k + \cdots + \beta_i^n \prod_{j=1}^{n}(-a_{ij} p_j^k)\right] - \delta_i p_i^k.$$

Remark 3. *If we assume* $\beta_i < 1$ $\forall i$*, the model in* (2.12) *can be approximated by truncating the terms with powers of* β_i *greater than one, giving:*

$$p_i^{k+1} \approx p_i^k + (1-p_i^k)\beta_i \sum_{j=1}^{n} a_{ij} p_j^k - \delta_i p_i^k. \tag{2.13}$$

The preceding discussion leads us to the following observation.

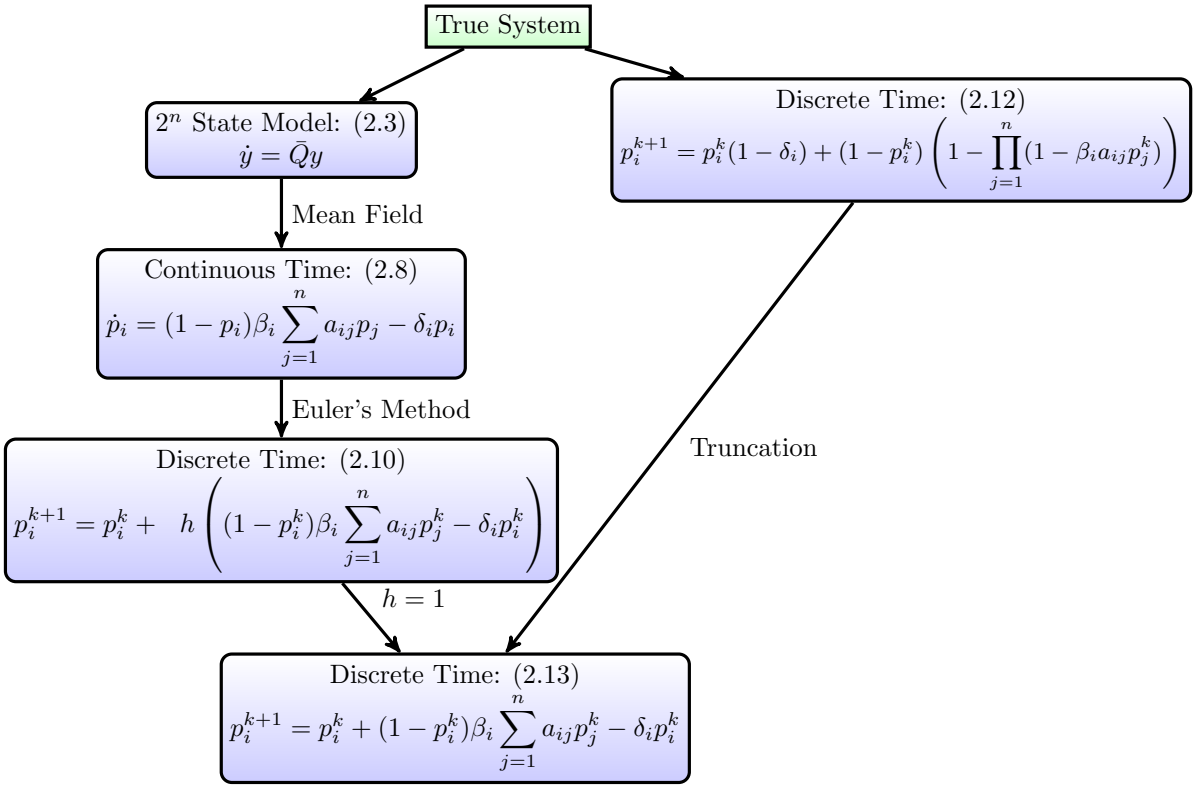

Figure 2.10: A graphical illustration of the discussion in Section 2.2 and the point in Observation 2, showing how the two discrete time spread models are related. The first modeling layer shows the 2^n state models. The arrows indicate different approximations taken.

Observation 2. *The approximation given by* (2.13) *and the discrete approximation of the mean field approximation of the continuous* 2^n *state Markov model in* (2.10) *are equivalent given* $h = 1$*.*

Proof. The approximation in (2.13) is clearly equivalent to (2.10) if $h = 1$. □

Remark 4. *Recall that* (2.8) *and* (2.12) *are different models of the same system. Observation 2 shows us that their approximations,* (2.10) *and* (2.13)*, are equivalent, giving reason to believe that* (2.10) *and* (2.13) *are good approximate models of the true system.*

The relationships between the models introduced in this section are depicted in Figure 2.10. The first layer of modeling is the most detailed, where the left side is the model given by (2.3) and the right side is that given by (2.12).

2.2.1 Model Well-Posedness

To assure well-posedness of the model we include the following. A more generic version of the model in (2.10) will be analyzed in this and the following sections:

$$p^{k+1} = p^k + h((I - P^k)B - D)p^k, \tag{2.14}$$

where $[B]_{ij} = \beta_{ij}$, and β_{ij} could be factored into $\beta_i a_{ij}$ as in (2.10).

Assumption 1. *For all* $i \in [n]$*, we have* $p_i^0 \in [0, 1]$*.*

Assumption 2. *For all* $i \in [n]$*, we have* $\delta_i \geq 0$ *and, for all* $j \in [n]$*,* $\beta_{ij} \geq 0$*.*

Assumption 3. *For all* $i \in [n]$*, we have* $h\delta_i \leq 1$ *and* $h \sum_{j \neq i} \beta_{ij} \leq 1$*.*

Lemma 2. *For the system in* (2.14)*, under the conditions of Assumptions 1, 2, and 3,* $p_i^k \in [0, 1]$ *for all* $i \in [n]$ *and* $k \geq 0$*.*

Proof. Suppose that at some time k, $p_i^k \in [0, 1]$ for all $i \in [n]$. Consider an index $i \in [n]$. Rearranging (2.10),

$$p_i^{k+1} = p_i^k(1 - h\delta_i) + (1 - p_i^k)\left(h \sum_{j=1}^{n} \beta_{ij} p_j^k\right),$$

we see that p_i^{k+1} is a convex combination of $(1 - h\delta_i)$ and $h \sum_{j=1}^n \beta_{ij} p_j^k$. Therefore since, by Assumptions 2 and 3, $h\delta_i, h \sum_{j=1}^n \beta_{ij} p_j^k \in [0, 1]$, $p_i^{k+1} \in [0, 1]$.

Therefore, by Assumption 1, $p_i^0 \in [0, 1]$ for all $i \in [n]$, it follows that $p_i^k \in [0, 1]$ for all $i \in [n]$ and $k \geq 0$. □

2.2.2 Accuracy of Approximation

We examine the accuracy of the model in (2.10) in this section via simulation. Similar to Section 2.1.4, we explore the discrepancies between (2.10), and (2.6) and (2.3).

To quantify the error between the approximation in (2.10) and the full probabilistic 2^n state model in (2.3) and its continuous-time mean field approximation in (2.6) we simulate the models over a path

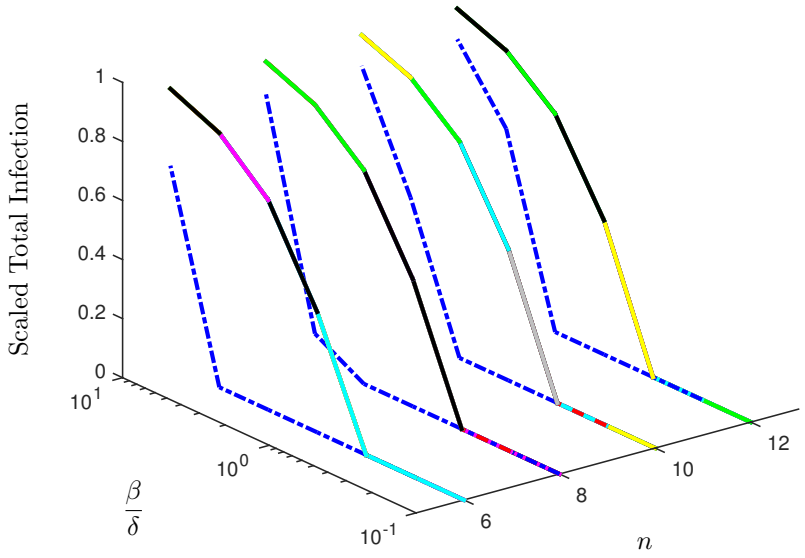

Figure 2.11: The lines show the average final infection for (2.3), (2.6), (2.10) with $h = 0.001, 0.01., 0.1, 0.5, 0.9, 1$, in blue, red, green, magenta, cyan, black, yellow, and gray, respectively. All models are simulated with the same graph structure of n nodes in a line, the same initial condition with every node infected, and for the same period of time, 10000 time steps (except for $h = 0.001$, the simulations were run for 100000 time steps, because since h was so small it took longer to reach the equilibrium).

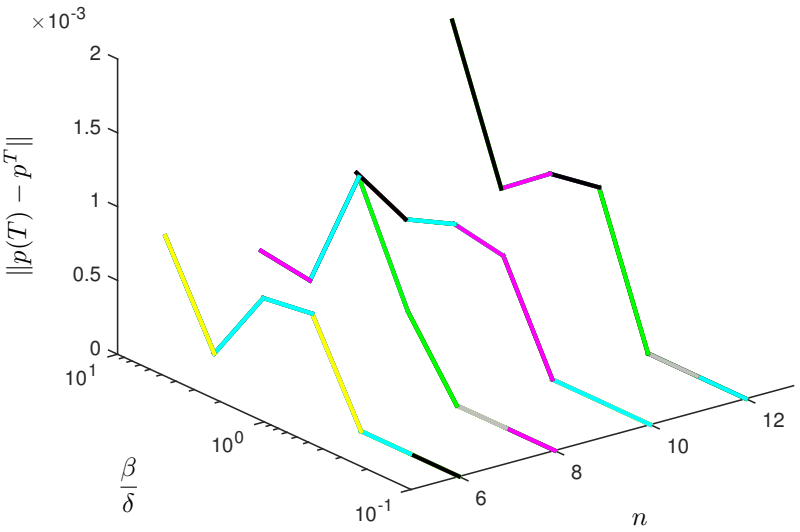

Figure 2.12: The lines show the 2-norm error between the final states of (2.6) and (2.10) with the different $h = 0.001, 0.01., 0.1, 0.5, 0.9, 1$ values, in green, magenta, cyan, black, yellow, and gray, respectively. All models are simulated with the same graph structure of n nodes in a line and the same initial condition with every node infected.

graph with every node completely infected initially (different initial conditions performed similarly). The (β, δ) pairs used are $[(0.1, 1), (0.215, 1), (0.464, 1), (0.5, 0.5), (1, 0.464), (1, 0.215), (1, 0.1)]$, and the number of nodes, $n = 6, 8, 10, 12$. We simulate (2.10) for $h = 0.001, 0.01., 0.1, 0.5, 0.9, 1$. Due to the constraints of Assumption 3 and the presence of numerical error, several of the simulations of (2.10) failed, namely, the tuples $(\beta, \delta, h) = (1, 0.464, 0.9), (1, 0.464, 1), (1, 0.215, 1), (1, 0.1, 1)$.

The comparisons of the simulation results depicted by the final average infection are in Figure 2.11. As the simulations indicate, the model in (2.10) is very similar to (2.6), and, consistent with Section 2.1.4, (2.6) is different from (2.3) in the cases where δ and β are close to each other in value. Therefore (2.10) has similar disadvantages to (2.6) as an approximation of (2.3), which is logical since (2.10) is an approximation of (2.6).

To better quantify the quality of (2.10) as an approximation of (2.6) we plot the Euclidean distance (2-norm) between the final states of (2.6) and (2.10) with all of the different h values in Figure 2.12. As can be seen, the error is quite low. Therefore we conclude that (2.10) is a good model when Assumption 3 is met. Also, (2.10) is a decent approximation of (2.3) when δ and β are not too similar in magnitude, and a good approximation of (2.6).

2.3 Analysis of the Static Graph, Discrete Time Virus Model

Lemma 2 implies that the set $[0, 1]^n$ is positively invariant with respect to the system defined by (2.14). Since p_i denotes the probability of infection of individual i, or the fraction of group i infected, and $1 - p_i$

denotes probability of individual i being healthy, or the fraction of group i that is healthy, it is natural to assume that their initial values are in the interval $[0,1]$, since otherwise the values will lack any physical meaning for the epidemic model considered here. Therefore, we focus on the analysis of (2.14) only on the domain $[0,1]^n$.

We need an assumption to ensure *non-trivial* homogeneous virus spread.

Assumption 4. *We have $B, h \neq 0$.*

Definition 2. *Consider an autonomous system*

$$x^{k+1} = f(x^k), \tag{2.15}$$

where $f : \mathcal{X} \to \mathbb{R}^n$ is a locally Lipschitz map from a domain $\mathcal{X} \subset \mathbb{R}^n$ into $\mathbb{R}^n$. Let z be an equilibrium of (2.15) and $\mathcal{E} \subset \mathcal{X}$ be a domain containing z. If the equilibrium z is asymptotically stable such that for any $x^0 \in \mathcal{E}$ we have $\lim_{k\to\infty} x^k = z$, then $\mathcal{E}$ is said to be a domain of attraction for z.

Proposition 3. *Let z be an equilibrium of (2.15) and $\mathcal{E} \subset \mathcal{X}$ be a domain containing z. Let $V : \mathcal{E} \to \mathbb{R}$ be a continuously differentiable function such that $V(z) = z$, $V(x) > 0$ in $\mathcal{E} \setminus \{z\}$, and $\Delta V^k := V(x^{k+1}) - V(x^k) < 0$ in $\mathcal{E} \setminus \{z\}$. If $\mathcal{E}$ is a positively invariant set, then the equilibrium z is asymptotically stable with a domain of attraction $\mathcal{E}$.*

This proposition is a direct consequence of Lyapunov's stability theorem for discrete time systems and the definition of domain of attraction.

Finally, we need an assumption on the structure of the B matrix. Note, a square matrix is called *irreducible* if it cannot be permuted to a block upper triangular matrix.

Assumption 5. *The matrix B is irreducible.*

Note, this assumption is equivalent to the underlying graph being strongly connected, which means that there exists a path from any node to every other node in the graph.

Theorem 1. *Suppose that Assumptions 1-5 hold for (2.14). If $\rho(I - hD + hB) \leq 1$, then the healthy state is asymptotically stable with domain of attraction $[0,1]^n$.*

To prove the theorem we need the following lemmata.

Lemma 3. [30] *Suppose that M is an irreducible nonnegative matrix such that $\rho(M) < 1$. Then, there exists a positive diagonal matrix P_1 such that $M^\top P_1 M - P_1$ is negative definite.*

Lemma 4. *Suppose that M is an irreducible nonnegative matrix such that $\rho(M) = 1$. Then, there exists a positive diagonal matrix P_2 such that $M^\top P_2 M - P_2$ is negative semi-definite.*

Proof. From the Perron Frobenius Theorem for irreducible nonnegative matrices, there exists $v \gg 0$ such that $Mv = v$. Since $M^\top$ is also irreducible and nonnegative, there exists $u \gg 0$ such that $M^\top u = u$. Let P_2 be a diagonal matrix whose ith diagonal entry is equal to u_i/v_i, which gives $P_2 v = u$. Therefore

$$(M^\top P_2 M - P_2)v = M^\top P_2 v - P_2 v = M^\top u - u = 0.$$

Then by Lemma 2.3 in [31], $\rho(M^\top P_2 M - P_2) = 0$. □

The proof of Theorem 1 is included in Appendix A.

Proposition 4. *Let Assumptions 1-5 hold. If* $\rho(I - hD + hB) > 1$*, then* (2.14) *has two equilibria,* $\mathbf{0}$ *and* p^**, where* $p^* \gg \mathbf{0}$*.*

Proof. Clearly $\mathbf{0}$ is always an equilibrium of (2.14).

By the Perron Frobenius Theorem for irreducible nonnegative matrices (Theorem 8.4.4 in [32]), $\rho(I - hD + hB) = s_1(I - hD + hB)$ and there exists $v \gg 0$ such that

$$(I - hD + hB)v = \rho(I - hD + hB)v > v,$$

since $\rho(I - hD + hB) > 1$. Therefore

$$(-hD + hB)v = \rho(-hD + hB)v = s_1(-hD + hB)v > 0v,$$

which implies

$$\rho(I - hD + hB) > 1 \iff h(s_1(-D + B)) > 0.$$

This condition is the same as the condition of Proposition 3 in [33, 23], and the proof follows similarly, showing that there exists $p^* \gg \mathbf{0}$ such that

$$h((-D + B) - P^*B)p^* = \mathbf{0}.$$

Therefore, $\mathbf{0}$ and p^* are equilibria of (2.14). □

From Theorem 1 and Proposition 4 we have the following result.

Theorem 2. *Under Assumptions 1-5, the healthy state is the unique equilibrium of* (2.14) *if and only if* $\rho(I - hD + hB) \leq 1$*.*

In [8] a counterexample is provided to show that the nontrivial equilibrium of (2.12) is unstable. However this example does not apply to the models in (2.10) and (2.14) because it does not meet Assumption 3. Consequently the state of the system does not stay in the domain of interest, $[0, 1]^n$.

Chapter 3

Epidemic Processes over Time–Varying Networks

The aforementioned work in Chapter 1 considers only static graph structures. Although contributing to the understanding of virus spread and the ensuing eradication, in most cases static graph structures are fundamentally too simple to capture the essential dynamics of infectious disease processes. Most applications that motivate these systems have agents that are mobile, which implies that the underlying graph structure is time–varying. For example, computer networks are comprised of smart phones, laptops, and other mobile devices which connect to different devices as they move around. In order to obtain a better understanding of these systems, a more realistic representation, that of *virus dynamics over time–varying networks*, is necessary. The majority of this chapter appeared in the IEEE Transactions on Control of Network Systems [19] and is used here with permission.

3.1 Background

The previous work on virus spread over time–varying networks is limited to unweighted and undirected graphs. In [34], Prakash *et al.* extend the discrete time model used in [9] to a model with a time–varying graph structure. The authors provide a sufficient condition for local exponential stability of the origin (the DFE), and propose a control scheme that removes agents from the system. In [35], Bokharaie *et al.* provide similar results to those in [34], extending the model from [9] to the time–varying case and proving local exponential convergence to the origin. The authors state that these results extend to the continuous time–varying case, without proof. The authors of both [34] and [35] consider unweighted, undirected graphs and extend the model from [9], which was shown in [6] to have significant shortcomings. In [36], Rami *et al.* extend the model from [3] to that of a switching virus model. The authors provide a sufficient condition for stability of the DFE, show the existence of a periodic NDFE, and give a sufficient condition for stability of the DFE for a Markovian switching virus model. Sanatkar *et al.*, in [37], present results similar to the ideas in [36], but for a discrete time model. Liu, in [38], also following the ideas in [36], examines a switching SI model for a system with trivial graph structures (i.e., similar to the model in (1.1)). In [39], Ogura and Preciado propose a less general version of the results given in Proposition 1 of [7], examining a subset of random graphs and giving sufficient conditions for almost sure, global exponential stability. Somewhat related results can also be found in the physics/network science literature, including, but not limited to, the references [40, 41, 17, 42]. In these references less general time–varying models are studied with some analysis provided.

In this chapter, we propose notable extensions to the models from [6] to include time–varying, weighted, directed and undirected graph structures. To the best of our knowledge, we are the first to derive results for weighted and directed time–varying graph structures. We provide sufficient conditions for global exponential

stability of the DFE for these models. We present additional simulations that give insight into stability, and from these formulate several corollaries.

This chapter is organized as follows. In Section 3.2 we introduce the time–varying extensions of the models from Section 2.1. In Section 3.3 we explore the stability properties of the time–varying extensions of the n-intertwined Markov chain model, and in Section 3.3.2 we introduce stochasticity into the model and perform some analysis. In Section 3.4 we illustrate the time–varying n-intertwined model via simulations. Based on one of these simulations, we state and prove a corollary.

3.2 Time-Varying Model

In this chapter, a time–varying extension of the model in (2.9) is considered, that is

$$\dot{p}(t) = (BA(t) - P(t)BA(t) - D)p(t), \tag{3.1}$$

where now $A(t)$ is a function of time. Note that $A(t)$ is not necessarily symmetric, and depicts the links between the n agents, similar to an adjacency matrix without the constraint to be binary-valued. The mean field approximation in (2.5) remains unaffected by this extension as long as the assumption is made that the $a_{ij}(t)$'s are deterministic and known functions. We assume that $p_i(0) \geq 0$ for all $i = 1, ..., n$. Note that Lemma 1 still holds assuming $A(t)$ is piece-wise continuous.

For completeness, we also include a time–varying extension of the model in (2.3). The extended model is

$$\frac{dy^\top(t)}{dt} = y^\top(t)\bar{Q}(t), \tag{3.2}$$

where

$$\bar{q}_{kl}(t) = \begin{cases} \delta, & \text{if } x_i = 1, k = l + 2^{i-1} \\ \beta \sum_{j=1}^{n} a_{ij}(t)x_j, & \text{if } x_i = 0, k = l - 2^{i-1} \\ -\sum_{j \neq l} \bar{q}_{jl}(t), & \text{if } k = l \\ 0, & \text{otherwise.} \end{cases}$$

Due to the immense size of the 2^n model it is quite costly to employ, which makes the mean field approximation particularly relevant.

3.3 Stability Analysis of the Time–Varying Model: Deterministic and Stochastic Cases

In this section, stability analysis of the disease-free equilibrium for the time–varying model in (3.1) is performed for the deterministic case and several stochastic cases.

3.3.1 Deterministic Case

The DFE is the state where $p_i(t) = 0$ for all i, which from (3.1) implies $\dot{p}_i(t) = 0$ for all i. We show global exponential convergence to the DFE under certain conditions, to be made precise.

First we consider the case with undirected graph structure and homogeneous β.

Theorem 3. *Suppose $\beta_i = \beta\ \forall i$, $A(t)$ is symmetric, piece-wise-continuous in t, and bounded, and $\sup_{t\geq 0} \lambda_1(BA(t) - D) < 0$. Then the DFE is globally exponentially stable (GES).*

Proof. To simplify notation we will write $p = p(t)$. Consider an arbitrary $p \geq 0$ and define a Lyapunov function $V(p) = \frac{1}{2}p^\top p$. For $p \neq 0$,

$$\begin{aligned}\dot{V}(p) &= p^\top \dot{p} = p^\top (BA(t) - P(t)BA(t) - D)p \\ &\leq p^\top (BA(t) - D)p \leq \lambda_1(BA(t) - D)\|p\|^2 \\ &\leq \left(\sup_{t\geq 0} \lambda_1(BA(t) - D)\right)\|p\|^2 < 0.\end{aligned}$$

The first inequality holds because $(P(t)BA(t))_{ij} \geq 0,\ \forall i, j,\ \beta \geq 0,\ a_{ij} \geq 0$ for all i, j, by assumption, and $p_i(t) \geq 0$ for all i, by Lemma 1. The second inequality holds by the Rayleigh-Ritz Quotient (RRQ) [32] because $BA(t) - D$ is symmetric (since $A = A^\top$ and $\beta_i = \beta\ \forall i$). The last inequality holds by definition of the supremum. Therefore, since the system is piece-wise continuous in t and, by the boundedness of $A(t)$, locally Lipschitz in $p\ \forall t, p \geq 0$, the system converges exponentially fast to the origin by Theorem 8.5 in [43]. □

Remark 5. *Theorem 3 requires $BA(t) - D$ to be symmetric because of the chosen Lyapunov function in the proof, which considerably simplifies the analysis. The RRQ cannot be applied unless the matrix under consideration is symmetric, which is not satisfied for BA when the virus is heterogeneous in infection rate. However, note if the Lyapunov function $V(p) = \frac{1}{2}p^\top B^{-1}p$ is used, assuming $\beta_i > 0$ for all i, the result of Theorem 3 can be shown in terms of $\lambda_1(A(t) - B^{-1}D)$.*

The following lemma and theorem explore the case where symmetry is not assumed, that is, for the heterogeneous model (different β_i's and δ_i's $\forall i$) and asymmetric matrices ($A \neq A^\top$).

Now we consider the more general case with directed graph structure and heterogeneous virus spread. The following result and proof are similar to Theorem 3.4.11 in [44] and the Lyapunov analysis is done point-wise in t.

Definition 3. *Assume that for all $t \geq 0$, there exist finite $c(t), \lambda(t) > 0$ such that*

$$\|BA(t) - D\| \leq c(t)e^{-\lambda(t)t} \quad \forall t \geq 0. \tag{3.3}$$

We then define

$$\gamma_1 := \sup_{t\geq 0} \int_0^\infty c(t)^2 e^{-2\lambda(t)\tau} d\tau \geq \left\| \int_0^\infty e^{(BA(t)-D)^\top \tau} e^{(BA(t)-D)\tau} d\tau \right\|. \tag{3.4}$$

Theorem 4. *Consider the system in (3.1) with $A(t)$ continuously differentiable and $BA(t) - D$ bounded, that is, there exists an $L > 0$ such that $\|BA(t) - D\| \leq L\ \forall t$. Assume that $\sup_{t\geq 0} s(BA(t) - D) < 0$, and γ_1 in Definition 3, is well-defined and finite. If $\sup_{t\geq 0} \|B\dot{A}(t) - D\| < \frac{1}{2\gamma_1^2}$ or $\int_t^{t+T} \|B\dot{A}(s) - D\| ds \leq \mu T + \alpha$ for small enough $\mu > 0$, then the DFE is globally exponentially stable.*

The proof can be found in Appendix A.

Next we consider the case where the linearized system is not always Hurwitz. We first introduce a lemma.

Lemma 5. *Consider the system*

$$\dot{p} = (BA(t) - D + B\Delta(t))p.$$

Assume

$$\lim_{T\to\infty} \frac{1}{T} \int_{t_0}^{t_0+T} \|BA(s) - D\|ds \leq a < \infty, \tag{3.5}$$

for all $t_0 \geq 0$, and for some $\nu > 0$ there exists an $h > 0$ such that

$$\|BA(t+h) - BA(t)\| \leq \nu h^{\gamma}, \tag{3.6}$$

for all $t \geq 0$ and some γ, $0 < \gamma \leq 1$. Assume

$$\lim_{T\to\infty} \frac{1}{T} \int_{t_0}^{t_0+T} s(BA(s) - D)ds \leq \bar{\alpha}, \tag{3.7}$$

for some negative scalar $\bar{\alpha}$ and for all $t_0 \geq 0$, and

$$\lim_{T\to\infty} \frac{1}{T} \int_{t_0}^{t_0+T} \|B\Delta(s)\|ds \leq \eta < \infty, \tag{3.8}$$

for all $t_0 \geq 0$. Then the DFE is exponentially stable.

Lemma 5 is a direct application of Theorem 2 in [45].

Theorem 5. *Consider*

$$\dot{p} = (B(A(t) + \Delta(t)) - P(t)B(A(t) + \Delta(t)) - D)p.$$

Assume (3.5)-(3.8) *hold, and $\forall i, j$ and $t \geq 0$ the perturbation*

$$|\Delta_{ij}(t)| \leq a_{ij}(t). \tag{3.9}$$

Then the DFE is exponentially stable.

Proof. Since $(P(t)B(A(t) + \Delta(t)))_{ij} \geq 0$ $\forall i, j$ by (3.9) and Lemma 1,

$$\dot{p} = (B(A(t) + \Delta(t)) - P(t)B(A(t) + \Delta(t)) - D)p \leq (B(A(t) + \Delta(t)) - D)p.$$

Therefore, by Grönwall's Inequality ([46]), the solution of the original system will be bounded above by the solution of the linear system. Thus by Lemma 5, the DFE for the system in (29) is exponentially stable. □

Remark 6. *In the context of disease propagation, these results tell us that the infection rates, β_i, can dominate the healing rates, δ_i, and nevertheless, if the interactions between the agents have certain behavior, the virus can still be eradicated.*

Note that the assumption in (3.5) states that the unperturbed linearized system cannot get too large on average. In the context of virus spread, this means that the element values of the matrix $A(t)$ combined with the corresponding infection rates cannot get too large with respect to the corresponding healing rate,

on average. The assumption in (3.6) is a uniform Lipschitz condition and states that the agents' interactions cannot change too quickly. The assumption in (3.7) imposes that the time average of the unperturbed linearized system is Hurwitz. Also, the assumption in (3.8) states that the perturbation $B\Delta(t)$ cannot be too large, on average.

3.3.2 Stochastic Models

In this section we explore introducing randomness using two different models, a generic additive noise model and an Ito's formula-type model. Note that the mean-field step in (2.5), in essence, removes the randomness that was included in the original 2^n model in (2.3). Therefore, an exploration of random graph structures, while interesting as an extension of the n-intertwined Markov model in (3.1), does not accurately approximate the 2^n model with random graph structure. Alternatively, in this section we consider the measurement of the virus probabilities to be corrupted with additive noise, which allows for a greater range of potential behaviors to be evaluated. Also, this approach acknowledges that the underlying model is stochastic, without necessitating the high-dimensionality of the 2^n state model.

Consider the system

$$\dot{p}(t) = \underbrace{(BA(t) - P(t)BA(t) - D)p(t)}_{F(t,p)} + g(t,p)\xi(t,\omega), \tag{3.10}$$

which represents a perturbation to the model in (3.1), where $\xi(t,\omega) \in \mathbb{R}^k$ is a zero mean, measurable stochastic process, $A(t)$, B, D, and $g(t,p)$ are deterministic, $g(t,p) \in \mathbb{R}^{n\times k}$, and $g(t,0) = 0$ for all t. We assume that $p_i(0) \geq 0$ for all $i = 1, ..., n$.

Lemma 6. *Consider the system in* (3.10) *with* $p_i(0) \geq 0$*, for all* $i = 1, ..., n$*. If* $\xi(t,\omega) \in \mathbb{R}^k$ *is a zero mean, measurable stochastic process and, for all* $i = 1, ..., n$ *there exists* $k_i > 0$ *such that* $\|g_i(t,p)\| \leq k_i|p_i|^2$ *for all* $t \geq 0$*, then* $p_i(t) \geq 0$ *for all* $t \geq 0$*,* $i = 1, ..., n$*.*

Proof. By Lemma 1, the deterministic part of (3.10), $F(t,p)$, is non-negative for all $t \geq 0$. Therefore we turn our attention to the $g_i(t,p)\xi(t,\omega)$ term, where i refers to the ith row of $g(t,p)$. By the zero mean and independence assumptions, $\xi(t,\omega)$ can be negative for any $t \geq 0$. However, by our assumption that $\|g_i(t,p)\| \leq k_i|p_i|^2$ for all t, we have, for any $t \geq 0$,

$$\lim_{p_i\to 0} \|g_i(t,p)\xi(t,\omega)\| \leq \lim_{p_i\to 0} \|g_i(t,p)\|\|\xi(t,\omega)\| \leq \lim_{p_i\to 0} k_i|p_i|^2\|\xi(t,\omega)\| = 0.$$

Therefore if $p_i(0) \geq 0$ then as p_i approaches zero, the random part of the derivative vanishes. Therefore if $p_i(t) = 0$ then $\dot{p}_i(t) \geq 0$, and consequently $p_i(t) \geq 0$ for all $t \geq 0$. □

We have the following result:

Theorem 6. *Consider the system in* (3.10) *with* $\beta_i = \beta\ \forall i$*,* $A(t)$ *symmetric, piece-wise continuous in* t*, and bounded, and* $\sup_{t\geq 0} \lambda_1(BA(t) - D) < 0$*. If* $\xi(t,\omega) \in \mathbb{R}^k$ *is a zero mean, measurable stochastic process and, for all* $i = 1, ..., n$ *there exists* $k_i > 0$ *such that* $\|g_i(t,p)\| \leq k_i|p_i|^2$ *for all* $t \geq 0$*, then the DFE is globally exponentially stable in expectation.*

Proof. Consider an arbitrary p and define a Lyapunov function $V(p) = \frac{1}{2}p^\top p$. For $p \neq 0$,

$$\begin{aligned} E[\dot{V}(p)|p] &= E[p^\top \dot{p}|p] \\ &= p^\top (BA(t) - P(t)BA(t) - D)p + p^\top g(t,p)E[\xi(t,\omega)] \quad (3.11) \\ &= p^\top (BA(t) - P(t)BA(t) - D)p \quad (3.12) \\ &\leq p^\top (BA(t) - D)p \quad (3.13) \\ &\leq \lambda_1(BA(t) - D)\|p\|^2 \leq \left(\sup_{t\geq 0} \lambda_1(BA(t) - D)\right)\|p\|^2 < 0, \end{aligned}$$

where (3.11) and (3.12) hold because, by assumption, $E[\xi(t,\omega)|p] = E[\xi(t,\omega)] = 0$, and (3.13) holds by our assumption that $p_i(0) \geq 0$ for all $i = 1, ..., n$, and by Lemma 6. Thus, since the system is piece-wise continuous in t and locally Lipschitz in p $\forall t, p \geq 0$, and the system converges exponentially fast to the origin in expectation by Theorem 8.5 in [43]. □

Remark 7. *The assumption that for each $i = 1, ..., n$ there exists $k_i > 0$ such that $\|g_i(t,p)\| \leq k_i|p_i|^2$ for all $t \geq 0$, may appear to be strong. However, consider the case where $g(t,p)$ is monotonic in p. An explicit real-life example could be the germs of the ith agent spreading to objects in its surroundings as a source of the noise. As agent i becomes healthy, this noise reduces to zero.*

We will use the result stated in Lemma 7, from [47], to prove Theorem 7. Note that d^0V/dt is defined as

$$\frac{d^0V}{dt} := \frac{\partial V}{\partial t} + \sum_{i=1}^{n} \frac{\partial V}{\partial p_i} F_i(t,p), \quad (3.14)$$

where $F_i(t,p)$ is the ith entry of $F(t,p)$ as defined in (3.10).

Lemma 7. (Theorem 1.12, in [47]) Consider the system (3.10) with a Lyapunov function $V(p,t)$ that is positive definite uniformly in t and $V(0,t) = 0$. If $\xi(t,\omega)$ satisfies the strong law of large numbers,

$$\sup_{t\geq 0} E|\xi(t,\omega)| < \frac{c_1}{bc_2}, \quad (3.15)$$

$$\frac{d^0V}{dt} \leq -c_1 V, \text{ and } \|g\| \leq c_2 V, \quad (3.16)$$

for some constants $c_1, c_2, b > 0$, then the origin is almost surely asymptotically stable.

Theorem 7. *Consider the system in* (3.10) *with $\beta_i = \beta$ $\forall i$, $A(t)$ symmetric, and $\sup_{t\geq 0} \lambda_1(BA(t) - D) < 0$. If $\xi(t,\omega)$ is a zero mean, independent, identically distributed (i.i.d.), measurable stochastic process, and for all $i = 1, ..., n$ there exists $k_i > 0$ such that $\|g_i(t,p)\| \leq k_i|p_i|^2$ for all $t \geq 0$, then the origin is almost surely asymptotically stable.*

The proof is included in Appendix A.

A similar result can be shown for the case of non-symmetric $A(t)$. Note that here the graph can still be undirected, we just do not require symmetric $A(t)$.

Theorem 8. *Consider the system in* (3.10) *with $A(t)$ continuously differentiable and $BA(t) - D$ bounded, that is, there exists an $L > 0$ such that $\|BA(t) - D\| \leq L$ $\forall t$. Further suppose $\xi(t,\omega)$ are zero mean and i.i.d., and for all $i = 1, ..., n$ there exists $k_i > 0$ such that $\|g_i(t,p)\| \leq k_i|p_i|^2$ for all $t \geq 0$. Assume that*

$\sup_{t\geq 0} s(BA(t)-D)<0$, *and* γ_1 *in Definition 3, is well-defined and finite. If* $\sup_{t\geq 0}\|B\dot{A}(t)-D\|<\frac{1}{2\gamma_1^2}$ *or* $\int_t^{t+T}\|B\dot{A}(s)-D\|ds\leq \mu T+\alpha$ *for small enough* $\mu>0$*, then the origin is almost surely asymptotically stable.*

Proof. Similar to the proof of Theorems 4 and 7, it can be shown $\frac{d^0V}{dt}\leq -c_1V$.

By our assumption $\|g_i(t,p)\|\leq k_i|p_i|^2$ and (A.18)-(A.20), we have that $\|g(t,p)\|\leq\sqrt{c}V$ for all $t\geq 0$, where $c=n(\max_i k_i^2)$. Also, since $\xi(t,\omega)$ is i.i.d., it satisfies the strong law of large numbers and (3.15) is satisfied by the zero mean assumption. Therefore, by Lemma 7, the origin is almost surely asymptotically stable. □

Consider the system

$$dp(t)=\underbrace{(BA(t)-P(t)BA(t)-D)p(t)dt}_{F(t,p)}+g(t,p)dw, \tag{3.17}$$

which represents a perturbation to the model in (3.1), where w is a d-dimensional vector of independent standard Wiener processes and $A(t)$, B, D, and $g(t,p)$ are deterministic. Again assume that $g(t,0)=0$ for all t, and $p_i(0)\geq 0$ for all $i=1,...,n$.

Similar to Lemma 1 and Lemma 6, we can state a positivity result for $p(t)$ in (3.17):

Lemma 8. *Consider the system in* (3.17) *with* $p_i(0)\geq 0$ *for all* $i=1,...,n$*. If, for all* $i=1,...,n$ *there exists* $k_i>0$ *such that* $\|g_i(t,p)\|\leq k_i|p_i|$ *for all* $t\geq 0$*, then* $p_i(t)\geq 0$ *for all* $t\geq 0$*,* $i=1,...,n$*.*

Proof. By Lemma 1 the deterministic part of (3.17), $F(t,p)$, is non-negative for all $t\geq 0$. Therefore we turn our attention to the $g_i(t,p)\xi(t,\omega)$ term, where i refers to the ith row of $g(t,p)$. By our assumption that $\|g_i(t,p)\|\leq k_i|p_i|$ we have, for any $t\geq 0$,

$$\lim_{p_i\to 0}\|g_i(t,p)dw\|\leq\lim_{p_i\to 0}\|g_i(t,p)\|\|dw\|\leq\lim_{p_i\to 0}k_i|p_i|\|dw\|=0.$$

Therefore if $p_i(0)\geq 0$ then as p_i approaches zero, the random part of the derivative vanishes. Further if $p_i(t)=0$, then $\dot{p}_i(t)\geq 0$, and consequently $p_i(t)\geq 0$ for all $t\geq 0$. □

We now call several results from [47] in order to develop a result analogous to Theorem 1 for the stochastic model in (3.17). Consider the system

$$dp=b(t,p)dt+\sum_{r=1}^{k}\sigma_r(t,p)dw_r(t), \tag{3.18}$$

where w_i's are independent standard Wiener processes and $p(t)$, $b(t,p)$, and $\sigma_r(t,p)$ are vectors in $\mathbb{R}^d$. The *generator operator* (see Chapter 5 in [47]), which generalizes the operation of differentiating a Lyapunov function V, is given by

$$\mathcal{L}=\frac{\partial}{\partial t}+\langle b,\frac{\partial}{\partial p}\rangle+\sum_r\langle\sigma_r,\frac{\partial}{\partial p}\rangle^2 \tag{3.19}$$

where $\langle\cdot,\cdot\rangle$ is the inner product and $\frac{\partial}{\partial p}=\left[\frac{\partial}{\partial p_1},\ldots,\frac{\partial}{\partial p_n}\right]^\top$.

Definition 4. (Section 5.7 in [47]) A system is *exponentially 2-stable* if for some constants a,b, and $\forall t\geq 0$,

$$E\|p(t)\|^2\leq a\|p(0)\|^2e^{bt}.$$

Theorem 9. (Theorem 5.11,15, Section 5.7 in [47]) Given a system as in Equation (3.18), if there exists a, twice continuously differentiable with respect to p and continuously differentiable with respect to t, Lyapunov function $V(t,p)$ such that

$$k_1\|p\|^2 \leq V(t,p) \leq k_2\|p\|^2, \tag{3.20}$$

$$\mathcal{L}V(t,p) \leq -k_3\|p\|^2, \tag{3.21}$$

for some positive constants k_1, k_2, k_3, then the origin is exponentially 2-stable. Furthermore, the origin is almost surely exponentially stable.

Theorem 10. *Consider the system in* (3.17) *with $g(t,p)$ bounded and locally Lipschitz in $p(t)$ uniformly in t, w are independent standard Wiener processes, and for all $i = 1, ..., n$ there exists $k_i > 0$ such that $\|g_i(t,p)\| \leq k_i|p_i|$ for all $t \geq 0$. If $\beta_i = \beta\ \forall i$, $A(t)$ is symmetric, piece-wise continuous in t, and bounded, and $\sup_{t\geq 0} \lambda_1(BA(t) - D) < -c$, with $c := \sum_{i=1}^n k_i^2 + \epsilon$, $\epsilon > 0$, then the origin is exponentially 2-stable and almost surely exponentially stable.*

Proof. Consider the Lyapunov function candidate $V(p) = \frac{1}{2}p^\top p$. Clearly Equation (3.20) is satisfied. Since $\frac{\partial V}{\partial p} = \nabla V = p$ and $\nabla^2 V = I$, we have

$$\begin{aligned}
\mathcal{L}V(p) &= \langle b(t,p), \frac{\partial V}{\partial p}\rangle + \langle g(t,p), \frac{\partial V}{\partial p}\rangle^2 \\
&= p^\top b(t,p) + \frac{1}{2}\sum_{i,j}(g(t,p)g^\top(t,p))_{ij}\frac{\partial V}{\partial p_i \partial p_j} \\
&= p^\top(BA(t) - PBA(t) - D)p + \frac{1}{2}\sum_{i=1}^n g_i(t,p)g_i^\top(t,p) \\
&\leq p^\top(BA(t) - D)p + \frac{1}{2}\sum_{i=1}^n (k_i|p_i|)^2 \qquad (3.22) \\
&\leq \left(\sup_{t\geq 0}\lambda_1(BA(t) - D) + \frac{1}{2}\sum_{i=1}^n k_i^2\right)\|p\|^2 \qquad (3.23) \\
&< \left(-c + \frac{1}{2}\sum_{i=1}^n k_i^2\right)\|p\|^2 \\
&= -\epsilon\|p\|^2, \qquad (3.24)
\end{aligned}$$

where (3.22) holds because $PBA(t) \geq 0$, by construction and Lemma 8 and $\|g_i(t,p)\| \leq k_i|p_i|$, for all i, by assumption; (3.23) holds by the symmetry of $BA(t)$; and (3.24) holds by definition of c. Thus (3.21) is satisfied and therefore by Theorem 9, the origin is exponentially 2-stable and almost surely exponentially stable. □

Remark 8. *Note that the results in Theorems 4 and 5 could similarly be extended to the models in* (3.10) *and* (3.17).

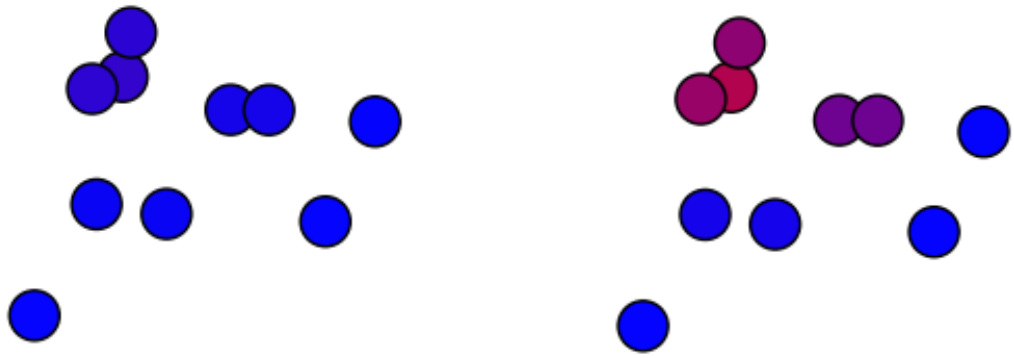

Figure 3.1: This system has constant drift as given by (3.26) for each node with $r = 1$. The 2^n model is on the left and the n-intertwined model is on the right. Blue indicates the agent is healthy and red indicates the agent is infected. This figure gives a snapshot of the system at time 40. For a video of this simulation please see youtu.be/-LmPj7oynLs.

3.4 Time–Varying Simulations and Extensions

A variety of time–varying simulations are presented, leading to a series of corollaries and observations. Since the infection rate $p(t)$ and the location of the states, $z(t)$, are both time dependent, the simulations are best viewed in video format with links provided in the captions of the figures.

3.4.1 Dynamic Graphs

In this section we use several examples to highlight the effectiveness and ineffectiveness of the n-intertwined model in (3.1) as a mean field approximation of (3.2) for dynamic graph structures. For these simulations, the weighting matrix $A(t)$ is dependent on the agents' relative positions, that is, using the definition from [48], for some radius r and $i \neq j$,

$$a_{ij}(t) = \begin{cases} e^{-\|z_i(t)-z_j(t)\|^2}, & \text{if } \|z_i(t) - z_j(t)\| < r \\ 0, & \text{otherwise,} \end{cases} \tag{3.25}$$

where $z_i(t) \in \mathbb{R}^d$ is the position of agent i in d-space. Note that under the construction in (3.25), $A(t)$ is symmetric.

First consider the case of constant drift for the positional dynamics of the agents, that is,

$$\dot{z}(t) = \phi, \tag{3.26}$$

where ϕ is some constant vector. As we see in Figure 3.1, the upper bounding nature of the n-intertwined Markov chain model leads to a decent approximation; at time step 40, the 2^n model has reached the DFE, whereas the n-intertwined Markov chain model has not. However, the n-intertwined model reaches the DFE shortly thereafter (see the link referenced in the caption of Figure 3.1).

For another comparison we will use a piece-wise constant drift so that the agents remain confined to a fixed region. Without loss of generality, let the constrained region be a hypercube l^d, where d is the dimension of

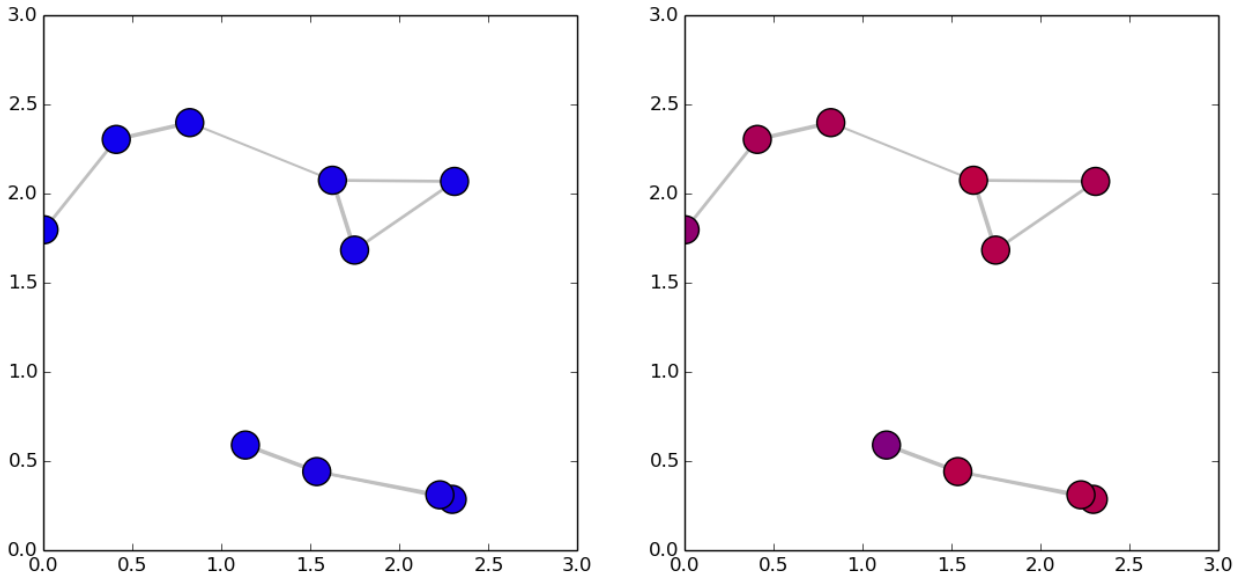

Figure 3.2: This system has piece-wise constant drift as given by (3.27) for each node with $r = 1.5$. The 2^n model is on the left and the n-intertwined model is on the right. Blue indicates the agent is healthy and red indicates the agent is infected. This figure gives a snapshot of the system at time 40. For a video of this simulation please see youtu.be/BMn4FGnBZX0.

the space, centered at some point z_c. That is, the dynamics follow (3.26) but instead of a constant ϕ term for each agent, we have

$$\phi_k = \begin{cases} -\phi_k, & \text{if } z_k = z_{c_k} + l/2 \text{ or } z_k = z_{c_k} - l/2 \\ \phi_k, & \text{otherwise,} \end{cases} \tag{3.27}$$

for each dimension $k = 1, \ldots, d$. That is, if an agent hits a boundary, the velocity of the agent in the dimension corresponding to that boundary flips sign. As illustrated in Figure 3.2, the upper bounding nature of the n-intertwined Markov chain model leads to an inaccurate approximation, as the 2^n model reaches the DFE but the n-intertwined model does not and does not appear to be tending towards the DFE.

3.4.2 Exploratory Time–Varying Networks and Extensions

If the agents have constant (non-equal) drift, as defined in (3.26), they will eventually float away from each other far enough that, assuming they have non-zero healing rate, the disease will be eradicated. This is illustrated in the simulations depicted in Figure 3.1.

This behavior is captured in the following corollary:

Corollary 1. *If $B = \beta I$ and $A(t)$ is symmetric, piece-wise continuous in t, and bounded $\forall t \geq T$, and for some fixed T, $\sup_{t \geq T} \lambda_1(BA(t) - D) < 0$, then $\forall t \geq T$ the DFE is globally exponentially stable.*

Proof. Let $\hat{t} = t - T$. The result follows immediately from applying Theorem 3 to $\dot{p}(\hat{t})$ for $\hat{t} \geq 0$. □

Consider the n-intertwined model with piece-wise constant drift illustrated in Figure 3.3. At several time instances the disease appears to be approaching the DFE, but when the graph structure changes, due to agents coming into close proximity of each other, the system is pushed away from the DFE.

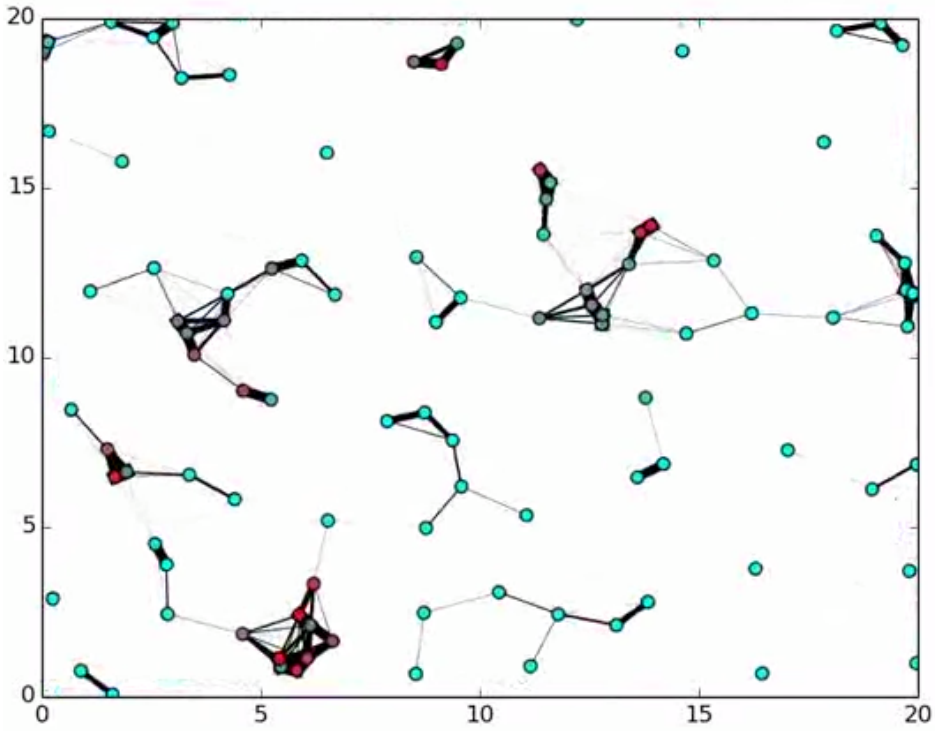

Figure 3.3: This system has 100 agents with random initial conditions and piece-wise constant drift as explained in (3.27) for each node with $r = 3$. Teal indicates the agent is healthy and red indicates the agent is infected. This figure gives a snapshot of the system. For a video of this simulation please see youtu.be/Q05TPES5VNU.

Chapter 4

Multiple Viruses

In this chapter we explore the case of competing viruses. The majority of this work has been published, submitted, or is being prepared for submission in [23, 33, 22, 49, 50, 51] and is used here with permission.

4.1 Background

The idea of competing SIS virus models is pursued in [52, 53, 54, 55, 56, 57]. This work is motivated by the competition of different viral strains [52]. These models have a wide range of applications, including, as one example, social networks, where the goal is to understand how competing opinions spread on different social networks [54]. Competing SIS models were first introduced in [52], which is an extension of [2] in (1.1), where the model considers the dynamics of three groups: 1) susceptible, 2) infected with virus one, and 3) infected with virus two, illustrated in Figure 4.1. These dynamics are modeled by three differential equations where full connectivity of the agents is assumed (i.e., the infection graph is a complete graph), and it is also assumed that the two viruses are both homogeneous. In [53], a model of two competing homogeneous viruses spreading over the same nontrivial (not necessarily fully connected), undirected, connected network is studied. The set of equilibrium points is determined and sufficient conditions for local stability are given for all equilibria except the coexisting equilibrium. In [54], the equilibria of two competing homogeneous virus models over the same as well as different undirected graph structures are studied. Existence of the coexisting epidemic states, where both viruses are at nontrivial (nonzero) equilibria, is shown, but no stability analysis is provided. Note that all this previous work is conducted for homogeneous viruses over undirected graph structures with limited/local stability analysis. The following are the two exceptions: in [55], a sufficient condition for the global asymptotic survival of a single virus is given for a model of two competing viruses, both homogeneous in the healing rate and propagating over undirected, regular graphs. In [57], a necessary and sufficient condition for local exponential stability of the origin is provided for two competing heterogeneous viruses over strongly connected graphs. In addition, a geometric program is formulated, working toward optimal stabilization and rate control of the virus. However, stability of the epidemic equilibria is not explored. Note that none of the existing studies consider heterogeneous viruses over directed graph structures or perform global stability analysis, exploring all of the system's equilibria.

Competing viruses are also explored for an SIR model in [58].

The main motivations for studying the bi-virus model are those of competing viral strains [52] and competing ideas spreading on different social networks [54]. However, these models can have broader applications to political stances, adaptation of competing products, competing practices in farming, etc., and can be generalized to more than two viruses. Consider, for example, the case of three competing viruses; then each node has four possible conditions: susceptible, infected with virus 1, 2, or 3. This is depicted in Figure 4.2.

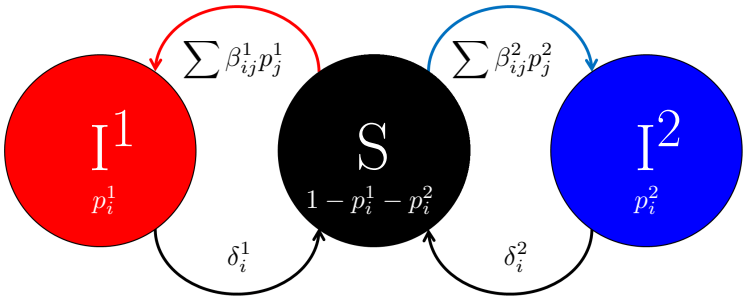

Figure 4.1: There are three states for each group i, with a portion of the group in each state: a percentage of the group, $1 - p_i^1(t) - p_i^2(t)$, is susceptible (S); a percentage of the group, $p_i^1(t)$, is infected with virus 1 (I^1); and a percentage of the group, $p_i^2(t)$, is infected with virus 2 (I^2). The healing and infection rates are indicated by δ_i^k and $\sum \beta_{ij}^k p_j^k$, respectively, for $k \in [2]$.

Restricting to only two competing viruses limits the applicability of the model.

To the best of our knowledge, the only work that has considered more than two competing SIS viruses is presented in [59], where Xu *et al.* propose a multi-virus model to capture the behavior of the spread of computer viruses. The model is different than the one considered herein, in that it allows viruses to "rob" each other and requires the viruses to spread on the same static graph. In addition, the analysis presented in [59] considers only the healthy state.

Some work has been done to model mutating viruses [60, 61, 62]. In [60], Kutch and Gurfil introduce differential equations describing infection by viruses immune to different HIV drugs. In [61], Singh models the mutation using the addition of another virus. In [62], Gubar and Zhu use evolutionary dynamics to model the virus mutations. To the best of our knowledge no work has been done on studying mutating viruses over nontrivial networks. In this work we model the mutating viruses by allowing the infection and healing rates to change over time, which we believe is novel.

All of the previous work on competing viruses has focused on non-mutating viruses over static graph structures. There are recent results for the single-virus model over time–varying networks [7, 19, 34, 35, 36]. Some of the ideas from Chapter 3 will be employed in this chapter.

There is a body of literature that extends virus spread models to include human awareness [63, 64, 65, 66, 67, 68, 69, 70]. In [64], the single virus SIS model is modified to reflect the scenario that individuals may become alert, if not yet infected, when their neighbors are infected. Based on this modified model, the effects of information dissemination were considered in [65, 66] and an optimal dissemination strategy was studied to promote preventive behaviors in the network. The only work that includes human awareness with competing viruses is our work in [70], where only the bi-virus case is considered. In this chapter, we include the extension of these results where we capture the effect of human awareness on a multi-virus model.

There has also been some work in the literature that allows viruses to be coupled and not purely competitive, i.e., that a node can be infected with more than one virus. This behavior is more realistic in many applications, e.g. sicknesses, computer viruses, and fake news spread. In [71], Beutel *et al.* proposed a bi-virus model that allows people to be infected with both viruses simultaneously; however, their model had a trivial graph structure, assuming full connectivity and modeling the system as three groups: 1) infected with virus one, 2) infected with virus two, and 3) infected with both viruses. Beutel *et al.* characterize the set of equilibria but do not provide any conditions for convergence to these equilibria. In [59], Xu *et al.* study a model with a similar transition graph that is dependent on a non-trivial graph structure; however,

it is a probabilistic model, and not an ODE model as the one we study here.

4.2 Competing Virus Model

The single-virus model in (2.8) has been extended to have two viruses, providing a generalization of the model introduced in [54],

$$\begin{aligned}\dot{p}_i^1(t) &= (1 - p_i^1(t) - p_i^2(t)) \sum_{j=1}^{n} \beta_{ij}^1 p_j^1(t) - \delta_i^1 p_i^1(t), \\ \dot{p}_i^2(t) &= (1 - p_i^1(t) - p_i^2(t)) \sum_{j=1}^{n} \beta_{ij}^2 p_j^2(t) - \delta_i^2 p_i^2(t),\end{aligned} \tag{4.1}$$

where $p_i^1(t)$ and $p_i^2(t)$ are the probabilities that agent i has virus 1 and 2 respectively, and each virus has its own infection rates and healing rates. Each virus spreads over a (possibly different) spanning subgraph of $\mathbb{G}$, where their union is the neighbor graph $\mathbb{G}$. It will be assumed that both of the two subgraphs are strongly connected and, thus, so is $\mathbb{G}$.[1]

We need not restrict ourselves to two viruses, however. A direct generalization leads to the following multi-virus model:

$$\dot{p}_i^k(t) = (1 - p_i^1(t) - \cdots - p_i^m(t)) \sum_{j=1}^{n} \beta_{ij}^k p_j^k(t) - \delta_i^k p_i^k(t), \tag{4.2}$$

for all $k \in [m]$ (note that the superscript k here refers to the virus that is spreading, not the time index as in the case in the discrete time model in Section 2.2). This representation can be written in matrix form as:

$$\dot{p}^k(t) = ((I - P^1(t) - \cdots - P^m(t))B^k - D)p^k(t), \tag{4.3}$$

where the matrices are the same as in (2.9), but now they are dependent on to which virus they correspond. Since the subgraph for each virus k is strongly connected, it follows that B^k is irreducible, meaning that it cannot be permuted into block triangular matrix form. The assumption that B^k is bounded means $\forall i, j,\ \beta_{ij}^k < \infty$.

The set

$$\mathcal{D} = \{(p^1, \ldots, p^m) \mid p^k \geq \mathbf{0},\ k \in [m],\ \sum_{k=1}^{m} p^k \leq \mathbf{1}\} \tag{4.4}$$

is invariant with respect to the system defined by (4.3). If p_i^k denotes the probability of agent i being infected by virus k and $1 - \sum_{k=1}^{m} p_i^k$ denotes the probability of agent i being healthy, it is natural to assume that their initial values are in $[0, 1]$, since otherwise the values will lack any physical meaning for the epidemic model considered herein. Similarly, if the states were representative of the density of infected members of a sub-population, they would also be bounded between zero and one.

Lemma 9. *Suppose that for all $i \in [n], k \in [m]$, we have $\delta_i^k \geq 0$, and the matrices B^k are non-negative. If for all $i \in [n], k \in [m]$, we have $p_i^k(0), (1 - p_i^1(0) - \cdots - p_i^m(0)) \in [0, 1]$, then $p_i^k(t), p_i^1(t) + \cdots + p_i^m(t) \in [0, 1]$ for all $i \in [n], k \in [m]$ and $t \geq 0$.*

[1] A directed graph is *strongly connected* if for any two distinct vertices i and j, there is a directed path from i to j.

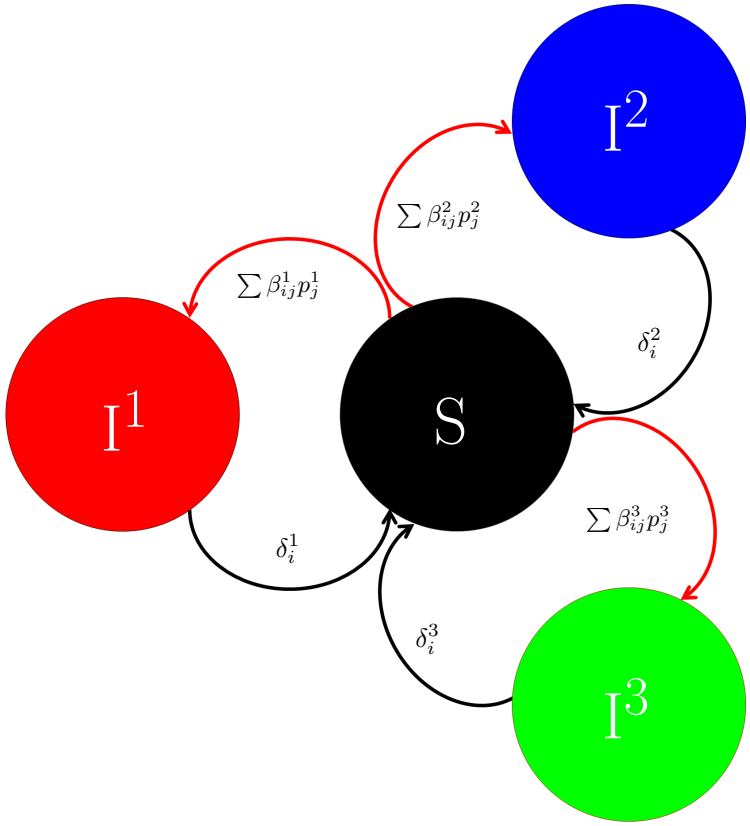

Figure 4.2: The ith node can be either in a susceptible or infected condition (the summations are over j).

Proof. Suppose that at some time τ, $p_i^1(\tau) + \cdots + p_i^m(\tau) \in [0,1]$ and $p_i^k(\tau) \in [0,1]$ for all $i \in [n], k \in [m]$. Consider an index $i \in [n]$. If $p_i^k(\tau) = 0$, then from (4.2) and the assumption that the matrices B^k are non-negative, $\dot{p}_i^k(\tau) \geq 0$. The same holds for $p_i^1(\tau) + \cdots + p_i^m(\tau)$. If $p_i^k(\tau) = 1$, then from (4.2) and the assumption that the matrices B^k are non-negative, $\dot{p}_i^1(\tau) \leq 0$. The same holds for $p_i^1(\tau) + \cdots + p_i^m(\tau)$. It follows that $p_i^k(t), p_i^1(t) + \cdots + p_i^m(t) \in [0,1]$ for all $i \in [n], k \in [m]$ and $t \geq \tau$.

Since, by assumption, $p_i^k(0), (1 - p_i^1(0) - \cdots - p_i^m(0)) \in [0,1]$ for all $i \in [n], k \in [m]$, it follows that $p_i^k(t), p_i^1(t) + \cdots + p_i^m(t) \in [0,1]$ for all $i \in [n], k \in [m]$ and $t \geq 0$. □

For the rest of the chapter we assume $p_i^k(0), (1 - \sum_j^m p_i^j(0)) \in [0,1]$ for all $i \in [n], k \in [m]$.

4.3 Analysis

In this section we provide the details of the analysis for the competing virus model.

4.3.1 Stability Analysis of the Healthy State

First, we explore stability of the healthy state for both the static and dynamic graph cases. We begin by analyzing competing viruses spreading over static graph structures.

We first give conditions under which the healthy state is asymptotically stable.

Lemma 10. *Suppose that for all $i \in [n], k \in [m]$, we have $\delta_i^k \geq 0$ and the matrices B^k are non-negative and irreducible. If $s(B^k - D^k) \leq 0$ for all $k \in [m]$, then the healthy state is the unique equilibrium of (4.3), which is asymptotically stable with domain of attraction $\mathcal{D}$, as defined in (4.4).*

Proof. To prove the lemma, it is sufficient to show that for all $k \in [m]$, $p^k(t)$ will asymptotically converge to $\mathbf{0}$ as $t \to \infty$ for any initial condition.

Since for all $k \in [m]$, $p_i^k(t)$ is always non-negative by Lemma 9, from (4.2),

$$\dot{p}_i^1(t) \leq -\delta_i^1 p_i^k(t) + (1 - p_i^k(t)) \sum_{j=1}^{n} \beta_{ij}^k p_j^1(t),$$

which implies that the trajectories of $p_i^k(t)$ are bounded above by a single-virus model. Since the B^k's are non-negative and irreducible, by Proposition 1 (Proposition 3 in [23]), $p_i^k(t)$ will asymptotically converge to $\mathbf{0}$ as $t \to \infty$ for all $k \in [m]$, and thus the healthy state is the unique equilibrium of (4.3). □

We can show that the condition in Lemma 10 is necessary and sufficient for eradication of all viruses.

Theorem 11. *Suppose that $\delta_i^k \geq 0$ for all i, k, and the matrices B^k are non-negative and irreducible for all k. The healthy state (all k viruses eradicated) is the unique equilibrium of (4.3) if, and only if, $s(B^k - D^k) \leq 0$ for all $k \in [m]$.*

Proof. Sufficiency has been shown in Lemma 10. Therefore, to prove the theorem, all that needs to be shown is that if for any $j \in [m]$ $s(B^j - D^j) > 0$, the system (4.3) admits an epidemic state.

Without loss of generality, suppose that $s(B^1 - D^1) > 0$. Set $p^k = \mathbf{0}$ for all $k = 2, \ldots, m$. Then, the dynamics of p^1 simplifies to a single-virus system, which admits an epidemic state by Proposition 1

(Proposition 4 in [23]). Therefore, in the case when $s(B^1 - D^1) > 0$, the system (4.3) always admits an equilibrium of the form $(\tilde{p}^1, \mathbf{0}, \ldots, \mathbf{0})$ with $\tilde{p}^1 \gg \mathbf{0}$. □

We next state a result on global exponential stability for the case when the underlying subgraphs are undirected and the infection rates are symmetric.

Theorem 12. *Suppose that B^k is symmetric, and the maximum eigenvalue of $B^k - D^k$ is less than zero, that is $\lambda_1(B^k - D^k) < 0$. Then, the healthy state is exponentially stable for virus k, with domain of attraction $\mathcal{D}$, in (4.4).*

Proof. Consider the Lyapunov function $V(p^k) = \frac{1}{2}(p^k)^\top p^k$. For $p^k \neq 0$,

$$\begin{aligned}
\dot{V}(p^k) &= (p^k)^\top \dot{p}^k \\
&= (p^k)^\top \left(B^k - \sum_{l=1}^{m} P^l B^k - D^k \right) p^k \\
&\leq (p^k)^\top (B^k - D^k) p^k \\
&\leq \lambda_1(B^k - D^k) \|p^k\|^2 < 0.
\end{aligned}$$

The first inequality holds because $(P^l B^k)_{ij} \geq 0,\ \forall l, i, j$ by construction since each $p_i^l(t)$ is a probability. The second inequality holds by the Rayleigh-Ritz Quotient [32] because $B^k - D^k$ is symmetric. Therefore, the system converges exponentially fast to the origin by Theorem 8.5 in [43]. □

We now generalize the model from (4.2) to have dynamic graph structure and allow the viruses to mutate over time as

$$\dot{p}_i^k(t) = (1 - p_i^1(t) - \cdots - p_i^m(t)) \sum_{j=1}^{n} \beta_{ij}^k(t) p_j^k(t) - \delta_i^k(t) p_i^k(t), \tag{4.5}$$

where $\beta_{ij}^k(t)$ and $\delta_i^k(t)$ are functions of time and the equation holds for $k = 1, \ldots, m$. We now provide a sufficient condition for global exponential stability of the healthy state that is a corollary of Theorem 3.

Corollary 2. *Suppose that $B^k(t)$ is symmetric, $B^k(t) - D^k(t)$ is piece-wise continuous in t and bounded, and $\sup_{t \geq 0} \lambda_1(B^k(t) - D^k(t)) < 0$. Then, the healthy state is exponentially stable for virus k, with domain of attraction $\mathcal{D}$, in (4.4).*

Proof. Consider the Lyapunov function $V(p^k) = \frac{1}{2}(p^k)^T p^k$. For $p^k \neq 0$,

$$\begin{aligned}
\dot{V}(p^k) &= (p^k)^T \dot{p}^k \\
&= (p^k)^T \left(B^k(t) - \sum_{l=1}^{m} P^l B^k(t) - D^k(t) \right) p^k \\
&\leq (p^k)^T (B^k(t) - D^k(t)) p^k \\
&\leq \lambda_1(B^k(t) - D^k(t)) \|p^k\|^2 \\
&\leq (\sup_{t \geq 0} \lambda_1(B^k(t) - D^k(t))) \|p^k\|^2 < 0.
\end{aligned}$$

The first inequality holds because $(P^l B^k(t))_{ij} \geq 0,\ \forall l, i, j, t$ by construction since each $p_i^l(t)$ is a probability. The second inequality holds by the Rayleigh-Ritz Theorem because $B^k(t) - D^k(t)$ is symmetric. The last

inequality holds by definition of the supremum. Therefore, the system converges exponentially fast to the origin by Theorem 8.5 in [43]. □

We can also show exponential stability for the case when the infection rates are not symmetric and the underlying subgraphs are undirected, with some added assumptions, as a corollary of Theorem 4. Similar to Definition 3 we need the following.

Definition 5. *For a given virus k, assume that for all $t \geq 0$, there exist $c^k(t), \lambda^k(t) > 0$ such that*

$$\|B^k(t) - D^k(t)\| \leq c^k(t)e^{-\lambda^k(t)t} \quad \forall t \geq 0. \tag{4.6}$$

We then define

$$\gamma_1^k := \sup_{t\geq 0} \int_0^\infty c^k(t)^2 e^{-2\lambda^k(t)\tau} d\tau. \tag{4.7}$$

Note that

$$\gamma_1^k \geq \left\| \int_0^\infty e^{(B^k(t)-D^k(t))^T\tau} e^{(B^k(t)-D^k(t))\tau} d\tau \right\|, \tag{4.8}$$

which follows from the definition of γ_1^k and the upper bound assumption in (4.6).

Corollary 3. *Consider the dynamics for virus k in (4.5) with $B^k(t) - D^k(t)$ continuously differentiable and bounded, that is, there exists an $L > 0$ such that $\|B^k(t) - D^k(t)\| \leq L \ \forall t$. Assume that $\sup_{t\geq 0} s(B^k(t) - D^k(t)) < 0$ and γ_1^k in Definition 5 is finite. If $\sup_{t>0} \|\dot{B}^k(t) - \dot{D}^k(t)\| < \frac{1}{2(\gamma_1^k)^2}$ or $\int_t^{t+T} \|\dot{B}^k(s) - \dot{D}^k(s)\| ds \leq \mu T + \alpha$ for small enough $\mu > 0$, then the healthy state is exponentially stable for virus k, with domain of attraction $\mathcal{D}$, as given in (4.4).*

Proof. Note that since $(P^l(t)B^k(t))_{ij} \geq 0 \ \forall l, i, j$, by construction,

$$\begin{aligned} \dot{p}^k &= (B^k(t) - \sum_{l=1}^m P^l B^k(t) - D^k(t))p^k \\ &\leq (B^k(t) - D^k(t))p^k. \end{aligned}$$

Therefore, by Grönwall's Inequality (pg 651, [43]), the solution of the original system will be bounded above by the solution of the linear system. Thus, by Lemma 2 in [72] (a subset of the proof of Theorem 4 in Appendix A), the healthy state is exponentially stable for virus k. □

Note that this theorem is a generalization of a single-virus result provided in Theorem 4 ([19, 72]), which is for a less general model; however the arguments for Lemma 5 hold by replacing $BA(t)$ with $B^k(t)$, D with $D^k(t)$, and $B\dot{A}(t) - D$ with $\dot{B}^k(t) - \dot{D}^k(t)$.

Now we consider a case where the linearized system is not required always to be Hurwitz, a corollary of Theorem 5.

Corollary 4. *Consider the dynamics for single virus k:*

$$\dot{p}^k = (B^k(t) + \Delta^k(t) - \sum_{l=1}^m P^l(B^k(t) + \Delta^k(t)) - D^k(t))p^k.$$

Assume that

$$\lim_{T\to\infty} \frac{1}{T} \int_{t_0}^{t_0+T} \|B^k(s) - D^k(s)\| ds \leq a < \infty, \tag{4.9}$$

for all $t_0 \geq 0$, and for some $\nu > 0$, there exists an $h > 0$ such that

$$\|B^k(t+h) - D^k(t+h) - (B^k(t) - D^k(t))\| \leq \nu h^\gamma, \tag{4.10}$$

for all $t \geq 0$ and some γ, $0 < \gamma \leq 1$. Assume further that

$$\lim_{T\to\infty} \frac{1}{T} \int_{t_0}^{t_0+T} s(B^k(s) - D^k(s))ds \leq \bar{\alpha}, \tag{4.11}$$

for some negative scalar $\bar{\alpha}$ and for all $t_0 \geq 0$,

$$\lim_{T\to\infty} \frac{1}{T} \int_{t_0}^{t_0+T} \|\Delta^k(s)\|ds \leq \eta < \infty, \tag{4.12}$$

for all $t_0 \geq 0$, and for all i, j and $t \geq 0$, the perturbation satisfies the inequality

$$|\Delta_{ij}^k(t)| \leq \beta_{ij}^k(t). \tag{4.13}$$

Then, the origin is exponentially stable for virus k.

Proof. Since $(P^l(t)(B^k(t) + \Delta^k(t)))_{ij} \geq 0 \ \forall i, j$ by (4.13) and Lemma 9,

$$\begin{aligned}\dot{p}^k &= (B^k(t) + \Delta^k(t) - \sum_{l=1}^{m} P^l(B^k(t) + \Delta^k(t)) - D^k(t))p^k \\ &\leq (B^k(t) + \Delta^k(t)) - D^k(t))p^k.\end{aligned}$$

Therefore, by Grönwall's Inequality ([43]), the solution of the original system will be bounded above by the solution of the linear system. Thus, by Lemma 5, the origin is exponentially stable for virus k. □

This result says that if the linearized system is bounded on the average, slowly time–varying, Hurwitz on the average (but not necessarily strictly Hurwitz for all $t \geq 0$), and the perturbations are bounded but not too large (so that the model remains in the sensible domain), then the system converges to the healthy state. Note that the arguments for Lemma 5 hold by replacing $BA(t)$ with $B^k(t)$, D with $D^k(t)$, and $B\dot{A}(t) - D$ with $\dot{B}^k(t) - \dot{D}^k(t)$.

4.4 Stability Analysis of the Epidemic States

There are a number of different epidemic equilibria. The simplest scenario is when one virus is in an epidemic state and the remaining viruses are eradicated.

Theorem 13. *Suppose that $\delta_i^k \geq 0$ for all i, k, and the matrices B^k are non-negative and irreducible for all k. If for some $i \in [m]$, $s(B^i - D^i) > 0$ and $s(B^k - D^k) \leq 0$ for all $k \neq i$, then (4.3) has two equilibria, the healthy state $(\mathbf{0}, \ldots, \mathbf{0})$, where the system converges to this equilibrium for all initial conditions in $\{(p^1, \ldots, p^m) | p^i = \mathbf{0}$ and $p^k \in [0,1]^n \ \forall k \neq i\}$, and a unique epidemic state of the form $(\mathbf{0}, \ldots, \mathbf{0}, \tilde{p}^i, \mathbf{0}, \ldots, \mathbf{0})$ with $\tilde{p}^i \gg \mathbf{0}$, which is asymptotically stable with domain of attraction $\mathcal{D} \setminus \{(p^1, \ldots, p^m) | p^i = \mathbf{0}$ and $p^k \in [0,1]^n \ \forall k \neq i\}$, with $\mathcal{D}$ defined in (4.4).*

Note that the healthy state can be shown to be an unstable equilibrium by evaluating the Jacobian linearization at the origin. A small perturbation of virus i from the origin will drive the system to the unique epidemic state.

Proof of Theorem 13: From the proof of Lemma 10, $p^k(t)$ will asymptotically converge to $\mathbf{0}$ as $t \to \infty$ for all initial values $(p^1(0), \dots p^m(0)) \in \{(p^1, \dots, p^m) | p^i = \mathbf{0} \text{ and } p^k \in [0,1]^n \ \forall k \neq i\}$, for $k \neq i$. From (4.3),

$$\dot{p}^i(t) = (B^i - D^i - P^i(t)B^i)p^i(t) - \sum_{k \neq i} P^k(t)B^k p^k(t).$$

Thus, we can regard the dynamics of $p^i(t)$ as an autonomous system

$$\dot{p}^i(t) = (B^i - D^i - P^i(t)B^i)p^i(t), \tag{4.14}$$

with a vanishing perturbation $-\sum_{k \neq i} P^k(t)B^i p^i(t)$, which converges to $\mathbf{0}$ as $t \to \infty$. From Proposition 1, the autonomous system (4.14) will asymptotically converge to a unique epidemic state $(\mathbf{0}, \dots, \mathbf{0}, \tilde{p}^i, \mathbf{0}, \dots, \mathbf{0})$ for any $(p^1(0), \dots, p^m(0)) \in \mathcal{D} \setminus \{(p^1, \dots, p^m) | p^i = \mathbf{0} \text{ and } p^k \in [0,1]^n \ \forall k \neq i\}$, with $\mathcal{D}$ defined in (4.4).

Let $y(t) = p^i(t) - \tilde{p}^i$. Then,

$$\dot{y}(t) = f(y(t)) + g(t, y(t)),$$

where

$$\begin{aligned} f(y(t)) &= (-D^i + (I - \tilde{P}^i)B^i - \operatorname{diag}(B^i p^i(t)))y(t) \\ g(t, y(t)) &= -\sum_{k \neq i} P^k(t)B^i(y(t) + \tilde{p}^i). \end{aligned}$$

Consider the Lyapunov function candidate

$$V(y(t)) = \max_{l \in [n]} \frac{|y_l(t)|}{\tilde{p}^i_l}.$$

Then,

$$\dot{V}(y(t)) = \frac{\partial V}{\partial y} f(y(t)) + \frac{\partial V}{\partial y} g(t, y(t)).$$

From the proof of Proposition 1, $\frac{\partial V}{\partial t} + \frac{\partial V}{\partial y} f(t, y) < 0$ unless $y(t) = \mathbf{0}$, i.e., $p^i(t) = \tilde{p}^i$. Since, $\forall k \neq i$, $p^k(t)$ asymptotically converges to $\mathbf{0}$, so does $\frac{\partial V}{\partial y} g(t, y(t))$. This implies that after a sufficiently long time, $\dot{V}(y(t)) < 0$ if $p^i(t)$ does not equal $\tilde{p}^i$. Since $(p^1(t), \dots, p^m(t))$ will asymptotically converge to the unique epidemic state $(\mathbf{0}, \dots, \mathbf{0}, \tilde{p}^i, \mathbf{0}, \dots, \mathbf{0})$ for any $(p^1(0), \dots, p^m(0)) \in \mathcal{D} \setminus \{(p^1, \dots, p^m) | p^i = \mathbf{0} \text{ and } p^k \in [0,1]^n \ \forall k \neq i\}$, with $\mathcal{D}$ defined in (4.4). □

Another possible epidemic state is that of coexisting equilibria, that is, where more than one virus survives.

Theorem 14. *Consider the model in (4.2) with each virus propagating over the same strongly connected graph $\mathbb{G}$ with the corresponding adjacency matrix A, and each virus homogeneous in healing and infection rates, that is, for each $k \in [m]$ $\delta^k_i = \delta^k > 0 \ \forall i \in [n]$ and $\beta^k_i = \beta^k > 0 \ \forall i \in [n]$. Suppose that $s(A) > \frac{\delta^1}{\beta^1} = \dots = \frac{\delta^m}{\beta^m}$. If $(\tilde{p}^1, \dots, \tilde{p}^m)$ with $\tilde{p}^k > \mathbf{0} \ \forall k \in [m]$ is an equilibrium of (4.2), then $\tilde{p}^k \gg \mathbf{0} \ \forall k \in [m]$ and $\tilde{p}^i = \alpha^{ik} \tilde{p}^k \ \forall i, k \in [m]$, for some constant $\alpha^{ik} > 0$.*

The proof is included in Appendix A.

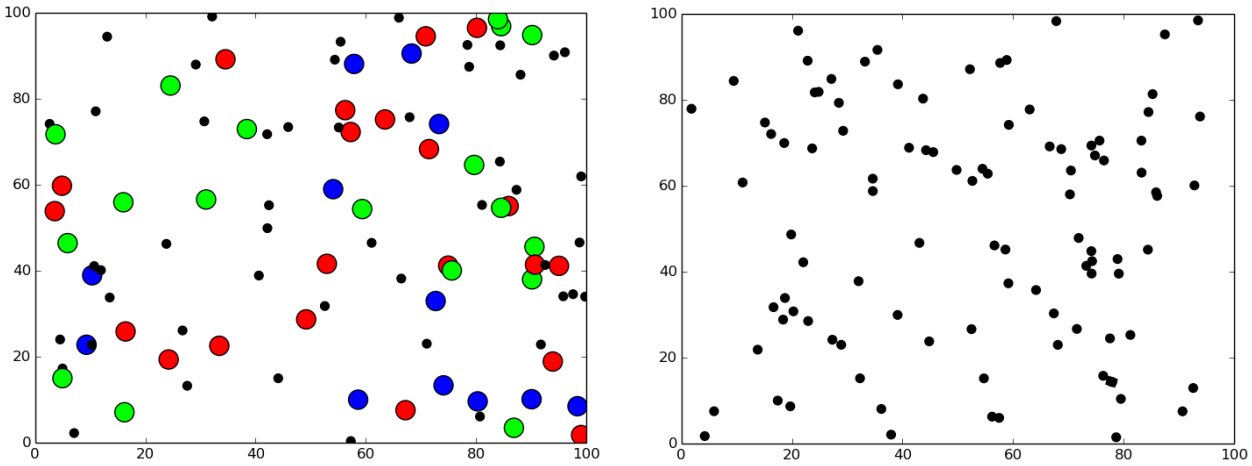

(a) The system at time zero.

(b) The system at time 1000.

Figure 4.3: Viruses 1 and 2 of this three-virus system meets the assumptions of Corollary 2 so they converge quickly to the healthy state, as does the third one as well. The colors and diameters follow (4.15) and (4.16) and the graph structure follows (3.25)-(3.27). A video of this simulation can be found at youtu.be/j_MHm08dA_o.

We follow by exploring another possible coexisting equilibrium when the viruses are heterogeneous in infection and healing rates, but for each node every virus has the same infection rate and healing rate.

Theorem 15. *Suppose that* $\delta_i^1 = \cdots = \delta_i^m > 0$, $\forall i \in [n]$ *(which implies that* $D^1 = \cdots = D^m = D$*),* $\beta_{ij}^1 = \cdots = \beta_{ij}^m \ \forall \beta_{ij}^k \neq 0$, $k \in [m]$ *(which implies that* $B^1 = \cdots = B^m = B$*), the matrix* B *is non-negative and irreducible, and* $s(-D+B) > 0$*. If* $(\tilde{p}^1, \ldots, \tilde{p}^m)$ *with* $\tilde{p}^k > \mathbf{0}$ $\forall k \in [m]$ *is an equilibrium of (4.2), then* $\tilde{p}^k \gg \mathbf{0}$ $\forall k \in [m]$, $\tilde{p}^1 + \cdots + \tilde{p}^m$ *is unique, and* $\tilde{p}^i = \alpha^{ik}\tilde{p}^k$ $\forall i, k \in [m]$*, for some constant* $\alpha^{ik} > 0$.

The proof is included in Appendix A.

4.5 Multi-Virus Simulations

In this section, we present a set of illuminating simulations of various competing virus models over static and time–varying graph structure networks. Due to the difficulty in adequately displaying multiple viruses over networks of high dimensions, for the simulations we employ only three competing viruses, $m = 3$. Virus 1 is depicted by the color red (r), virus 2 is depicted by the color blue (b), and virus 3 is depicted by the color green (g). For all $i \in [n]$, the color at each time t for node i is given by

$$\frac{p_i^1(t)}{\sum_{k=1}^3 p_i^k(t)} r + \frac{p_i^2(t)}{\sum_{k=1}^3 p_i^k(t)} b + \frac{p_i^3(t)}{\sum_{k=1}^3 p_i^k(t)} g. \tag{4.15}$$

When $p_i^1(t) + p_i^2(t) + p_i^3(t) = 0$, the color is black, indicating completely healthy, susceptible. These color variations are used to facilitate the depiction of the parallel equilibrium ($\tilde{p}^1 = \alpha^2\tilde{p}^2 = \alpha^3\tilde{p}^3$), which are illustrated by all the nodes converging to the same color. For all $i \in [n]$, the diameter of node i is given by

$$d_0 + (p_i^1(t) + p_i^2(t) + p_i^3(t))r_0, \tag{4.16}$$

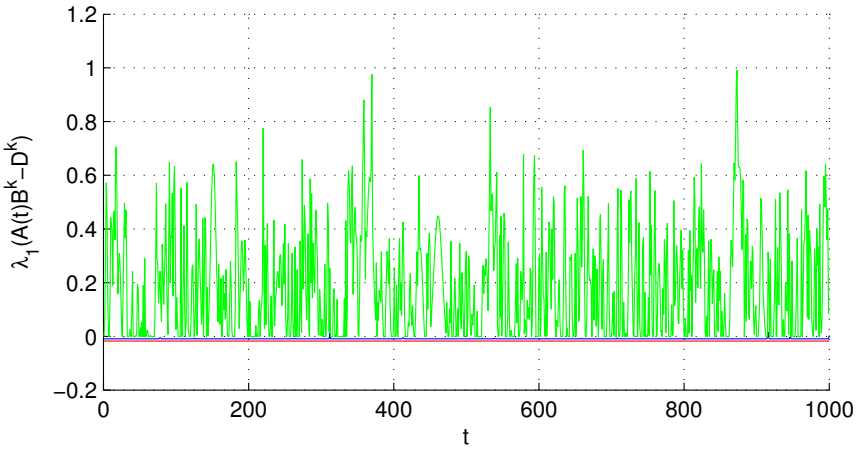

Figure 4.4: The maximum eigenvalues of the three viruses from the simulation in Figure 4.3. Note that the maximum eigenvalues for viruses 1 and 2 are indicated by horizontal lines (red and blue, resp.) just below the 0 axis.

with d_0 being the default/smallest diameter and r_0 being the scaling factor depending on the total sickness of node i. Therefore, the color indicates the type of virus(es) each agent, or group, has and the diameter indicates degree of sickness for each agent, or group.

For systems that have three different subgraphs, viruses 1, 2, and 3 spread on the graphs depicted by gray, green, and pink edges, respectively. If all viruses spread on the same graph, the edges are gray.

The simulation in Figure 4.3 has three viruses spreading over the same time–varying graph. Similar to Chapter 3, the graph structure is determined by (3.25), where $z_i(t) \in \mathbb{R}^2$ is the position of node i, with $\hat{r} = 10$. The nodes have piece-wise constant drifts following (3.26), where $\phi(t) \in \mathbb{R}^2$ and is determined, for each dimension $l \in [2]$, by (3.27), that is, the nodes hover around a square, centered at some point z_c. The initial positions and ϕ's are chosen randomly. Each virus is homogeneous in infection rate. The first two viruses meet the assumptions of Corollary 2, while the maximum eigenvalue of the third virus fluctuates between being positive and negative. See Figure 4.4 for a plot of the maximum eigenvalues of the three-virus dynamics. Consistent with the corollary, the first two viruses are eradicated quite quickly. The third virus is also eliminated, but it takes a little longer. This eradication is illustrated in Figure 4.3b.

The simulation in Figure 4.5 meets the assumptions of Theorem 13, where $s(B^1 - D^1) > 0$, and $s(B^2 - D^2) < 0$ and $s(B^3 - D^3) < 0$. Therefore, the first virus, depicted in red, reaches an epidemic equilibrium, while the other two viruses are eradicated.

The simulation shown in Figure 4.6 meets the assumptions of Theorem 14, that is, the three viruses are each homogeneous, with $\frac{\delta^1}{\beta^1} = \frac{\delta^2}{\beta^2} = \frac{\delta^3}{\beta^3}$, and propagate over the same graph structure. There are 15 nodes and the initial conditions are given in Figure 4.6a. Consistent with the theorem, the system converges to a co-existing parallel equilibrium.

Similarly, the simulation shown in Figure 4.7 meets the assumptions of Theorem 15, that is, the viruses are heterogeneous but identical for each node, with $\delta_i^1 = \cdots = \delta_i^m$, $\beta_i^1 = \cdots = \beta_i^m$ $\forall i \in [n]$, and propagate over the same graph structure. There are 15 nodes and the initial conditions are given in Figure 4.7a. Consistent with the theorem, the system converges to a co-existing parallel equilibrium, shown in 4.7b.

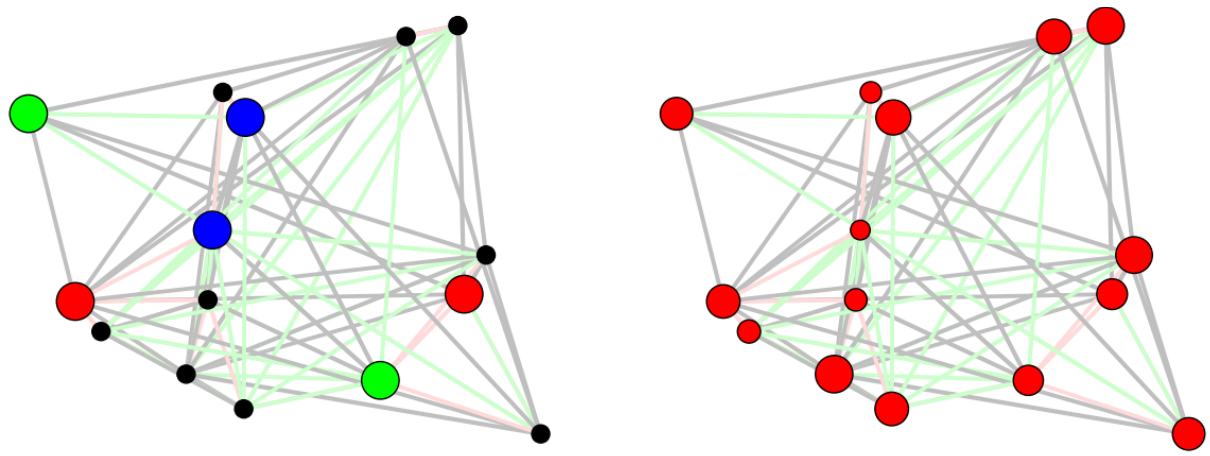

(a) The system at time zero.

(b) The system at time 300.

Figure 4.5: This three-virus system meets the assumptions of Theorem 13 so virus 1 reaches an epidemic state while the other viruses are eradicated. The colors and diameters follow (4.15) and (4.16). A video of this simulation can be found at youtu.be/gPGwAdLo_DU.

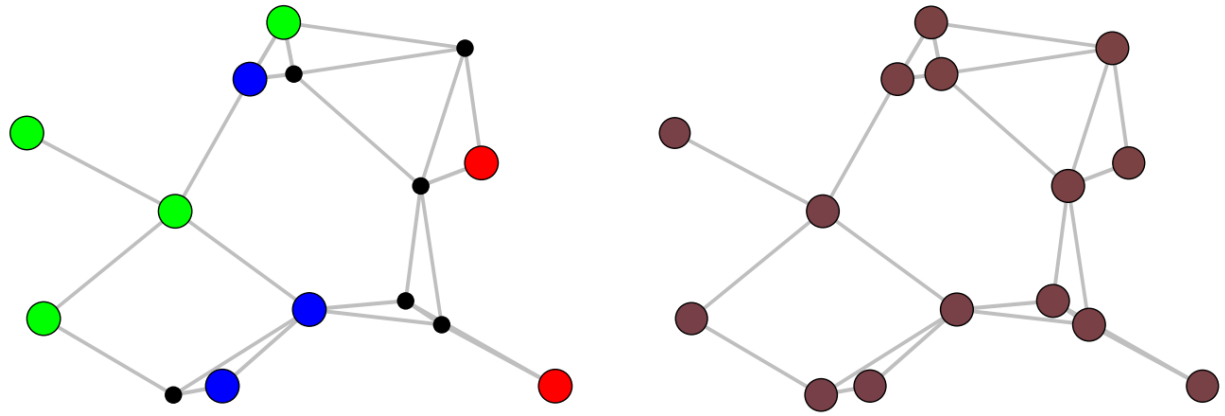

(a) The system at time zero.

(b) The system at time 400.

Figure 4.6: This three-virus system meets the assumptions of Theorem 14 and the viruses converge to a parallel equilibrium. The colors and diameters follow (4.15) and (4.16). A video of this simulation can be found at youtu.be/yzV8HxDkEJc.

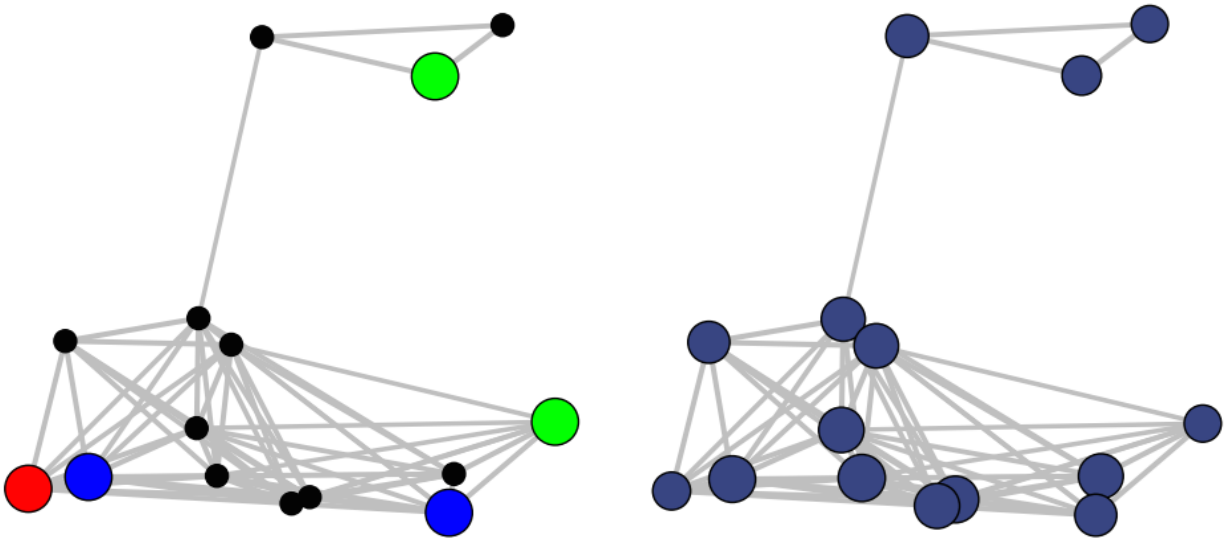

(a) The system at time zero.

(b) The system at time 150.

Figure 4.7: This three-virus system meets the assumptions of Theorem 15 and the viruses converge to a parallel equilibrium. The colors and diameters follow (4.15) and (4.16). A video of this simulation can be found at youtu.be/VIgoHe74P1w.

4.6 Human Awareness

In this section, we extend the model in (4.2) to allow agents to become alerted to the fact that viruses are pervading the system. This state of awareness reduces the likelihood of becoming infected by scaling the spread parameters.

Each individual has four possible states including susceptible, infected with virus 1, infected with virus 2, and an alert state. An alert individual is still susceptible but is cautious, and therefore less susceptible than when not alert. Let $S_i(t)$ and $A_i(t)$ respectively denote the number of susceptible and alert individuals in group i at time $t \geq 0$, and let $I_i^1(t)$ and $I_i^2(t)$ respectively denote the number of individuals infected with virus 1 and virus 2 in group i at time $t \geq 0$. Assume that the total number of individuals in each group i, denoted by N_i, does not change over time. In other words, $S_i(t) + I_i^1(t) + I_i^2(t) + A_i(t) = N_i$, for all $i \in [n]$ and $t \geq 0$, which implies that birth rate equals death rate.

The transitions among the four states are described as follows. Individuals infected with virus 1 (or virus 2) in group i become susceptible at a curing rate γ_i^1 (or γ_i^2). Infected individuals will not become alert since they may become careless about the diseases after getting recovered. A susceptible individual may become infected or alert when contacting other infected individuals. Specifically, susceptible individuals in group i become infected with virus 1 (or virus 2), at an infection rate α_{ij}^1 (or α_{ij}^2) times the portion of susceptible individuals in group i and the number of infected individuals with virus 1 (or virus 2) in group j, when contacting individuals in their own and neighboring group j. Here the portion of susceptible individuals in group i represents the possibility that a susceptible individual contacts individuals in group j. Similarly, susceptible individuals in group i become alert, at an apprehension (trepidation) rate κ_i times the portion of susceptible individuals in group i and the number of infected individuals (with virus 1 and virus 2) in group j, when contacting infected individuals in their own and neighboring group j. Susceptible individuals in group i may also become alert when contacting alert individuals in their own and neighboring

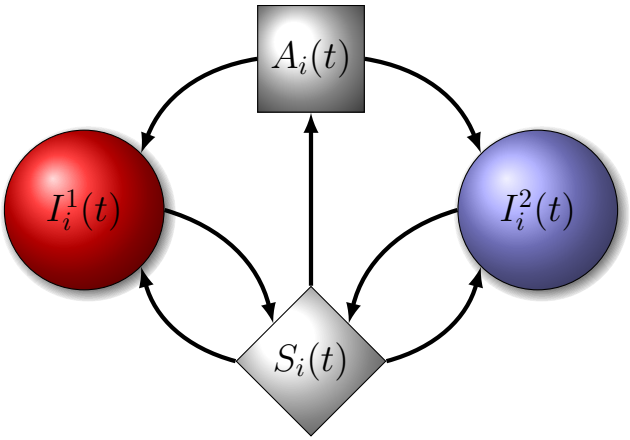

Figure 4.8: The possible states and transitions for agents in group i.

group j, at an admonition rate $\bar{\kappa}_i$ times the portion of susceptible individuals in group i and the number of alert individuals in group j. Alert individuals may also become infected when contacting other infected individuals. Similar to susceptible individuals, alert individuals in group i become infected with virus 1 (or virus 2) at an infection rate $\bar{\alpha}_{ij}^1$ (or $\bar{\alpha}_{ij}^2$). We assume that $\bar{\alpha}_{ij}^1 < \alpha_{ij}^1$ and $\bar{\alpha}_{ij}^2 < \alpha_{ij}^2$, which implies that alert individuals get infected with smaller infection rates than susceptible individuals. We also assume that an alert individual will not return to the susceptible state. The above transitions are illustrated in Figure 4.8.

We introduce the notation $y_i(t)$ to denote the portion of alert individuals in group i. Therefore, for every virus $k \in [m]$,

$$\dot{p}_i^k(t) = \big(1 - p_i^1(t) - \cdots - p_i^m(t) - y_i(t)\big) \sum_{j=1}^{n} \beta_{ij}^1 p_j^k(t) - \delta_i^k p_i^k(t) + y_i(t) \sum_{j=1}^{n} \bar{\beta}_{ij}^k p_j^k(t) \tag{4.17}$$

$$\begin{aligned} \dot{y}_i(t) = &-\mu_i y_i(t) - y_i(t) \sum_{k=1}^{m} \sum_{j=1}^{n} \bar{\beta}_{ij}^k p_j^k(t) + (1 - p_i^1(t) - \cdots - p_i^m(t) - y_i(t)) \sum_{j=1}^{n} \kappa_{ij} \sum_{k=1}^{m} p_j^k(t) \\ &+ (1 - p_i^1(t) - \cdots - p_i^m(t) - y_i(t)) \sum_{j=1}^{n} \bar{\kappa}_{ij} y_j(t), \end{aligned} \tag{4.18}$$

where μ_i is the death rate, κ_{ij} and $\bar{\kappa}_{ij}$ are the alerting rates of the system, and $\bar{\beta}_{ij}^1$ and $\bar{\beta}_{ij}^2$ are the infection rates associated with the alert state, with $\bar{\beta}_{ij}^1 < \beta_{ij}^1$ and $\bar{\beta}_{ij}^2 < \beta_{ij}^2$ for all $i, j \in [n]$. Note that κ_{ij} allows for awareness from infected individuals and $\bar{\kappa}_{ij}$ allows for awareness from individuals who are already aware. We define K and $\bar{K}$ as the matrices of κ_{ij}'s and $\bar{\kappa}_{ij}$'s, respectively. The model in (4.18) can be derived in a manner similar to that of the bi-virus case in [70].

Lemma 11. *Suppose that for all $i \in [n], k \in [m]$, we have $\delta_i^k \geq 0$, $\mu_i \geq 0$, and the matrices B^k, $\bar{B}^k$, K, $\bar{K}$ are non-negative. If for all $i \in [n], k \in [m]$, we have $p_i^k(0), y_i(0), (1 - p_i^1(0) - \cdots - p_i^m(0) - y_i(0)) \in [0, 1]$, then $p_i^k(t), y_i(t), p_i^1(t) + \cdots + p_i^m(t) + y_i(t) \in [0, 1]$ for all $i \in [n], k \in [m]$ and $t \geq 0$.*

The proof follows the lines similar to those of Lemma 9.

Following the definitions in [70], an equilibrium $(p^1, \ldots, p^m, y)$ of (4.17)-(4.18) is a *healthy state* if $p^1 = \cdots = p^m = \mathbf{0}$, independent of the value of y, since at such an equilibrium, all individuals in the network are healthy. We call the equilibrium where $p^1 = \cdots = p^m = y = \mathbf{0}$ the trivial healthy state. If a healthy state

has $y > \mathbf{0}$, it is an *alert state*, which implies that all individuals are healthy, but some of them are alert. Similar to the multi-virus model, the system with human awareness also admits *epidemic states* which are equilibria with nonzero p^k's.

The following theorem provides a sufficient condition for global stability of healthy states.

Theorem 16. *Suppose that for all $i \in [n], k \in [m]$, we have $\delta_i^k \geq 0$ and the matrices B^k, $\bar{B}^k$ are nonnegative and irreducible. If $s(B^k - D^k) \leq 0$ for all $k \in [m]$, then the system in (4.17)-(4.18) asymptotically enters the set of healthy states. Suppose, in addition, that $\bar{K}$ is irreducible. If $s(-M + \bar{K}) \leq 0$, then the system in (4.17)-(4.18) has a unique equilibrium $(\mathbf{0}, \ldots, \mathbf{0})$, which is asymptotically stable with domain of attraction $\mathcal{D}$ defined in (4.4). If $s(-M + \bar{K}) > 0$, then the system in (4.17)-(4.18) has two equilibria, the trivial healthy state $(\mathbf{0}, \ldots, \mathbf{0})$, which is asymptotically stable with domain of attraction $\{(p^1, \ldots, p^m, \mathbf{0}) | p^1 \geq \mathbf{0}, \ldots, p^m \geq \mathbf{0}, p^1 + \cdots + p^m \leq \mathbf{1}\}$, and a unique alert state $(\mathbf{0}, \ldots, \mathbf{0}, \tilde{y})$ with $\tilde{y} \gg \mathbf{0}$, which is asymptotically stable with domain of attraction $\mathcal{D} \setminus \{(p^1, \ldots, p^m, \mathbf{0}) | p^1 \geq \mathbf{0}, \ldots, p^m \geq \mathbf{0}, p^1 + \cdots + p^m \leq \mathbf{1}\}$.*

Proof. Since $p_i^1(t)$, $\ldots$, $p_i^m(t)$, and $y_i(t)$ are always nonnegative by Lemma 11, from (4.17)-(4.18), we have, for every virus $k \in [m]$,

$$\dot{p}_i^k(t) \quad \leq \quad -\delta_i^k p_i^k(t) + (1 - p_i^k(t)) \sum_{j=1}^{n} \beta_{ij}^k p_j^k(t),$$

which implies that each of the trajectories of each $p_i^k(t)$ is bounded above by a single-virus model. Therefore, if $s(-D^k + B^k) \leq 0$ for every virus $k \in [m]$, both $p_i^k(t)$ will asymptotically converge to $\mathbf{0}$ as $t \to \infty$, for every virus $k \in [m]$, and thus the system asymptotically enters the set of healthy states.

Next suppose, in addition, that $\bar{K}$ is irreducible. From (4.18), we have

$$\dot{y}(t) = -My(t) - Y(t) \sum_{k=1}^{m} \bar{B}^k p^k(t) + (I - P^1(t) - \cdots - P^m(t) - Y(t))(K(p^1(t) + \cdots + p^m(t)) + \bar{K}y(t)).$$

Thus, we can regard the dynamics of $y(t)$ as an autonomous system

$$\dot{y}(t) = (\bar{K} - Y(t)\bar{K} - M)y(t),$$

with a vanishing perturbation

$$-Y(t) \sum_{j=1}^{n} \beta_{ij}^1 p_j^k(t) + (I - P^1(t) - \cdots - P^m(t) - Y(t))K(p^1(t) + \cdots + p^m(t)) - (P^1(t) + \cdots + P^m(t))\bar{K}y(t),$$

which converges to $\mathbf{0}$ as $t \to \infty$ since all $p^1(t), \ldots, p^m(t)$ converge to $\mathbf{0}$. From (2.9), we see that $y(t)$ will asymptotically converge to $\mathbf{0}$ for any $y(0) \in [0,1]^n$ if $s(-M + \bar{K}) \leq 0$, or a unique nonzero state $\tilde{y} \gg \mathbf{0}$ for any $y(0) \in [0,1]^n \setminus \{\mathbf{0}\}$ if $s(-M + \bar{K}) > 0$. Therefore, if $s(-M + \bar{K}) \leq 0$, the system in (4.17)-(4.18) has a unique equilibrium $(\mathbf{0}, \ldots, \mathbf{0})$, which is asymptotically stable with domain of attraction $\mathcal{D}$, and if $s(-M + \bar{K}) > 0$, the system in (4.17)-(4.18) has a unique alert state $(\mathbf{0}, \ldots, \mathbf{0}, \tilde{y})$ with $\tilde{y} \gg \mathbf{0}$, which is asymptotically stable with domain of attraction $\mathcal{D} \setminus \{(p^1, \ldots, p^m, \mathbf{0}) | p^1 \geq \mathbf{0}, \ldots, p^m \geq \mathbf{0}, p^1 + \cdots + p^m \leq \mathbf{1}\}$, and $(\mathbf{0}, \ldots, \mathbf{0})$ is asymptotically stable with domain of attraction $\{(p^1, \ldots, p^m, \mathbf{0}) | p^1 \geq \mathbf{0}, \ldots, p^m \geq \mathbf{0}, p^1 + \cdots + p^m \leq \mathbf{1}\}$. $\square$

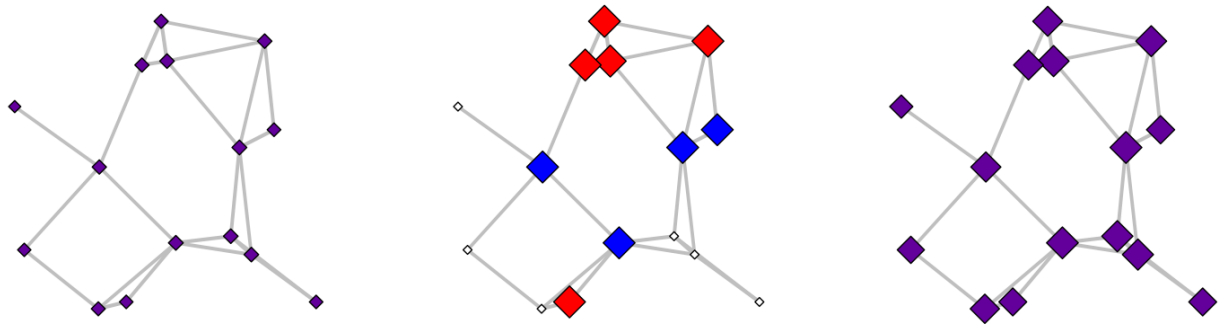

Figure 4.9: The initial conditions for the bi-virus system with awareness. The colors and diameters follow (4.19) and (4.20).

4.6.1 Human Awareness Simulations

We illustrate the behavior of the model with $m = 2$, i.e., for two viruses or a bi-virus system. Virus 1 is depicted by the color red ($r = [1\ 0\ 0]$) and virus 2 is depicted by the color blue ($b = [0\ 0\ 1]$). For all $i \in [n]$, the color at each time t for group (agent) i is given, similar to (4.15) by

$$\frac{p_i^1(t)}{p_i^1(t) + p_i^2(t)} r + \frac{p_i^2(t)}{p_i^1(t) + p_i^2(t)} b. \tag{4.19}$$

When $p_i^1(t) + p_i^2(t) = 0$, the color goes to white, indicating completely healthy, susceptible. These are used to facilitate the depiction of the parallel equilibrium ($\tilde{p}^1 = \alpha \tilde{p}^2$), which will be shown by all nodes converging to the same color. For all $i \in [n]$, the length of the node representing group (agent) i is given, similar to (4.16), by

$$d_0 + (p_i^1(t) + p_i^2(t)) r_0, \tag{4.20}$$

with d_0 being the default/smallest length and r_0 being the scaling factor depending on the total sickness of group i. Therefore the color shows which sickness the group has and the size shows how much of the sickness or how sick each group is. The awareness variable is depicted by the rotation of the polygon; $y_i = 0$ corresponds to a diamond orientation and $y_i = 1$ corresponds to a square orientation.

The system in Figures 4.9-4.10 has homogeneous virus spread such that

$$\frac{1}{1} = \frac{\delta^1}{\beta^1} = \frac{\delta^2}{\beta^2} = \frac{2}{2},$$

factoring the matrices into $B^1 = \beta_1 A$, $B^2 = \beta_2 A$, $\bar{B}^1 = .9B^1$, $\bar{B}^2 = .9B^2$, $D^1 = \delta_1 A$, $D^2 = \delta_2 A$, where A is the weighted adjacency matrix, and simulates over the same graph structure for all the matrices and $M = 0$. The system converges to a parallel equilibrium, that is $\tilde{p}^1 = 0.2488\tilde{x}^2$, depicted by the nodes being the same color for all three initial conditions in Figure 4.9. Rerunning the simulation with $M = I$, gives almost the exact same parallel equilibrium, i.e. $\tilde{p}^1$ and $\tilde{p}^2$, as in Figure 4.10 (each agent differing by an average of 0.0011) but non-trivially changes $\tilde{y}$ (average difference of 0.0698).

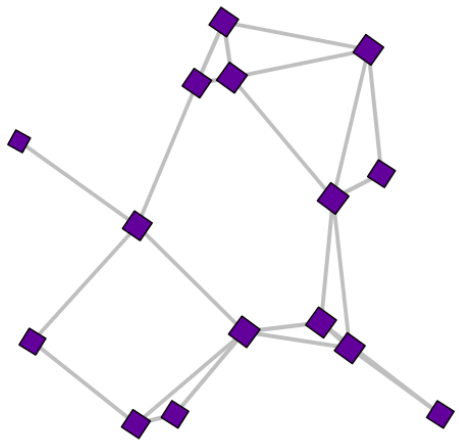

Figure 4.10: The parallel equilibrium for a bi-virus system with awareness. The stable equilibrium at time 100 is the same parallel equilibrium for all three initial conditions in Figure 4.9. The colors and diameters follow (4.19) and (4.20).

4.7 Coupled Competing Viruses

It is well known that false and/or misleading information spreads over the internet. One of the most natural places for this information to spread on is social networks. This problem has been highlighted by recent revelations that fake Facebook accounts were purchased by a Russian-linked firm to influence the November 2016 presidential election in the United States [73]. In this case one virus could be an untrue or exaggerated story from the right-wing site, or one of these fake accounts, and the other virus could be another exaggerated story from a left-wing site. If a person accepts one of the stories, they are less likely to accept a story from the other side, although not necessarily completely averse to it. The model proposed herein incorporates non-trivial graph structures and allows the viruses (fake news) to spread on different graphs; the social media networks referred to could be the same or different platforms (including a Twitter network since symmetry is not assumed).

There has recently been increasing attention paid to security issues in computer networks [74, 75, 76]. Of particular interest is the spread of computer viruses which may paralyze the whole network [77, 78, 79]. There have been a few existing models for computer viruses [79, 80, 81]. For the case of a single computer virus, these models are closely related to SIS models in epidemic networks.

The key difference between the bi-virus model in (4.1) and the model proposed in this section is that it is possible for a node to be infected with both viruses simultaneously. Once infected with one virus, a node can become infected with the other virus in a similar fashion by the infection parameters scaled by the sum of infections of its neighbors; however, it becomes discounted, or scaled, by a factor $\epsilon \in [0, 1]$. If $\epsilon = 0$, the model is exactly the bi-virus model studied in previous work, given in (4.1). If $\epsilon = 1$, the viruses become decoupled; therefore they are independent, and can practically be studied as two single viruses.

One interpretation of the coupling strength ϵ in computer networks is the following. If a computer becomes infected with a virus by a user clicking on a corrupted link in an email and the user realizes that, then the user's subsequent actions will most likely be different, i.e. she will become less likely to click on similar suspicious links for the second virus. In fake news spreading, one interpretation of ϵ is that given that a node accepts one piece of fake news as truth they are less likely to believe a piece of fake news from an

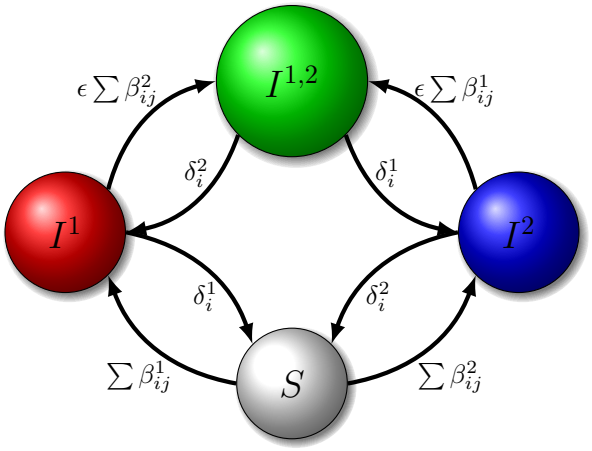

Figure 4.11: The possible states and transitions for node i. State S stands for being healthy but susceptible. States I^1, I^2, and $I^{1,2}$ stand for being infected by virus 1, virus 2, and both virus 1 and virus 2, respectively.

opposing-view, biased source.

The spread of computer viruses in a computer network and fake news spreading in social networks are not necessarily mutually exclusive, and therefore do not necessarily compete with each other, in the sense that a node can be infected with only one at a time. Our goal here is to propose a novel bi-virus model for computer and social networks, in which the two viruses are not competitive but are coupled, and we expect the model can be generalized to the case of more than two viruses. The work in this section appears in [82].

4.7.1 Coupled Bi-Virus Model

Suppose that two viruses are spreading in a computer network or a social network. It is not reasonable to assume that the two viruses are completely competitive, that is, a node can only be infected with one virus at a time, as studied in epidemic networks [53] and economic marketing [83]. We consider the following model in which a node (representing a computer, or an agent or subpopulation in a social network) can be simultaneously infected by the two viruses.

Consider a network of n agents. Each agent may be infected with a virus through external attacks and contagion. Specifically, each agent can be infected if one of its neighbors is infected. The neighbor relationships among the n agents are described by an n-vertex directed graph. A directed edge from node j to node i means that agent i can be infected by agent j, i.e., agent j is a neighbor of agent i. We use $\mathcal{N}_i$ to denote the set of neighbors of agent i. The two viruses may spread through different routes in the network. We use $\mathcal{N}_i^k$ to denote the set of neighbors of agent i from which virus k spreads. It is clear that $\mathcal{N}_i^1 \cup \mathcal{N}_i^2 = \mathcal{N}_i$ for all $i \in [n]$.

For each virus $k \in \{1, 2\}$, each agent i has its curing rate δ_i^k and infection rates β_{ji}^k when $i \in \mathcal{N}_j^k$. The former means that if agent i is infected by virus k, it is cured with rate δ_i^k, and the latter means that if agent i is infected by virus k and its neighbor j is not, agent i can infect agent j at rate β_{ji}^k. The two viruses can simultaneously infect the same node, but not independently. Specifically, they are coupled in the following manner. Let i and j be any pair of integers in $[n]$ such that agent j is a neighbor of agent i. If agent j has been infected by only one virus, say virus 1, and agent i is infected by the other virus, virus 2, then agent

i can infect agent j with virus 2 at a discounted rate $\epsilon\beta_{ji}^2$. See Figure 4.11 for a depiction of the model. It is worth noting that there is no transition link from state $I^{1,2}$ (infected by both two viruses) to state S (healthy state), as the probability that the two viruses are cured at the same time is zero. We call ϵ the *coupling strength* between the two viruses, and assume that ϵ takes value in the interval $[0,1]$. If $\epsilon = 1$, then the two viruses are independent. If $\epsilon = 0$, then the two viruses are competitive. We will discuss these two special cases shortly.

Let p_i^1, p_i^2, and z_i denote the probability of agent i being infected with virus 1, virus 2, and both viruses 1 and 2, respectively. Their dynamics are as follows:

$$\dot{p}_i^1(t) = -\delta_i^1 p_i^1(t) + \delta_i^2 z_i(t) + (1 - p_i^1(t) - p_i^2(t) - z_i(t)) \sum_{j=1}^n \beta_{ij}^1 (p_j^1(t) + z_j(t)) - p_i^1(t) \sum_{j=1}^n \epsilon\beta_{ij}^2 (p_j^2(t) + z_j(t)), \tag{4.21}$$

$$\dot{p}_i^2(t) = -\delta_i^2 p_i^2(t) + \delta_i^1 z_i(t) + (1 - p_i^1(t) - p_i^2(t) - z_i(t)) \sum_{j=1}^n \beta_{ij}^2 (p_j^2(t) + z_j(t)) - p_i^2(t) \sum_{j=1}^n \epsilon\beta_{ij}^1 (p_j^1(t) + z_j(t)), \tag{4.22}$$

$$\dot{z}_i(t) = -(\delta_i^1 + \delta_i^2) z_i(t) + p_i^1(t) \sum_{j=1}^n \epsilon\beta_{ij}^2 (p_j^2(t) + z_j(t)) + p_i^2(t) \sum_{j=1}^n \epsilon\beta_{ij}^1 (p_j^1(t) + z_j(t)). \tag{4.23}$$

The above continuous-time dynamics can be derived from a 4^n state Markov chain using a mean field approximation, similar to the single virus case in Section 2.1, which will be detailed in a future extended version of [82].

The above equations can be combined into vector form, as follows:

$$\dot{p}^1(t) = -D^1 p^1(t) + D^2 z(t) + (I - P^1(t) - P^2(t) - Z(t)) B^1 (p^1(t) + z(t)) - \epsilon P^1(t) B^2 (p^2(t) + z(t)), \tag{4.24}$$

$$\dot{p}^2(t) = -D^2 p^2(t) + D^1 z(t) + (I - P^1(t) - P^2(t) - Z(t)) B^2 (p^2(t) + z(t)) - \epsilon P^2(t) B^1 (p^1(t) + z(t)), \tag{4.25}$$

$$\dot{z}(t) = -(D^1 + D^2) z(t) + \epsilon P^1(t) B^2 (p^2(t) + z(t)) + \epsilon P^2(t) B^1 (p^1(t) + z(t)), \tag{4.26}$$

where $p^1(t)$, $p^2(t)$, $z(t)$ are the column vectors obtained by stacking $p_i^1(t)$, $p_i^2(t)$, and $z_i(t)$, respectively, B^1, B^2 are the matrices of β_{ij}^1, β_{ij}^2, respectively, $P^1(t) = \mathrm{diag}(p^1(t))$, $P^2(t) = \mathrm{diag}(p^2(t))$, $Z(t) = \mathrm{diag}(z(t))$, $D^1 = \mathrm{diag}(\delta^1)$, and $D^2 = \mathrm{diag}(\delta^2)$.

It is worth emphasizing that the two viruses may spread in different routes, that is, the graphs of B^1 and B^2 are not necessarily the same. We call the graphs of B^1 and B^2 the spreading graphs of viruses 1 and 2, respectively. Both the graphs of B^1 and B^2 are subgraphs of the neighbor graph. Specifically, for each $k \in \{1,2\}$, the ijth entry of B^k, i.e., β_{ij}^k, is nonzero whenever $i \in \mathcal{N}_j^k$. In social networks, this is very natural; the two graphs correspond to two different social media platforms. In computer networks, different neighboring computers may exchange information using different manners, such as emails versus shared folders, which results in different spreading routes for viruses.

We make the following assumptions on the model to ensure that it is well defined.

Assumption 6. *For all $i \in [n]$, we have $p_i^1(0), p_i^2(0), z_i(0), (1 - p_i^1(0) - p_i^2(0) - z_i(0)) \in [0,1]$.*

Assumption 7. *For all $i \in [n]$, we have $\delta_i^1, \delta_i^2 \geq 0$. The matrices B^1 and B^2 are nonnegative and irreducible.*

If $\delta_i^1, \delta_i^2 = 0$ for $i \in [n]$, the model simplifies to two coupled SI viruses. The assumption that B^1 and B^2 are nonnegative and irreducible implies that the graphs of B^1 and B^2 are both strongly connected.

4.7.2 Coupled Bi-Virus Analysis

In this section, we analyze the system defined by (4.24)-(4.26). We begin with the following lemma which establishes the invariant set of the system.

Lemma 12. *Under Assumptions 6 and 7,* $p_i^1(t), p_i^2(t), z(t),\ p_i^1(t) + p_i^2(t) + z(t) \in [0,1]$ *for all* $i \in [n]$ *and* $t \geq 0$.

Proof: Suppose that at some time τ, $p_i^1(\tau), p_i^2(\tau), z_i(\tau),\ p_i^1(\tau)+p_i^2(\tau)+z_i(\tau) \in [0,1]$ for all $i \in [n]$. Consider an index $i \in [n]$. If $p_i^1(\tau) = 0$, then from (4.21) and Assumption 7, $\dot{p}_i^1(\tau) \geq 0$. The same holds for $p_i^2(\tau)$, $z_i(\tau)$ and $p_i^1(\tau)+p_i^2(\tau)+z_i(\tau)$. If $p_i^1(\tau) = 1$, then from (4.22) and Assumption 7, $\dot{p}_i^1(\tau) \leq 0$. The same holds for $p_i^2(\tau)$, $z_i(\tau)$, and $p_i^1(\tau)+p_i^2(\tau)+z_i(\tau)$. It follows that $p_i^1(t), p_i^2(t), z_i(t), p_i^1(t)+p_i^2(t)+z_i(t)$ will be in $[0,1]$ for all times $t \geq \tau$. Since the above arguments hold for all $i \in [n]$, $p_i^1(t), p_i^2(t), z_i(t), p_i^1(t) + p_i^2(t) + z_i(t)$ will be in $[0,1]$ for all $i \in [n]$ and $t \geq \tau$. Since by Assumption 1, $p_i^1(0), p_i^2(0), z_i(0), p_i^1(0) + p_i^2(0) + z_i(0) \in [0,1]$ for all $i \in [n]$, it follows that $p_i^1(t), p_i^2(t), z_i(t), p_i^1(t) + p_i^2(t) + z_i(t) \in [0,1]$ for all $i \in [n]$ and $t \geq 0$. □

Lemma 12 implies that the set

$$\mathcal{D} = \{(p^1, p^2, z) \mid p^1 \geq \mathbf{0},\ p^2 \geq \mathbf{0},\ z \geq \mathbf{0},\ p^1 + p^2 + z \leq \mathbf{1}\} \tag{4.27}$$

is positively invariant with respect to the system defined by (4.24)-(4.26). Since p_i^1, p_i^2, and z_i denote the probabilities of sickness of agent i, or fractions of group i, infected by viruses 1, 2, and both 1 and 2 simultaneously, respectively, and $1 - p_i^1 - p_i^2 - z_i$ denotes the probability of agent i, or fraction of group i that is healthy, it is natural to assume that their initial values are in the interval $[0,1]$, since otherwise the values will lack any physical meaning for the spread model considered here.

To begin we consider two special cases of the model. First, let $\epsilon = 0$. Then, the system defined by (4.24)-(4.26) simplifies to

$$\dot{p}^1(t) = -D^1 p^1(t) + D^2 z(t) + (I - P^1(t) - P^2(t) - Z(t))B^1(p^1(t) + z(t)), \tag{4.28}$$

$$\dot{p}^2(t) = -D^2 p^2(t) + D^1 z(t) + (I - P^1(t) - P^2(t) - Z(t))B^2(p^2(t) + z(t)), \tag{4.29}$$

$$\dot{z}(t) = -(D^1 + D^2)z(t). \tag{4.30}$$

In this case, as long as the matrix $D^1 + D^2$ is positive definite, i.e., $\delta_i^1 + \delta_i^2 > 0$ for all $i \in [n]$, it holds that $z(t)$ converges to $\mathbf{0}$ exponentially fast, and thus the system will eventually become a competitive bi-virus model which has been studied in [53, 55, 33]. In the second case, we let $\epsilon = 1$. To proceed, we define $y_i^1(t) = p_i^1(t) + z_i(t)$ and $y_i^2(t) = p_i^2(t) + z_i(t)$ for each $i \in [n]$, which represents the total probabilities of agent i being infected by viruses 1 and 2, respectively. From (4.21)-(4.23), the dynamics of y_i^1 and y_i^2 are

$$\dot{y}_i^1(t) = -\delta_i^1 y_i^1(t) + (1 - y_i^1(t)) \sum_{j=1}^{n} \beta_{ij}^1 y_j^1(t),$$

$$\dot{y}_i^2(t) = -\delta_i^2 y_i^2(t) + (1 - y_i^2(t)) \sum_{j=1}^{n} \beta_{ij}^2 y_j^2(t),$$

which are two independent single SIS dynamics. Therefore, the system defined by (4.24)-(4.26) subsumes the single SIS virus (two single, independent viruses) and the competitive, two SIS virus models. In the sequel, we study the behavior of the system defined by (4.24)-(4.26) when $\epsilon \in (0, 1)$.

Let $(\tilde{p}^1, \tilde{p}^2, \tilde{z})$ be an equilibrium of system (4.24)-(4.26). Then, the Jacobian matrix of the equilibrium, denoted by $J(\tilde{p}^1, \tilde{p}^2, \tilde{z})$, with $\tilde{B}^i = \text{diag}(B^i(\tilde{p}^i + \tilde{z}))$, $\tilde{Z}^i = Z\text{diag}(B^i\mathbf{1})$, $i \in [2]$, and $W = (I - \tilde{P}^1 - \tilde{P}^2 - \tilde{Z})$, is

$$J(\tilde{p}^1, \tilde{p}^2, \tilde{z}) = \begin{bmatrix} J_{1,1} & -\tilde{B}^1 - \epsilon\tilde{P}^1B^2 & WB^1 + D^2 - \tilde{B}^1 - \epsilon\tilde{P}^1B^2 \\ -\tilde{B}^2 - \epsilon\tilde{P}^2B^1 & J_{2,2} & WB^2 + D^1 - \tilde{B}^2 - \epsilon\tilde{P}^2B^1 \\ \epsilon(\tilde{B}^2 + \tilde{P}^2B^1) & \epsilon(\tilde{B}^1 + \tilde{P}^1B^2) & J_{3,3} \end{bmatrix}, \tag{4.31}$$

where

$$J_{1,1} = WB^1 - D^1 - \tilde{B}^1 - \epsilon\tilde{B}^2 \tag{4.32}$$

$$J_{2,2} = WB^2 - D^2 - \tilde{B}^2 - \epsilon\tilde{B}^1 \tag{4.33}$$

$$J_{3,3} = -D^1 - D^2 + \epsilon\tilde{P}^1B^2 + \epsilon\tilde{P}^2B^1. \tag{4.34}$$

It is easy to see that $(\mathbf{0}, \mathbf{0}, \mathbf{0})$ is an equilibrium of the system. We call it the healthy state.

Theorem 17. *Under Assumptions 6 and 7, if $s(B^1 - D^1) \leq 0$ and $s(B^2 - D^2) \leq 0$, then the healthy state is the unique equilibrium of (4.24)-(4.26), and the system defined by (4.24)-(4.26) asymptotically converges to the healthy state for any initial state in $\mathcal{D}$, as defined in* (4.27).

Proof: Let $y_i^1(t) = p_i^1(t) + z_i(t)$ and $y_i^2(t) = p_i^2(t) + z_i(t)$ for each $i \in [n]$. From (4.21)-(4.23), the dynamics of $y_i^1(t)$ and $y_i^2(t)$ are

$$\begin{aligned} \dot{y}_i^1(t) &= -\delta_i^1 y_i^1(t) + (1 - y_i^1(t) - (1-\epsilon)p_i^2(t)) \sum_{j=1}^n \beta_{ij}^1 y_j^1(t), \\ \dot{y}_i^2(t) &= -\delta_i^2 y_i^2(t) + (1 - y_i^2(t) - (1-\epsilon)p_i^1(t)) \sum_{j=1}^n \beta_{ij}^2 y_j^2(t). \end{aligned} \tag{4.35}$$

Since $\epsilon \in [0, 1]$, it follows that

$$\begin{aligned} \dot{y}_i^1(t) &\leq -\delta_i^1 y_i^1(t) + (1 - y_i^1(t)) \sum_{j=1}^n \beta_{ij}^1 y_j^1(t), \\ \dot{y}_i^2(t) &\leq -\delta_i^2 y_i^2(t) + (1 - y_i^2(t)) \sum_{j=1}^n \beta_{ij}^2 y_j^2(t), \end{aligned}$$

which implies that the trajectories of $y_i^1(t)$ and $y_i^2(t)$ in (4.35) are both bounded above by the trajectory of a single-virus SIS model. From Proposition 1 (Proposition 3 in [33]), in the case when $s(B^1 - D^1) \leq 0$ and $s(B^2 - D^2) \leq 0$, then all $y_i^1(t)$ and $y_i^2(t)$ asymptotically converge to 0 for any initial condition, which implies that system (4.24)-(4.26) asymptotically converges to the healthy state for any initial state in $\mathcal{D}$. Therefore, the healthy state is the unique equilibrium of the system. □

From (4.31), we have

$$J(\mathbf{0},\mathbf{0},\mathbf{0}) = \begin{bmatrix} B^1 - D^1 & 0 & B^1 + D^2 \\ 0 & B^2 - D^2 & WB^2 + D^1 \\ 0 & 0 & -D^1 - D^2 \end{bmatrix}. \tag{4.36}$$

Thus, the healthy state is (locally) asymptotically stable if and only if $s(-D^1 + B^1) < 0$, $s(-D^2 + B^2) < 0$, and $\delta_i^1 + \delta_i^2 > 0$ for all $i \in [n]$. We therefore have the following corollary.

Corollary 5. *Under Assumption 7, if $s(-D^1 + B^1) < 0$, $s(-D^2 + B^2) < 0$, and $\delta_i^1 + \delta_i^2 > 0$ for all $i \in [n]$, then the healthy state is the unique equilibrium of (4.24)-(4.26), which is asymptotically stable with domain of attraction $\mathcal{D}$, as defined in* (4.4).

Next we consider the scenario in which one of $s(B^1 - D^1)$ and $s(B^2 - D^2)$ is greater than zero. Without loss of generality, we assume that $s(B^1 - D^1) > 0$ and $s(B^2 - D^2) \leq 0$. We call an equilibrium $(\tilde{p}^1, \tilde{p}^2, \tilde{z})$ an epidemic equilibrium if it does not equal $(\mathbf{0}, \mathbf{0}, \mathbf{0})$.

Theorem 18. *Under Assumptions 6 and 7, if $s(B^1 - D^1) > 0$ and $s(B^2 - D^2) \leq 0$, then system (4.24)-(4.26) has a unique epidemic equilibrium $(\tilde{p}^1, \mathbf{0}, \mathbf{0})$ with $\tilde{p}^1 \gg \mathbf{0}$, and the system asymptotically converges to the epidemic equilibrium for any initial state in $\mathcal{D} \setminus \{(\mathbf{0}, p^2, z) | p^2 \geq \mathbf{0}, z \geq \mathbf{0}, p^2 + z \leq \mathbf{1}\}$, where $\mathcal{D}$ is defined in* (4.27).

Proof: Let $y_i^2(t) = p_i^2(t) + z_i(t)$ for each $i \in [n]$. From the proof of Theorem 17, since $s(B^2 - D^2) \leq 0$, all $y_i^2(t)$ converge to zero, which implies all $p_i^2(t)$ and $z_i(t)$ converge to zero as well. From (4.21), with $p_i^2(t) = z_i(t) = 0$ for all $i \in [n]$, the dynamics of $p_i^1(t)$ simplify to a single-virus SIS model. The theorem is then a direct consequence of Proposition 1 (Proposition 5 in [33]). □

From the preceding results, if at least one of $s(B^1 - D^1)$ and $s(B^2 - D^2)$ is less than or equal to zero, the two viruses cannot coexist at equilibrium. We now turn to the case when both $s(B^1 - D^1)$ and $s(B^2 - D^2)$ are greater than zero. We provide the following lemma, a necessary condition for the occurrence of coexistence of the two viruses on individuals.

Lemma 13. *Suppose that Assumptions 6 and 7 hold and that $\delta_i^1, \delta_i^2 > 0$ for all $i \in [n]$. If $(\tilde{p}^1, \tilde{p}^2, \tilde{z})$ is an equilibrium of system (4.24)-(4.26) such that $\tilde{z}_i > 0$ for at least one $i \in [n]$, then $\tilde{p}^1, \tilde{p}^2, \tilde{z} \gg \mathbf{0}$.*

Proof: Suppose that, to the contrary, there exists an $i \in [n]$ such that $\tilde{p}_i^1 = 0$. From (4.21), it holds that $\tilde{z}_i = 0$. It follows from (4.23) that

$$\tilde{p}_i^2 \sum_{j=1}^{n} \epsilon \beta_{ij}^1 (\tilde{p}_j^1 + \tilde{z}_j) = 0,$$

which implies that $\tilde{p}_i^2 = 0$ or $\sum_{j=1}^n \epsilon \beta_{ij}^1 (\tilde{p}_j^1 + \tilde{z}_j) = 0$. If the latter is true, since $\beta_{ij} > 0$ whenever $j \in \mathcal{N}_i$, it holds that $\tilde{p}_j^1 = 0$ and $\tilde{z}_j = 0$ for all $j \in \mathcal{N}_i$. If $\tilde{p}_i^2 = 0$, it follows from (4.21) that $\sum_{j=1}^n \beta_{ij}^1 (\tilde{p}_j^1 + \tilde{z}_j) = 0$, which also implies that $\tilde{p}_j^1 = 0$ and $\tilde{z}_j = 0$ for all $j \in \mathcal{N}_i$. By repeating this argument, since the graph of B^1 is strongly connected, $\tilde{z}_i = 0$ for all $i \in [n]$, which is a contradiction. Therefore, $\tilde{p}_i^1 > 0$ for all $i \in [n]$.

Similarly, it must be true that $\tilde{p}_i^2 > 0$ for all $i \in [n]$. Now suppose that, to the contrary, there exists one $i \in [n]$ for which $\tilde{z}_i = 0$. From (4.23), it holds that $\tilde{p}_i^1 \sum_{j=1}^n \epsilon \beta_{ij}^2 (\tilde{p}_j^2 + \tilde{z}_j) = 0$ and $\tilde{p}_i^2 \sum_{j=1}^n \epsilon \beta_{ij}^1 (\tilde{p}_j^1 + \tilde{z}_j) = 0$, which respectively imply that $\tilde{p}_i^1 = 0$ or $\tilde{p}_j^2 = 0$ for all $j \in \mathcal{N}_i$, and $\tilde{p}_i^2 = 0$ or $\tilde{p}_j^1 = 0$ for all $j \in \mathcal{N}_i$. From the preceding discussion, each of these four cases implies that $\tilde{z}_i = 0$ for all $i \in [n]$, which is impossible. Therefore, $\tilde{z}_i > 0$ for all $i \in [n]$. This completes the proof. □

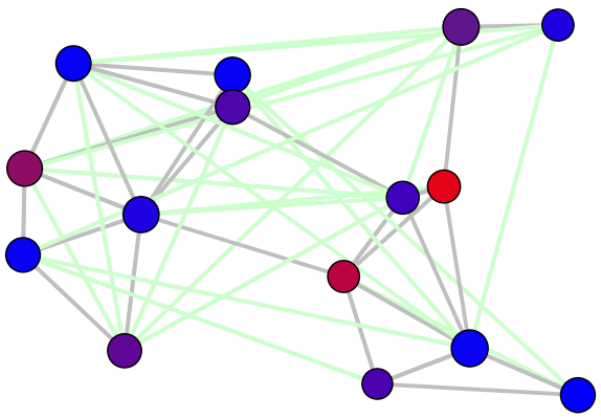

Figure 4.12: The final state of heterogeneous simulations with $s(-D^1 + B^1) = 1.4904$ and $s(-D^2 + B^2) = 2.2243$ and $\epsilon = 0.1$, for any initial condition that begins with both viruses being nonzero.

It turns out that the further analysis of the case when $s(B^1 - D^1), s(B^2 - D^2) > 0$ is very challenging, and we study it by extensive simulations in the next section, which show that coexistence of the two viruses may occur and that the behavior of the system defined by (4.24)-(4.26) depends on threshold values of ϵ.

4.7.3 Coupled Bi-Virus Simulations

In this section, we present a set of illuminating simulations of various coupled virus models. Virus 1 is depicted by the color red (r), virus 2 is depicted by the color blue (b), and the state of being infected with both states, $z(t)$, is depicted by the color green (g). For all $i \in [n]$, the color at each time t for node i is given, similar to (4.15), by

$$\frac{p_i^1(t)}{s_i(t)}r + \frac{p_i^2(t)}{s_i(t)}b + \frac{z_i(t)}{s_i(t)}g, \tag{4.37}$$

where $s_i(t) = p_i^1(t) + p_i^2(t) + z_i(t)$. When $p_i^1(t) + p_i^2(t) + z_i(t) = 0$, the color is black, indicating completely healthy, susceptible. These color variations are used to facilitate the depiction of the parallel equilibria ($\tilde{p}^1 = \alpha\tilde{p}^2$), a behavior that is exhibited by the $\epsilon = 0$ case (see [33]) and are illustrated by all the nodes converging to the same color. For all $i \in [n]$, the diameter of node i is given by

$$d_0 + s_i(t)r_0, \tag{4.38}$$

with d_0 being the default/smallest diameter and r_0 being the scaling factor depending on the total sickness of node i. Therefore, the color indicates the type of virus(es) each agent has and the diameter indicates the degree of sickness for each agent. The graph structure follows (3.25) with $\hat{r} = .35$.

For the first set of simulations, we have two heterogeneous viruses spreading on different graphs. Virus 1 spreads on the gray edges and virus 2 spreads on the green edges. We have $s(-D^1 + B^1) = 1.4904$ and $s(-D^2 + B^2) = 2.2243$. Independent of the initial condition (as long as both viruses are nonzero), the system always converges to the equilibrium in Figure 4.12. The behavior also appears to be independent of ϵ, that is, both viruses survive for any value of $\epsilon \in (0, 1)$ (however to different equilibria for each ϵ value). This leads to the following conjecture and remark.

Conjecture 1. *Suppose that $\epsilon \in (0, 1)$ and Assumptions 6 and 7 hold. If $s(B^1 - D^1) > 0$ and $s(B^2 - D^2) > 0$,*

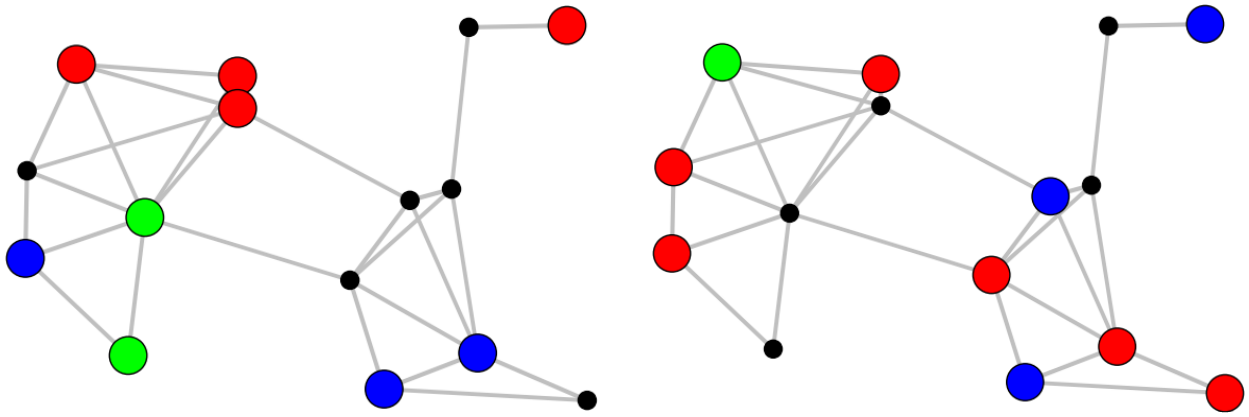

(a) First initial condition

(b) Second initial condition

Figure 4.13: These are the initial conditions for the simulations. The colors and diameters follow (4.37) and (4.38) and the graph structure follows (3.25) with $\hat{r} = .35$.

then there exists an $\epsilon_{\text{critical}} \in (0,1)$ *such that if* $\epsilon > \epsilon_{\text{critical}}$*, the system defined in (4.24)-(4.26) has at least one endemic equilibrium* (p^{1^*}, p^{2^*}, z^*) *with* $p^{1^*}, p^{2^*}, z^* \gg \mathbf{0}$*, and* z^* *is unique.*

Remark 9. *Simulations suggest that if the assumptions of Conjecture 1 are met and the viruses spread on two different spreading graphs (i.e.,* $\mathcal{N}_i^1 \neq \mathcal{N}_i^2$ *for at least one* $i \in [n]$*), then the endemic equilibrium* (p^{1^*}, p^{2^*}, z^*)*, with* $p^{1^*}, p^{2^*}, z^* \gg \mathbf{0}$*, is unique, and the system defined by (4.24)-(4.26) asymptotically converges to* (p^{1^*}, p^{2^*}, z^*) *for any initial condition in* $\mathcal{D} \setminus \mathcal{F}$*, where* $\mathcal{F} = \{\{(p^1, \mathbf{0}, \mathbf{0}) | p^1 \in [0,1]^n\} \cup (\mathbf{0}, p^2, \mathbf{0}) | p^2 \in [0,1]^n\} \cup \{(\mathbf{0}, \mathbf{0}, \mathbf{0})\}$.

If the two viruses spread on the same graph, that is, $\mathcal{N}_i^1 = \mathcal{N}_i^2$ *for all* $i \in [n]$*, the behavior of the system can change drastically. In certain cases, the endemic equilibrium of the form* (p^{1^*}, p^{2^*}, z^*)*, with* $p^{1^*}, p^{2^*}, z^* \gg \mathbf{0}$*, is no longer unique. However,* z^* *is still unique. This behavior will be illustrated by the next set of simulations.* □

Note that for homogeneous viruses (i.e., $\delta_i^1 = \delta^1$ and $\delta_i^2 = \delta^2$ for all $i \in [n]$, and $\beta_{ij}^1 = \beta^1$ and $\beta_{ij}^2 = \beta^2$ for all $i, j \in [n]$) spreading on the same graph (i.e., $\mathcal{N}_i^1 = \mathcal{N}_i^2$ for all $i \in [n]$), the system dynamics can be written as

$$\dot{p}^1(t) = -\delta^1 p^1(t) + \delta^2 z(t) + (I - P^1(t) - P^2(t) - Z(t))\beta^1 A(p^1(t) + z(t)) - \epsilon P^1(t)\beta^2 A(p^2(t) + z(t)), \quad (4.39)$$

$$\dot{p}^2(t) = -\delta^2 p^2(t) + \delta^1 z(t) + (I - P^1(t) - P^2(t) - Z(t))\beta^2 A(p^2(t) + z(t)) - \epsilon P^2(t)\beta^1 A(p^1(t) + z(t)), \quad (4.40)$$

$$\dot{z}(t) = -(\delta^1 + \delta^2) z(t) + \epsilon P^1(t)\beta^2 A(p^2(t) + z(t)) + \epsilon P^2(t)\beta^1 A(p^1(t) + z(t)), \quad (4.41)$$

where A is the adjacency matrix depicting the nearest-neighbor graph structure.

In the case of homogeneous viruses, $B^k = \beta^k A$ and $D^k = \delta^k I$ for each $k \in \{1, 2\}$. Thus, condition $s(B^k - D^k) > 0$ simplifies to $s(A) > \frac{\delta^k}{\beta^k}$, $k \in \{1, 2\}$.

For the next set of simulations, we have both viruses spreading on the same graph and use the two initial conditions in Figure 4.13. For the first set of simulations, we assume homogeneous spread with $\beta = 0.8145$ and $\delta = 0.8523$ for both viruses. With $\epsilon = 0.5$, using either initial condition the system converges to the same equilibria, shown in Figure 4.14. It appears, via simulation, that if ϵ is sufficiently far from zero, then the epidemic state is unique.

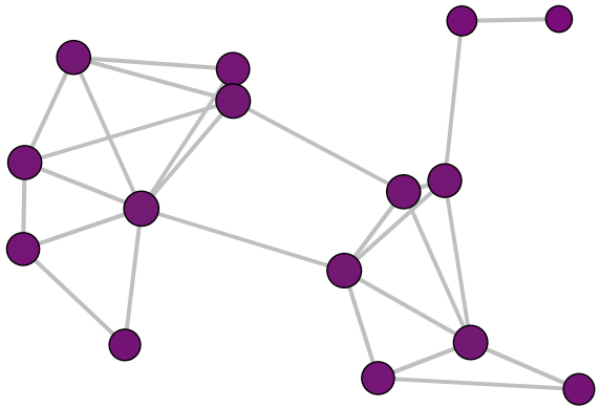

Figure 4.14: The final state of simulations with $\beta = 0.8145$ and $\delta = 0.8523$ for both viruses and $\epsilon = 0.5$, using either initial condition in Figure 4.13.

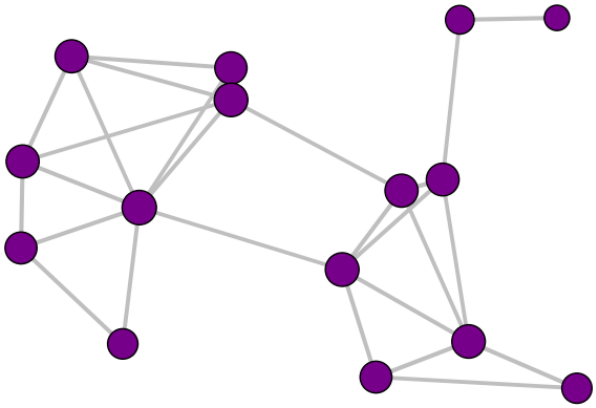

(a) Using Figure 4.13a as an initial condition

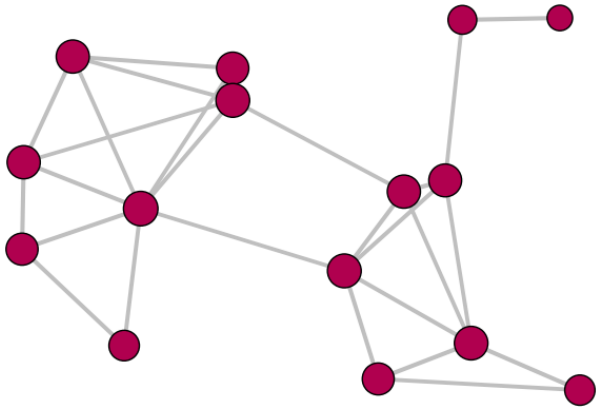

(b) Using Figure 4.13b as an initial condition

Figure 4.15: These are the endemic equilibria using the same parameters as Figure 4.14 except with $\epsilon = 0$.

Using the same parameters as above but setting $\epsilon = 0$ drastically changes the behavior. As was shown in (4.28)-(4.30), this essentially reduces to the competitive bi-virus case. So for the given parameters, the system reduces to the case of Theorem 7 of [33] (or similarly Theorem 14 herein with $m = 2$), which means that there are many endemic parallel equilibria, shown in Figure 4.15. Using the initial conditions in Figure 4.13, the endemic equilibria states are different. Note that every node is the same color, illustrating the parallel behavior. Note that $z_i^* = 0$ for all i. Also, note that the diameter of each node is equal for the two initial conditions, indicating that each node has the same amount of total sickness, just different proportions of the different states, that is, s_i^* is independent of initial condition.

By Theorem 5 in [33], in the competitive bi-virus case (i.e., $\epsilon = 0$) with two homogeneous viruses spreading on the same graph, both viruses will survive only if $s(A) > \frac{\delta_1}{\beta_1} = \frac{\delta_2}{\beta_2}$. However, with $\epsilon = 0.5$, setting $\beta_1 = 0.8145$ and $\delta_1 = 0.8523$, and $\beta_2 = 0.8145$ and $\delta_2 = .9\delta_1 = 0.7670$, so that $s(A) > \frac{\delta_1}{\beta_1} > \frac{\delta_2}{\beta_2}$, both viruses still survive. See Figure 4.16a for the endemic equilibria. However, if ϵ is small but not zero, the second virus can still dominate, driving out the first virus. This behavior is depicted in Figure 4.16b, where $\epsilon = 0.1$. Therefore, for ϵ sufficiently away from zero, viruses that would drive out weaker viruses in the purely competitive case can coexist. There appears to be a threshold, where, if ϵ is larger than it, both

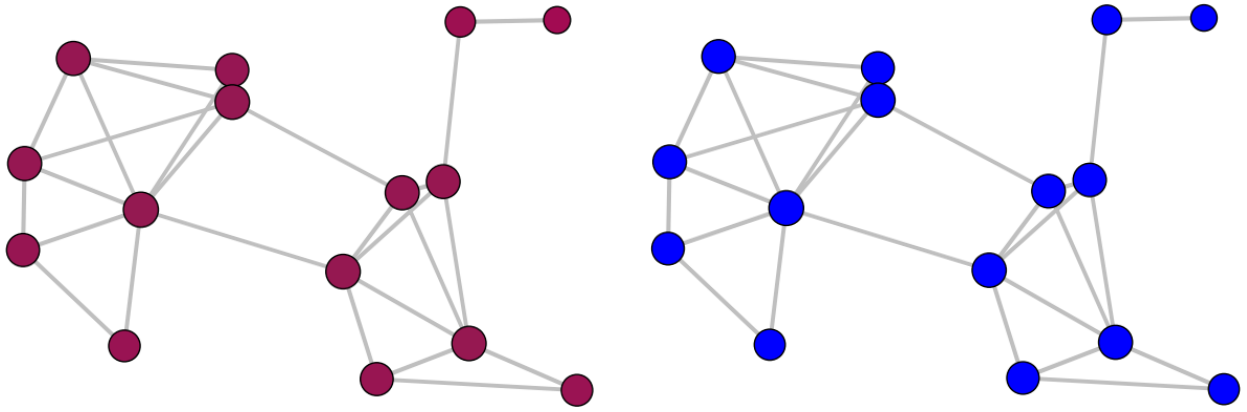

(a) $\epsilon = 0.5$ (b) $\epsilon = 0.1$

Figure 4.16: The final states of simulations with $\beta_1 = 0.8145$ and $\delta_1 = 0.8523$, and $\beta_2 = 0.8145$ and $\delta_2 = 0.7670$, using either initial condition in Figure 4.13.

viruses can survive even if $s(A) > \frac{\delta_1}{\beta_1} > \frac{\delta_2}{\beta_2}$, consistent with Theorem 1 in [71] for the group model with trivial graph structure. This leads to the following conjecture.

Conjecture 2. *Suppose that* $\epsilon \in (0,1)$ *and Assumptions 1 and 7 hold. If* $s(A) > \frac{\delta^1}{\beta^1} > \frac{\delta^2}{\beta^2}$, *then there exists an* $\epsilon_{\text{critical}} \in (0,1)$ *such that if* $\epsilon > \epsilon_{\text{critical}}$, *the system in* (4.39)-(4.41) *has a unique endemic state* (p^{1^*}, p^{2^*}, z^*), *with* $p^{1^*}, p^{2^*}, z^* \gg \mathbf{0}$, *to which the system asymptotically converges for any initial state in* $\mathcal{D} \setminus \mathcal{F}$, *with* $\mathcal{D}$ *defined in* (4.27) *and* $\mathcal{F} = \{(\mathbf{0}, p^2, \mathbf{0}) | p^2 \in [0,1]^n\} \cup \{(p^1, \mathbf{0}, \mathbf{0}) | p^1 \in [0,1]^n\} \cup \{(\mathbf{0}, \mathbf{0}, \mathbf{0})\}$.

If $\epsilon \leq \epsilon_{\text{critical}}$, virus 2 drives out virus 1, resulting in an equilibrium of the form $(\mathbf{0}, p^{2^*}, \mathbf{0})$. This behavior is illustrated in Figure 4.16b.

Chapter 5

Control of Virus Spread

In this chapter we explore several control techniques for mitigating virus spread in networks, appealing to theorems from previous chapters. The majority of this work has been published or is being prepared for submission in [7, 19, 49, 50, 51] and is used here with permission.

5.1 Background

Various control techniques have been applied to SIS virus systems [13, 14, 23, 57, 4, 5, 84]. These techniques regard the healing rate as a control variable. In [13], geometric programming ideas are used to control single SIS virus systems and the authors present a polynomial time algorithm illustrated on an air transportation network. In [57], ideas similar to [13] are applied to the bi-virus model. In [14], a network control technique is applied to a discretized, linearized version of the model from [6]. In [23], it is shown that there exists no distributed linear feedback control that can stabilize the system, and in fact, such a control structure will destabilize the system. Alternative approaches focus on reducing the maximum eigenvalue of the linearized system using the healing rate and/or the infection rate. In [4, 5], distributed control techniques for setting healing rate and quarantine protocols are proposed and implemented on a severe acute respiratory syndrome (SARS) simulation model. In [84], a bound is provided for the cost of fairness of mitigating the spread of disease, that is, the difference between the optimal solution and the fair or homogeneous solution, for several classes of graphs. In [85], distributed optimization techniques are used to solve several formulations of curing resource allocation problems.

5.2 Quarantine

If the system is too dense then the agents can be partitioned into distinct groups, spatially bounding them to separate regions. This technique is called a quarantine [4, 86], and is reflected in the model by removing edges in the graph, i.e. setting specific elements of the A matrix to zero. The quarantine essentially imposes a block diagonal structure on the A matrix, given that the states are properly ordered; this restricts interaction between certain agents, which can clearly reduce the spread of a virus.

A quarantine is difficult to implement, as was witnessed recently with the Ebola virus [87]. A quarantine could also be effected by less costly implementations, such as decreasing human contact via limiting handshakes and other greetings, instilling good habits of covering mouths, etc. Without restricting movement, these measures would decrease the weight of the links between agents, which would be reflected in the model by decreasing the values of a_{ij}.

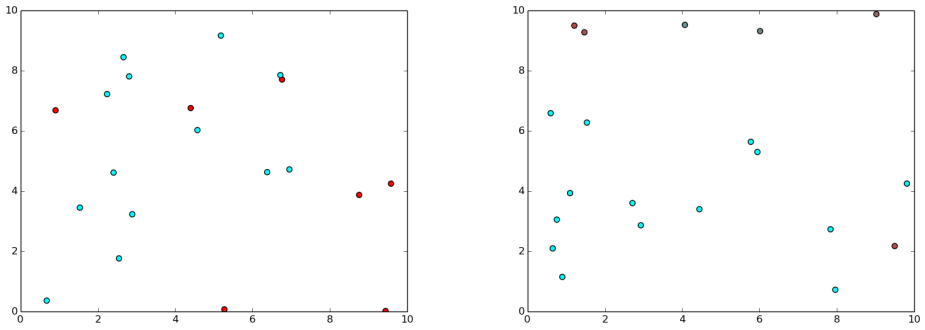

(a) The system at time zero.

(b) The system at time 400.

Figure 5.1: This system has piece-wise constant drift for each node and evolves for 400 time steps. After 50 time steps a quarantine is implemented, limiting the agents to certain regions. This separates the sick and the immuno-compromised from the other agents. For a video of this simulation please see youtu.be/NfskXS83FHI.

For the following discussion we assume A is symmetric. If the a_{ij}'s can be restricted such that, for $\epsilon_i < 0$,

$$\sup_{t\geq 0} \sum_{i=1}^{n} a_{ij}(t) \leq \epsilon_i + \frac{\delta_i}{\beta} \ \forall i,$$
$$\Rightarrow \beta \sup_{t\geq 0} \sum_{i=1}^{n} a_{ij}(t) - \delta_i \leq \epsilon_i \ \forall i.$$

Therefore, under the above assumption,

$$\sup_{t\geq 0} \lambda_1(BA(t) - D) < 0,$$

by the Gershgorin Disc Theorem [32]. Therefore by Theorem 1 the disease will be eradicated in exponential time.

We can implement a quarantine on the piece-wise constant drift case by imposing a block diagonal structure, limiting the movement of certain agents so that they do not interact with others. Consider a system with 20 agents, originally confined to a 40×40 box with certain random initial conditions (see Figure 5.1a). After 50 time steps a quarantine is imposed, limiting some agents to the region $[0, 25] \times [0, 25]$ and exiling the rest of the agents to the outside boundary. This separates the sick and the immuno-compromised agents from the others. One set of agents is tending towards the DFE and the other is not, which is consistent with the maximum eigenvalue plot in Figure 5.2. Note that the behavior of the maximum eigenvalue of the non-exiled group is consistent with Theorem 5, that is, the average is less than zero. This simulation leads to the following corollary:

Corollary 6. *Imposing a block diagonal graph structure, such that $A(t) = diag(A_1(t), \ldots, A_q(t))$, makes the DFE globally exponentially stable if $\lambda_1(B_l A_l(t) - D_l) < 0$ for all $t \geq 0$ and $l = 1, \ldots, q$, with $B_l = \beta_l I$ and $A(t)$ symmetric, piece-wise continuous in t, and bounded $\forall t \geq 0$.*

Proof. Since $A(t)$ is block diagonal and B and D are diagonal, $p(t)$ can be partitioned into q groups. Then the result follows immediately from applying Theorem 3 to each $\dot{p}_l(t)$. □

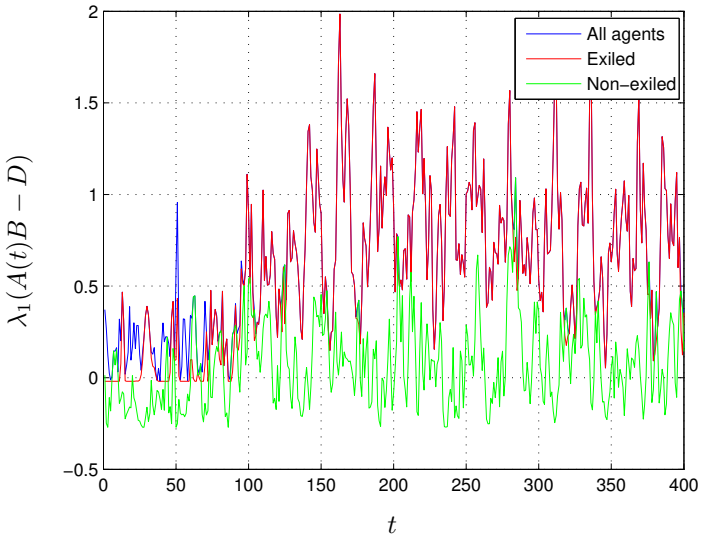

Figure 5.2: The maximum eigenvalues of the system shown in Figure 5.1 are plotted versus time. The blue line is the total system, the red line is the outside (sick) group, and the green line is the inside (healthy) group. Notice the max eigenvalue of the inside group is below zero on average.

This approach does not consider any reintegration process for healed agents. For this to be a feasible, effective control technique, healed agents would have to be allowed to rejoin the general population. Therefore, an agent-by-agent policy could be implemented so that once an agent was healed, i.e. $p_i(t) = 0$ for some t, re-admittance would be permitted, contingent on its remaining healthy during re-entrance.

5.3 Antidote Control Formulation

Let us assume that for each agent, or group (depending on which interpretation of the model is chosen), in addition to the healing rate, there is a control input $u_i(t)$ that acts as an additive boost to the healing rate. This implies that the controller can increase the ability of the agents, or groups, to recover from the virus, which can be thought of as the administration of an antidote or some other type of treatment. This effect is portrayed in the model as

$$\dot{p}_i^k(t) = (1 - p_i^1(t) - \cdots - p_i^m(t)) \sum_{j=1}^{n} \beta_{ij}^k(t) p_j^k(t) - (\delta_i^k(t) + u_i^k(t)) p_i^k(t).$$

We define $U^k(t) = \text{diag}(u^k(t))$ with $u^k(t) = [u_1^k(t), \ldots, u_n^k(t)]^\top$. To simplify the discussion in this section, we assume, $\forall t \geq 0$, that $B^k(t)$ is symmetric and that $B^k(t)$ and $D^k(t)$ are piece-wise continuous in t and bounded. Similar to the approaches in [4, 5, 84, 13, 14], we focus on minimizing the maximum eigenvalue of $B^k(t) - (D^k(t) + U^k(t))$. Even though these control techniques are generally effective, we believe the approaches herein are more general and simpler, and therefore more scalable. Also, the assumption that our control input is additive to the base healing rate is novel and more sensible for the main motivating example, that is, every agent, or group, should have some inherent healing rate that should not be affected by the controller.

While the solutions to the following posed problems may not meet the conditions of Theorems 3 and 12 and Corollary 2, that is, they may not result in the maximum eigenvalues being less than zero, they push the system towards those conditions, consistent with the principle of the average being less than zero, presented in Theorem 5 and Corollary 4. And in practice, illustrated by simulation in the next section, these techniques reduce the spread of the epidemics. Under the aforementioned assumptions we can formulate the following optimization problem for each virus k, appealing to Theorems 3 and 12 and Corollary 2 depending on whether B^k and D^k are constant or time dependent:

$$\begin{aligned} \underset{u_i^k(t)}{\textit{minimize}} \quad & \lambda_1(B^k(t) - (D^k(t) + U^k(t))) \\ \textit{subject to} \quad & \sum_{i=1}^{n} u_i^k(t) \leq c^k, \quad t \geq 0, \\ & U^k(t) = \text{diag}(u_1^k(t), \ldots, u_n^k(t)), \\ & u_i^k(t) \geq 0, \quad i = 1, \ldots, n, \ t \geq 0, \end{aligned}$$

given that $B^k(t)$ is symmetric for all $t \geq 0$. Note that if B^k and D^k are constant then this problem only needs to be solved once. However, if the system is time–varying then the problem must be solved heuristically over time to update the control inputs.

From the Gershgorin Disc Theorem [32] it is clear that by sufficiently increasing the u_i^k's, the conditions of Theorems 3 and 12 and Corollary 2 will be satisfied. Therefore, we can relax the above optimization problem to obtain the following:

Problem 1.

$$\begin{aligned} \underset{\eta^k, u_i^k(t)}{\textit{minimize}} \quad & \eta^k \\ \textit{subject to} \quad & \eta^k \geq \sum_{j=1}^{n} \beta_{ij}^k(t) - (\delta_i^k(t) + u_i^k(t)), \ i = 1, \ldots, n, \\ & \sum_{i=1}^{n} u_i^k(t) \leq c^k, \\ & u_i^k(t) \geq 0, \quad i = 1, \ldots, n, \ t \geq 0. \end{aligned}$$

This is clearly a linear program and can easily be solved.

To make this a more compelling and realistic problem, we can impose a constraint on the number of agents, or groups, that can be affected, which is a reasonable assumption because the cost of providing a low-dose treatment to all agents, or groups, is higher than that of providing that same amount of total treatment divided among a few select members of the population (such as the sickest or most susceptible agents, or groups). Define the sparsity metric $\|\cdot\|_0$ as the number of the non-zero entries in its argument.

Employing the sparsity metric, we have the following problem, with a capacity constraint and a sparsity

constraint:

$$\begin{aligned}
\underset{\eta^k, u_i^k(t)}{\textit{minimize}} \quad & \eta^k \\
\textit{subject to} \quad & \eta^k \geq \sum_{j=1}^{n} \beta_{ij}^k(t) - (\delta_i^k(t) + u_i^k(t)),\ i = 1, \ldots, n, \\
& \sum_{i=1}^{n} u_i^k(t) \leq c^k, \\
& \|u^k(t)\|_0 \leq d^k, \\
& u_i^k(t) \geq 0, \quad i = 1, \ldots, n,\ t \geq 0,
\end{aligned}$$

where d^k is the maximum number of agents, or groups, that can be treated for virus k. At first glance, the second and third constraints may seem redundant; however, the ℓ_1 constraint limits the total amount of antidote that can be used while the sparsity constraint limits the number of agents, or groups, that can be treated. The inclusion of the ℓ_1 constraint prevents an infinite amount of antidote being administered to the limited number of agents, or groups, allowed by the sparsity constraint.

It is well known that $\|\cdot\|_0$ is highly non-convex [88], making the above problem difficult to solve. Therefore, we employ another relaxation using the reweighted ℓ_1 norm [89].

Definition 6. *The weighted ℓ_1 norm is*

$$\|x^k\|_{\hat{\ell}_1} := \sum_{i=1}^{n} w_i^k |x_i^k|, \tag{5.1}$$

where w_i's are positive and can be a constant or depend on time.

In view of this, we can rewrite the above problem as the following:

Problem 2.

$$\begin{aligned}
\underset{\eta^k, u_i^k(t)}{\textit{minimize}} \quad & \eta^k + \kappa \|u^k(t)\|_{\hat{\ell}_1} \\
\textit{subject to} \quad & \eta^k \geq \sum_{j=1}^{n} \beta_{ij}^k(t) - (\delta_i^k(t) + u_i^k(t)),\ i = 1, \ldots, n, \\
& \sum_{i=1}^{n} u_i^k(t) \leq c^k, \\
& u_i^k(t) \geq 0, \quad i = 1, \ldots, n,\ t \geq 0,
\end{aligned}$$

where κ is a constant weighting factor.

An effective heuristic for the selection of the weights w_i^k's in (5.1), proposed in [89], is, for some small $\epsilon > 0$,

$$w_i^{k+1} = \frac{1}{|x_i^k| + \epsilon}. \tag{5.2}$$

For completeness, we include Algorithm 1, which explains the implementation of this heuristic to solve Problem 2. The notation Problem 2(w_{k-1}) indicates that w_{k-1} is used for the weighted ℓ_1 norm in the objective function of Problem 2 in the kth iteration. Employing this heuristic yields a good solution to Problem 2 but clearly is expensive, since it requires the calculation of multiple solutions.

Algorithm 1: Algorithm for solving Problem 2

$w^0 = vec(\frac{1}{n}, \ldots, \frac{1}{n})$;
$k = 1$;
while $\|u_k - u_{k-1}\| > \varepsilon$ **do**
  $u_k = \arg\min$ Problem 2(w_{k-1});
  $w_i^k = \frac{1}{|u_i^k| + \epsilon}$;
  $k = k + 1$;
end

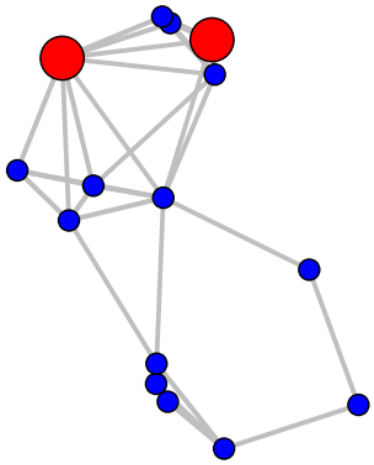

Figure 5.3: Initial condition for systems in Figure 5.4. Note the equilibria shown in Figures 5.4a-5.4c are not initial condition dependent (as long as it is nonzero).

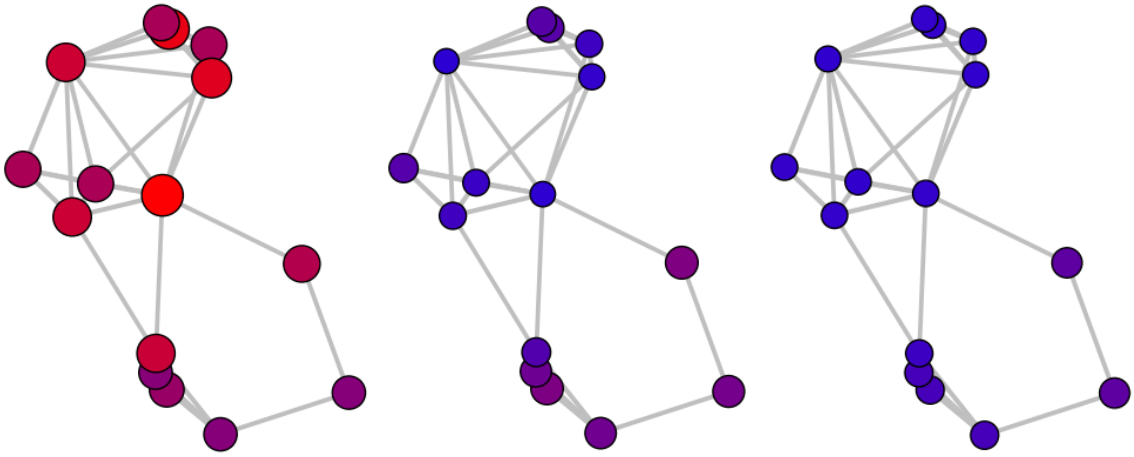

(a) Epidemic equilibrium with no control

(b) Epidemic equilibrium using Problem 1

(c) Epidemic equilibrium using Problem 2

Figure 5.4: Final state with no control, Problem 1, and implementing Algorithm 1 on Problem 2. For a video of this simulation please see youtu.be/MhW95R8s_Po.

Consider the single-virus system in Figure 5.3, with the initial condition shown. This system is homogeneous in infection rate, with $\beta = 0.4592$. We compare the system with no controller (Figure 5.4a), a controller using Problem 1 (Figure 5.4b), and a controller that uses Algorithm 1 to solve Problem 2 iteratively with $\kappa = .05$ (on the right). The sums of the final probabilities of infection for all nodes ($\sum_{i=1}^{n} p_i(100)$) for the three plots are 10.7, 4.92, and 3.6, respectively. Therefore, Algorithm 1 performed the best; however, both had significant improvements over the uncontrolled simulation. The maximum eigenvalues of the three linearized systems are, from left to right, 1.893, 0.557, and 0.421; so none of the linearized systems is Hurwitz. Therefore, consistent with Theorem 11, the systems are all at an epidemic state. However, even though the control efforts do not completely eradicate the virus, they do mitigate its effect. In other simulations Problem 1 outperformed Problem 2.

Chapter 6

Learning and Validation

In this chapter we explore several techniques for estimating the spread parameters of the network dependent, discrete-time spread models introduced in Section 2.2. The majority of the material in this chapter has been published in [28, 90] and is used here with permission.

6.1 Background

While parameter estimation of epidemic spread with real data has been carried out for some models [91, 92, 93, 94], the previous work has either not included network structure or has employed a large probabilistic model. Ignoring network structure is tantamount to making a strong simplifying assumption, and using a full probabilistic model can become very computationally expensive as the size of the network grows [6, 19]. For these reasons we focus on a nonlinear network-dependent ordinary differential equation model. To the best of our knowledge, no work has been done on the estimation of spread parameters from data for these models. Many virus spread papers using these models have claimed to use real data to test their models, but no true validation of non-trivial network-dependent SIS spread models has been done. Those papers that use real data only build the network structure using real data, but do not have real spreading process data over that network. In [4, 5], Wan *et al.* compare their model to a simulator of SARS, not real data. In [95], Chakrabarti *et al.* use a router network from the state of Oregon and simulate an artificial spreading process over that network. To the best of our knowledge, no work has been done that validates network-dependent SIS models using a set of real spread data. Similarly, in [13], Preciado *et al.* use data from an air transportation network but simulate using arbitrarily chosen healing and infection rates. To the best of our knowledge, no work has been done that validates network-dependent SIS models using a set of real spread data.

6.2 Learning Spread Parameters

In this section we provide the assumptions and the identification techniques for several of the models introduced in Section 2.2. We assume that the underlying graph structure A is known and that we have full-state measurement with no noise on the measurements, which we admit are strong assumptions. However, for the second application considered here these assumptions are well-founded because we aggregate the data by county and the adjacency of counties is known, i.e., the graph structure is known, and any farmer that received a subsidy payout is in the dataset, i.e., there are no hidden, unmeasured states.

We present several results on learning the spread parameters of the model in (2.10) from data. For the

reader's convenience we restate the model from (2.10):

$$p_i^{k+1} = p_i^k + h\left((1-p_i^k)\beta_i \sum_{j=1}^{n} a_{ij}p_j^k - \delta_i p_i^k\right).$$

Recall that for the discrete time models the superscript k refers to the time index. When we say *non-trivial* homogeneous virus spread this means that $[\beta\ \delta]', A, h \neq 0$.

Theorem 19. *Consider the model in* (2.10) *with non-trivial homogeneous virus spread and* $n > 1$. *Assume that* A, $p^0, \ldots, p^T$, *and* h *are known. Then, the spread parameters can be learned uniquely if and only if* $T > 0$, *and there exists* $l \in [T]$ *such that* $p^l \neq p^0$.

Proof. Since A, $p^0, \ldots, p^T$, and h are known, using the notation in (2.11) we can construct the matrix

$$\Phi = \begin{bmatrix} h(I - P^0)Ap^0 & -hp^0 \\ \vdots & \vdots \\ h(I - P^{T-1})Ap^{T-1} & -hp^{T-1} \end{bmatrix}. \tag{6.1}$$

Therefore we can rewrite (2.10) as

$$\begin{bmatrix} p^1 - p^0 \\ \vdots \\ p^T - p^{T-1} \end{bmatrix} = \Phi \begin{bmatrix} \beta \\ \delta \end{bmatrix}. \tag{6.2}$$

By the assumption that there exists $l \in [T]$ such that $p^l \neq p^0$, the left-hand side of the equation is nonzero, and by construction the left-hand side is in the range of Φ. This is clearly overdetermined if $T \geq 1$ and $n > 1$; therefore, it will have a unique solution using the pseudo-inverse.

If $T = 0$, then there is only one data point and learning the dynamic spread parameters uniquely is not possible. Similarly, if there does not exist $l \in [T]$ such that $p^l \neq p^0$, then

$$p^0 = \cdots = p^T. \tag{6.3}$$

This would only occur if p^0 were an equilibrium point of (2.10). So by (6.3), we have that the left-hand side of (6.2) equals zero, that is,

$$\begin{bmatrix} p^1 - p^0 \\ \vdots \\ p^T - p^{T-1} \end{bmatrix} = \mathbf{0}. \tag{6.4}$$

By Proposition 4, there are two cases where (6.3) can occur: 1) the healthy state ($p^0 = p^* = \mathbf{0}$) or 2) the endemic state ($p^0 = p^* > \mathbf{0}$).

1) If $p^0 = p^* = \mathbf{0}$, then, by (6.1) and (6.3), $\Phi = 0$. Therefore, by (6.2) and (6.4), β and δ can take any values, that is, they are not unique.

2) If $p^0 = p^* > \mathbf{0}$ then $\Phi \neq 0$. Therefore, by (6.2) and (6.4), $[\beta\ \delta]'$ is in the nullspace of Φ. This implies $[\beta\ \delta]'$ is not unique, unless the nullspace equals $\{\mathbf{0}\}$. If the nullspace equals $\{\mathbf{0}\}$, then $[\beta\ \delta]' = \mathbf{0}$, which is a contradiction because if $[\beta\ \delta]' = \mathbf{0}$, then there is no spread process and therefore there is no endemic state. □

Now we present two corollaries regarding how the ratio of the spread parameters, δ/β, can be recovered. The first covers the case for when h is unknown.

Corollary 7. *Consider the model in* (2.10) *with non-trivial homogeneous virus spread and* $n > 1$. *Assume that* A *and* $p^0, \ldots, p^T$ *are known. Then, the ratio of the spread parameters can be learned uniquely if and only if* $T > 0$ *and there exists* $l \in [T]$ *such that* $p^l \neq p^0$.

Proof. Since h factors out of the right-hand side of (6.1) and is nonzero by the non-trivial virus spread assumption, even if h is not known, a scaled version of β and δ, that is, $h\beta$ and $h\delta$, can be recovered exactly. Therefore the proportion of the two parameters can be found. □

The following corollary shows that the ratio of the spread parameters can be recovered for the heterogeneous case with different δ_i's and β_i's for each agent (and includes the homogeneous case as a special case) if A and the endemic state are known.

Corollary 8. *If* A *and the endemic state,* $p_i^* > 0\ \forall i$, *are known then*

$$\frac{\delta_i}{\beta_i} = \frac{(1 - p_i^*)}{p_i^*} \sum_{j=1}^{n} a_{ij} p_j^*. \tag{6.5}$$

Proof. By replacing p_i^{k+1} and p_i^k in (2.10) with p_i^* we have

$$\delta_i p_i^* = (1 - p_i^*)\beta_i \sum_{j=1}^{n} a_{ij} p_j^*.$$

Since $p_i^* > 0$, we can divide by p_i^* giving the result. □

These corollaries illustrate that under certain conditions, while the exact behavior of the system may not be recoverable, by Proposition 2, the limiting behavior of the system may be determined, following the discussion of the reproduction number R_0 in Section 2.1.2.

If the assumption is made that the underlying spread process is heterogeneous, a result similar to Theorem 19 can be achieved.

Theorem 20. *Consider the model in* (2.10) *with* $n > 1$. *Assume* A, $p^0, \ldots, p^T$, *and* h *are known. Then the spread parameters of node* i *can be learned uniquely if and only if* $T > 0$, *and there exists* $l \in [T]$ *such that* $p_i^l \neq p_i^0$.

Proof. Since A, $p^0, \ldots, p^T$, and h are known, for each i we can construct the matrix

$$\Phi_i = \begin{bmatrix} h(1 - p_i^0) \sum_{j=1}^{n} a_{ij} p_j^0 & -h p_i^0 \\ \vdots & \vdots \\ h(1 - p_i^{T-1}) \sum_{j=1}^{n} a_{ij} p_j^{T-1} & -h p_i^{T-1} \end{bmatrix}. \tag{6.6}$$

Then we have

$$\begin{bmatrix} p_i^1 - p_i^0 \\ \vdots \\ p_i^T - p_i^{T-1} \end{bmatrix} = \Phi_i \begin{bmatrix} \beta_i \\ \delta_i \end{bmatrix}. \tag{6.7}$$

The remainder of the proof follows that of Theorem 19. □

Note that (2.10) and (6.2), for $k = 0, 1, ..., T-1$, are an equivalent reformulation of (6.7).

Learning heterogeneous spread parameters, however interesting, will not help estimate the spread in other areas. Therefore, a homogeneous system should be more informative for some applications. For the Snow dataset in Section 6.4, we will employ the heterogeneous approach, using Corollary 8 and assuming $\beta_i = 1$ for all i. We will employ homogeneous formulation on the USDA dataset in Section 6.5.

Learning the spread parameters of the model in (2.12) is more difficult. Two approaches are attempted herein: 1) try to recover directly, and 2) use the approximation in (2.13) and then compare to the full model to determine how well it approximates the full model. For the first approach,

$$\begin{bmatrix} p_1^1 - p_1^0 \\ \vdots \\ p_n^T - p_n^{T-1} \end{bmatrix} = \hat{\Phi} \begin{bmatrix} \delta \\ \beta \\ \vdots \\ \beta^n \end{bmatrix}, \tag{6.8}$$

where

$$\hat{\Phi} = \begin{bmatrix} -p_1^0 & -(1-p_1^0)\sum_{j=1}^{n} a_{1j}p_j^0 & \cdots & -(1-p_1^0)\prod_{j=1}^{n}(-a_{1j}p_j^0) \\ \vdots & \vdots & & \vdots \\ -p_n^{T-1} & -(1-p_n^{T-1})\sum_{j=1}^{n} a_{nj}p_j^{T-1} & \cdots & -(1-p_n^{T-1})\prod_{j=1}^{n}(-a_{nj}p_j^{T-1}) \end{bmatrix}. \tag{6.9}$$

Note, for the second option, by Observation 2, learning the spread process parameters from (2.10) using (2.13) will be the same as learning those from (6.2) with $h = 1$. These two approaches will be explored in more detail via simulation in the next section.

6.3 Simulations

We present here simulations that implement the parameter estimation results from Section 6.2 to see how they perform in practice with clean and noisy data. While the data used in this section is artificially generated in Matlab, the insights gained from the exercises here contribute towards our approach using the USDA dataset in Section 6.5. We start with learning the spread parameters of (2.10), and then (2.12).

6.3.1 Learning Parameters of Discrete-Time Spread Process

We begin with an evaluation of the system given in (2.10). Consider a system with 40 agents, with a random set of initially infected agents, with $\beta = 1$, $\delta = 0.1$, $h = 0.1$ and the weighting matrix A determined by the agents' relative positions given by (3.25) (but with static positions) with radius $r = 2$ and $i \neq j$. See Figure 6.1 for plots of the initial and final conditions. Assuming the correct value for h and the A matrix are known, using (6.2) exactly recovers β and δ. If only two time-steps are used, the exact spread parameters can be recovered, consistent with Theorem 19. Using (6.2) with an incorrect h value to recover β and δ gives incorrect values for β and δ, but results in the correct proportion between the two, consistent with Corollary

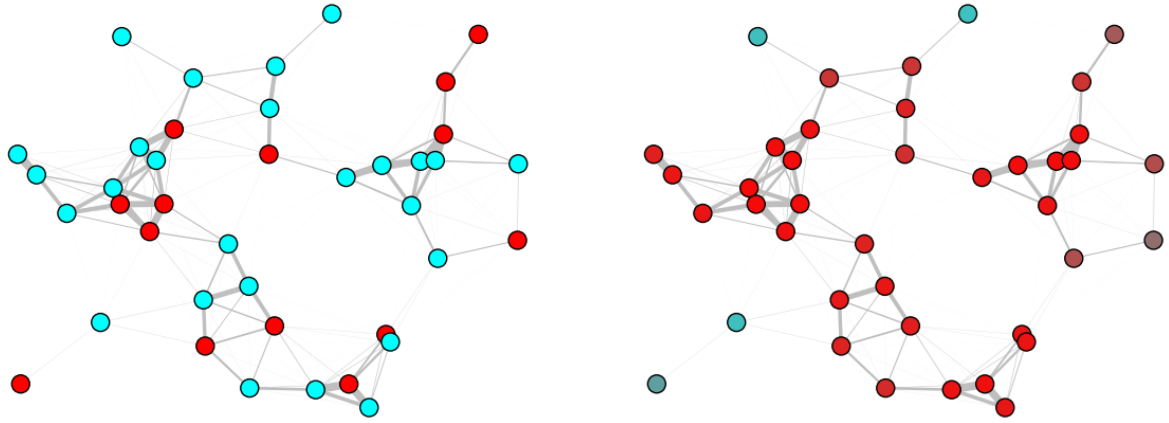

(a) The system at time zero.

(b) The system at time 100.

Figure 6.1: This virus system follows (2.10) with $\beta = 1$, $\delta = 0.1$, $h = .1$, and A depicted by the edges. Teal indicates healthy or susceptible, while red indicates infected. For a video of this simulation please see youtu.be/OxcwOEDiD9Y.

Table 6.1: Averages of 1000 estimates for the spread parameters given zero-mean Gaussian measurement noise with standard deviation σ. The parameters $\hat{\beta}$ and $\hat{\delta}$ are calculated using the noisy data. The parameters $\tilde{\beta}$ and $\tilde{\delta}$ are calculated using the noisy data restricted to the interval [0,1]. Recall the original parameters were $(\beta, \delta) = (1, 0.1)$.

σ	$\hat{\beta}$	$\hat{\delta}$	$\tilde{\beta}$	$\tilde{\delta}$
0.01	1.0473	0.1074	1.0412	0.1064
0.02	1.1840	0.1290	1.1708	0.1269
0.03	1.3976	0.1629	1.3654	0.1587
0.04	1.6645	0.2056	1.5977	0.1984
0.05	1.9679	0.2546	1.8532	0.2441

7. If the system is at the endemic state, the proportion between the spread parameters can be solved for exactly using Corollary 8.

When we add measurement noise

$$y^{k+1} = p^{k+1} + v^{k+1},$$

where y^{k+1} is the measurement, p^{k+1} is from (2.10), and each v_i^{k+1} is an i.i.d. zero-mean Gaussian random variable with standard deviation σ, and use the same learning technique from Theorem 19 the results are not as good. See Table 6.1 for the average values of estimates of β and δ for 1000 runs each, for different standard deviations σ. Future work is required for identification techniques that derive a maximum likelihood type estimator.

We also added zero-mean Gaussian noise to the A matrix as follows:

$$\hat{A} = A + \Delta,$$

Table 6.2: Averages of 1000 estimates for the spread parameters using $\hat{A}$ in (6.10). Recall the original parameters were $(\beta, \delta) = (1, 0.1)$.

σ	$\hat{\beta}$	$\hat{\delta}$
0.01	1.0721	0.0904
0.02	1.1363	0.0817
0.03	1.2012	0.0754
0.04	1.2685	0.0712
0.05	1.3336	0.0678

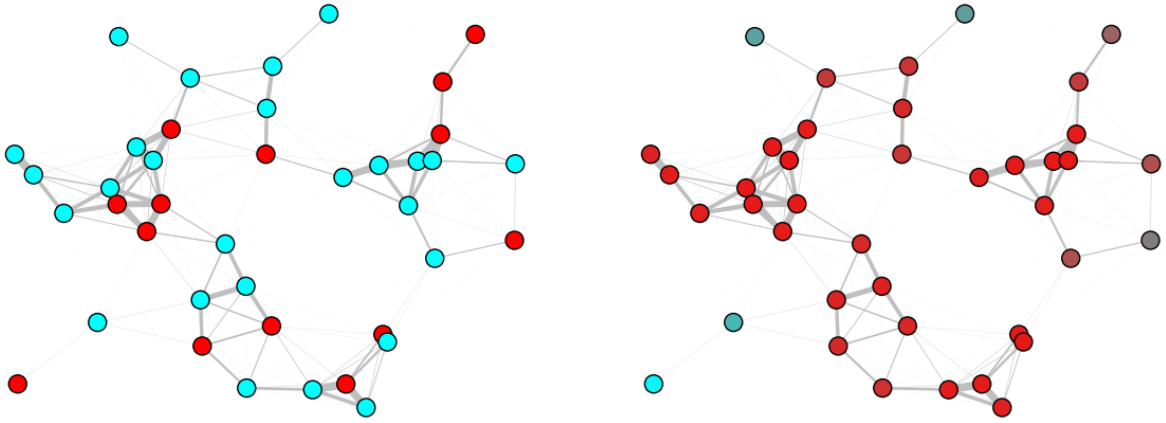

(a) The system at time zero.

(b) The system at time 100.

Figure 6.2: This virus system follows (2.12) with $\beta = 1$, $\delta = 0.1$, and A depicted by the edges. Teal indicates healthy or susceptible, while red indicates infected. For a video of this simulation please see youtu.be/FItrAx_MNGo.

where Δ is a matrix of i.i.d. zero-mean Gaussian random variables. We simulated the system with $\hat{A}'$, where

$$\hat{a}'_{ij} = \begin{cases} \hat{a}_{ij}, & \text{if } \hat{a}_{ij} \in [0, 1], \\ 1, & \text{if } \hat{a}_{ij} > 1, \\ 0, & \text{if } \hat{a}_{ij} < 0. \end{cases} \tag{6.10}$$

The restrictions on $\hat{A}'$ are imposed so that Assumption 2 and 3 are not violated, and the state does not lose its meaning of being the infection probability of an agent or the proportions of infected subpopulations. The average of 1000 runs of learning the spread parameters are given in Table 6.2.

6.3.2 Learning Parameters of Full Probabilistic Discrete-Time Spread Process

Now we will evaluate (2.12) in an attempt to determine how difficult it is to recover the parameters β and δ from data produced by the model first using (6.8), and then using the approximation of (2.13) by solving (6.2). Using the same parameters $(\beta, \delta, A, p^0$, etc.) as in the simulation in Figure 6.1, we simulate (2.12). The results of the simulation are shown in Figure 6.2. As was discussed in Remark 4, if the simulation in Figure 6.1 is an approximation of the system simulated in Figure 6.2, it appears, at least by comparing

Table 6.3: Learning the spread parameters of the system in Figure 6.2, where $\beta = 1$ and $\delta = 0.1$. The top row indicates the number of time steps (T) used to learn the parameters using (6.8).

	2	3	4	5	30
$\hat{\delta}$	0.1	0.1	0.1	0.1	0.1
$\hat{\beta}$	1.0	1.0	1.0	1.0	1.0
$\hat{\beta}^2$	1.0	1.0	1.0	1.0	1.0
$\hat{\beta}^3$	1.0	1.0	1.0	1.0	1.0
$\hat{\beta}^4$	1.0	1.0	1.0	1.0	1.0
$\hat{\beta}^5$	1.0	1.0	1.0	1.0	1.0
$\hat{\beta}^6$	0.9998	1.0	1.0	1.0	1.0
$\hat{\beta}^7$	-0.000	1.0	1.0	1.0	1.0
$\hat{\beta}^8$	0.0000	1.0	1.0	1.0	1.0
$\hat{\beta}^9$	-0.000	0.9974	0.9953	1.0	1.0
$\hat{\beta}^{10}$	0.0000	-0.002	-0.005	0.9974	0.9963
$\hat{\beta}^{11}$	-0.000	0.0000	0.0000	-0.003	-0.004
$\hat{\beta}^{12}$	0.0000	-0.000	-0.000	0.0000	0.0000
$\vdots$	$\vdots$	$\vdots$	$\vdots$	$\vdots$	$\vdots$

the equilibria reached at time 100, as shown in Figures 6.1b and 6.2b, to be a very good approximation, consistent with Section 2.2.2. To show this similarity quantitatively, let the time series data in Figures 6.1a and 6.2a be called p^k and $\tilde{p}^k$, respectively. Then the scaled error between the end states of the two models is given by

$$\frac{\left\|p^T - \tilde{p}^T\right\|}{\|p^T\|} = \frac{0.4479}{5.3233} = 0.0841, \tag{6.11}$$

where $T = 100$, is the last time step of the simulations.

The identification technique proposed in (6.8) is computationally expensive because the matrix can become very large very quickly. Also the powers of the p_j^k's become very small and lead to round-off error. Therefore solving (6.8) becomes more difficult, as more time steps are considered. However, under the assumption of homogeneous virus spread there are only $n+1$ unknowns; therefore only a limited number of time steps are required. See Table 6.3 for the results of using (6.8) on the system in Figure 6.2. Note that for even two time steps the parameters,

$$\begin{bmatrix} \delta \\ \beta \end{bmatrix} = \begin{bmatrix} 0.1 \\ 1.0 \end{bmatrix}, \tag{6.12}$$

are identified exactly up to the fifth power of β. Even without noise this seems somewhat surprising.

Remark 10. *Note that the difference between the results in Table 6.3 derived using 4 time steps and 30 time steps is almost negligible. This gives one reason to believe that even with limited data (since the USDA dataset is yearly and only includes four years of data) learning the spread process parameters may be possible.*

Using the approximation of the model given in (2.13) on this data gives similar results. The parameters were learned by using (6.2) with $h = 1$; the results are found in Table 6.4. While the results are not as good as those of the full model technique in (6.8), they are much less computationally expensive since Φ in (6.1) has significantly fewer columns than $\hat{\Phi}$ in (6.9) and provide a fairly good approximation of the true system. The approximate learning of the spread parameters combined with the small error shown in (6.11) support

Table 6.4: Learning the spread parameters of the system in Figure 6.2, where $\beta = 1$ and $\delta = 0.1$, using the approximation of the system in (2.13). The top row indicates the number of time steps (T) used to identify the parameters using (6.2) with $h = 1$.

	2	3	4	5	30	100
$\hat{\delta}$	0.1000	0.1128	0.1172	0.1189	0.1104	0.0878
$\hat{\beta}$	0.7871	0.7743	0.7730	0.7732	0.7061	0.5615

Table 6.5: Learning the spread parameters of the system, similar to Table 6.3, except where $\beta = 0.5$ and $\delta = 0.1$, and we truncate the table. The top row indicates the number of time steps (T) used to learn the parameters using (6.8).

	2	3	4	5	30
$\hat{\delta}$	0.1	0.1	0.1	0.1	0.1
$\hat{\beta}$	0.5	0.5	0.5	0.5	0.5
$\hat{\beta}^2$	0.25	0.25	0.25	0.25	0.25
$\hat{\beta}^3$	0.125	0.125	0.125	0.125	0.125
$\hat{\beta}^4$	0.0625	0.0625	0.0625	0.0625	0.0625
$\hat{\beta}^5$	0.0313	0.0312	0.0312	0.0312	0.0312
$\hat{\beta}^6$	0.0156	0.0156	0.0156	0.0156	0.0156
$\hat{\beta}^7$	0.0078	-0.000	0.0078	0.0078	0.0078
$\hat{\beta}^8$	0.0039	0.0000	0.0039	0.0039	0.0039
$\hat{\beta}^9$	0.0020	-0.000	0.0017	0.0020	0.0019
$\hat{\beta}^{10}$	0.0009	0.0000	-0.000	-0.000	-0.000
$\hat{\beta}^{11}$	0.0005	-0.000	0.0000	0.0000	0.0000
$\hat{\beta}^{12}$	0.0002	0.0000	-0.000	-0.000	0.0000
$\vdots$	$\vdots$	$\vdots$	$\vdots$	$\vdots$	$\vdots$

the hypothesis stated in Remark 4 that the model in (2.13) is a good approximation of (2.12). Adding more data allows more round-off error to affect the problem, leading to worse identification. Note in Table 6.4 that using the complete dataset of 100 time steps gives spread process parameters that are much further from the true parameters if fewer than 100 time steps are used. This outcome is logical since at time step 30 the system is very close to the equilibrium; therefore adding more data will not contribute any new information because the corresponding rows of the left-hand side of (6.2) will be practically equal to zero.

One may reason that using only two time steps gives the best solution is because $\beta \not< 1$; i.e., more time steps allow the terms with higher powers of β to have greater effect. However this is not the case; consider the system where everything is the same as the simulation in Figure 6.2, except $\beta = 0.5$. The results are found in Tables 6.5 and 6.6, and are very similar to those of the $\beta = 1$ case.

6.4 Validation: Snow Dataset

Now we employ the seminal cholera dataset collected by John Snow [96] (see Figure 6.3) for validation of the model in (2.10).

Table 6.6: Learning the spread parameters of the system, similar to Table 6.4, except where $\beta = 0.5$ and $\delta = 0.1$. The top row indicates the number of time steps (T) used to identify the parameters using (6.2).

	2	3	4	5	70	100
$\hat{\delta}$	0.1000	0.1022	0.1039	0.1050	0.1002	0.0967
$\hat{\beta}$	0.4436	0.4367	0.4346	0.4338	0.4025	0.3884

(a) Statue of Broad Street Pump with the handle removed, in the Soho District of London, installed in July 2018

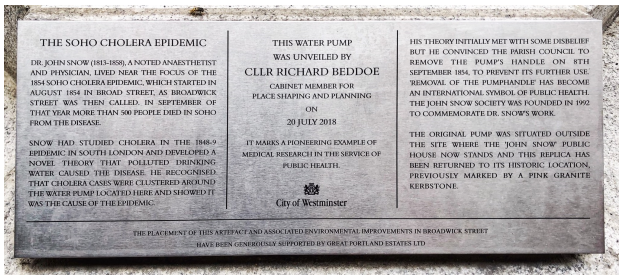

(b) Plaque underneath the pump statue

(c) Pub that bears John Snow's name

Figure 6.3: Tributes to John Snow in the Soho District London on Broadwick Street, formerly known as Broad Street. These pictures were taken when I was presenting the work from this section at the workshop *epiDAMIK: Epidemiology meets Data Mining and Knowledge Discovery, ACM SIGKDD 2018*.

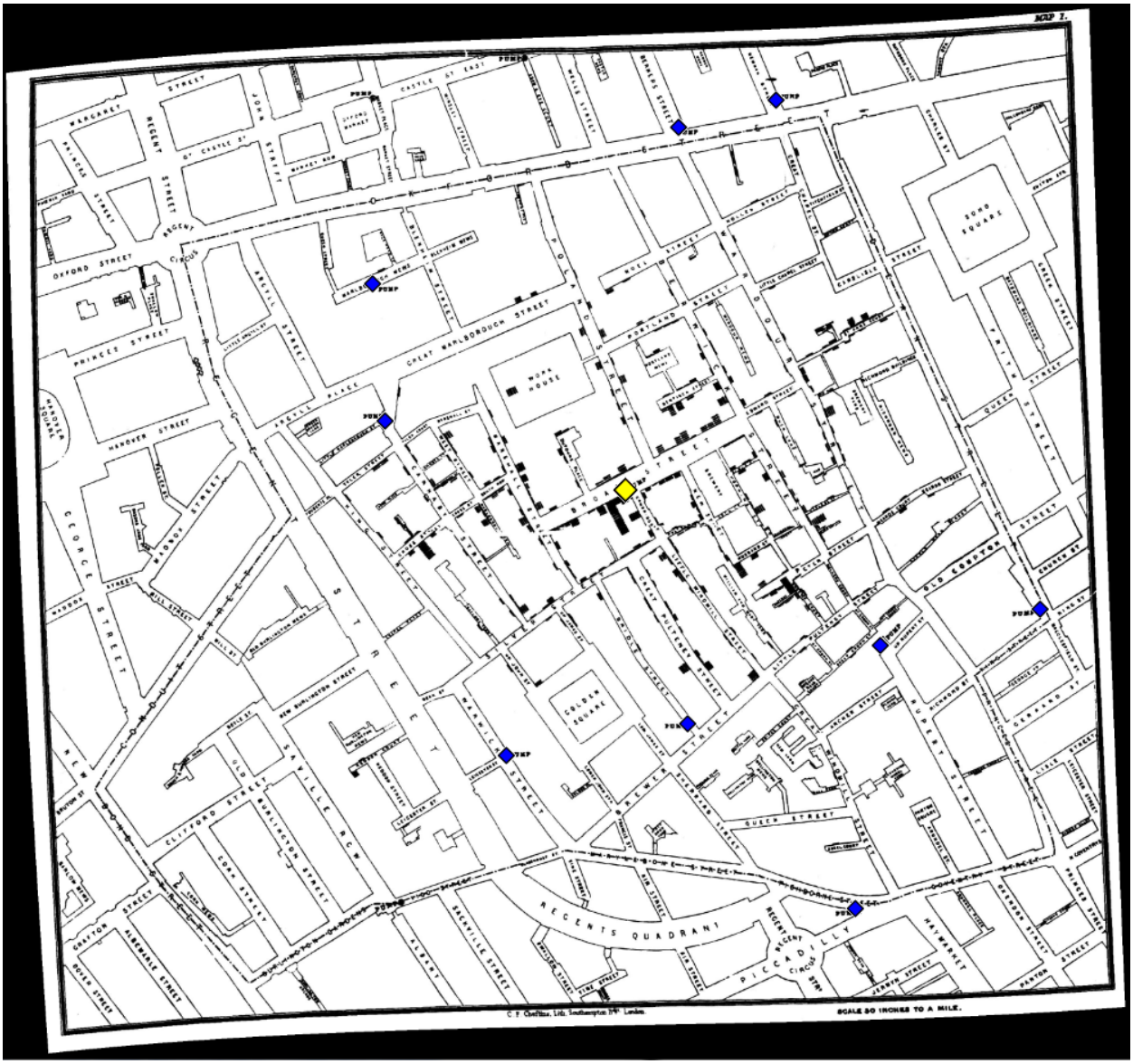

Figure 6.4: Map of cholera spread in London in 1854 compiled by John Snow [96]: healthy water pumps, the contaminated pump, and household deaths are depicted by blue diamonds, the yellow diamond, and black rectangles, respectively.

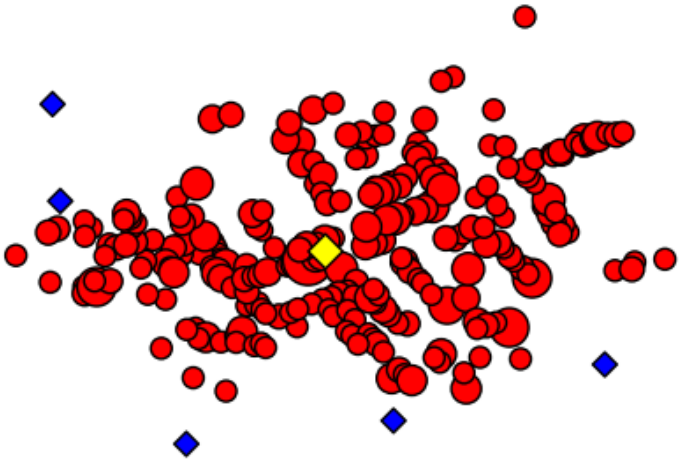

Figure 6.5: Digitization of Figure 6.4: The healthy water pumps, the contaminated pump, and the deaths are depicted by blue diamonds, the yellow diamond, and red dots with the diameters scaled by the number of deaths, respectively.

6.4.1 Snow Dataset

In the mid 19th century cholera was devastating many parts of the world; the outbreaks were especially severe in London. Dr. John Snow (Figure 6.3c) had been studying the disease for several years and devised a theory that the bacteria was spreading from contaminated water pumps instead of through the air, as was thought at the time. To illustrate this theory Snow depicted the number of deaths per household caused by cholera in the Soho District of London in 1854 on a map of the area. In Figure 6.4, the map is shown, where each small rectangle corresponds to one death at that address. Snow created this map to convince the officials that the cholera epidemic was being spread by polluted water from the Broad Street pump, and not through the air, as was the common belief of those times. After some initial reluctance the officials removed the pump handle (Figure 6.3a) and the epidemic stopped within a couple days.

We have plotted the data from the map in Figure 6.5, with diamonds indicating the water pumps and red dots indicating deaths. The dataset is comprised of 250 households with at least one death. Snow also documented the cumulative deaths per day in Table I of [96], plotted in Figure 6.6. The times of death for each address are not recorded. Note that the total cumulative deaths is 616, but the total number of deaths on the map is 489. Therefore, there is a discrepancy of 127 deaths, whose household addresses are not included in the map. For validation of the model in (2.10) we use the proportion of deaths in the households as the state of the disease spread system.

6.4.2 Spread Validation

For the validation, we consider three cases: 1) allowing cholera to spread through the air via nearest neighbor connection, 2) incorporating nearest neighbor connections and direct connections from the Broad Street pump, and 3) only allowing the pump to affect every relevant household. We make various assumptions in order to employ the model in (2.10). Each household with a death recorded by Snow in the map in Figure 6.4 corresponds to a node in the model. The last node in the model corresponds to the contaminated pump, the one on Broad Street, and we do not include the healthy water pumps in the model. We realize that ignoring

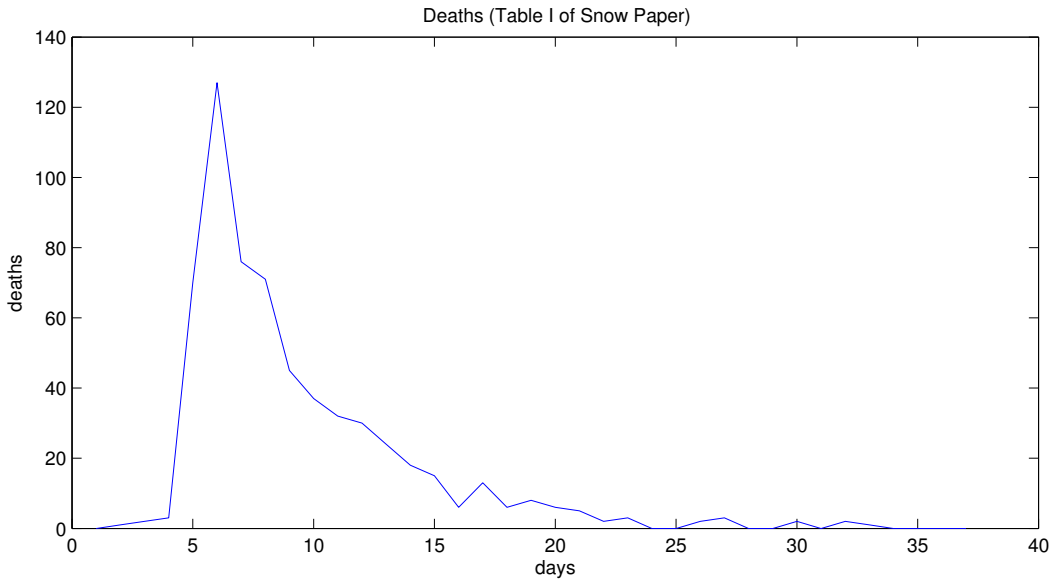

Figure 6.6: Deaths per day in the Soho District of London in 1854 compiled by John Snow [96].

the households with no recorded deaths and ignoring the healthy pumps are nontrivial assumptions. However, as was noted by Snow, many residents fled the city once they became aware of the outbreak [96]. For the households that did not flee, we assume they either had such a high healing rate that their inclusion would have been trivial and/or that these households exclusively drank from another pump and did not closely associate with neighbors who did drink from the Broad Street pump, and therefore were disconnected from the graph of interest. Despite these (and subsequent) relatively strong assumptions, the validation results are quite promising.

The state of the system, p^k, is the proportion of total deaths in each household up to time k. The three validation cases mentioned above, where we attempt to capture the behavior of the epidemic, use different graph structures and different household sizes to calculate the epidemic equilibrium.

The epidemic equilibrium of the system, which we call p^*, was calculated from the data in Figure 6.5, for the first two attempts, by dividing the total number of deaths in each household by 20, and therefore assuming that each household has 20 members. This number was chosen because the maximum number of deaths was 15. For the third attempt we approximated the household sizes using Figure 1 in [97]; see Table 6.7. We divide the total numbers of deaths in each household by these household sizes to obtain p^* for the third case. The last element of p^*, corresponding to the pump, was set to $\frac{19}{20}$ (alternatively, setting it to 1 makes the corresponding δ_i equal zero, which is clear by Corollary 8, and only slightly changes the rest of the estimated spread parameters).

We employed Corollary 8 to calculate the $\frac{\delta_i}{\beta_i}$ values. Then for simulation we set $\beta_i = 1$ for all i and chose h as large as possible while still meeting Assumption 3 (we wanted a large sample parameter h because a larger h makes the system evolve more quickly, and therefore makes a single time step be closer to a full day). Recall the Broad Street pump corresponds to the last agent in the model (agent n). For the initial condition in the simulations, we began with the Broad Street pump infected and all the households healthy:

$$p^0 = \begin{bmatrix} 0 & \dots & 0 & 1 \end{bmatrix}^\top. \tag{6.13}$$

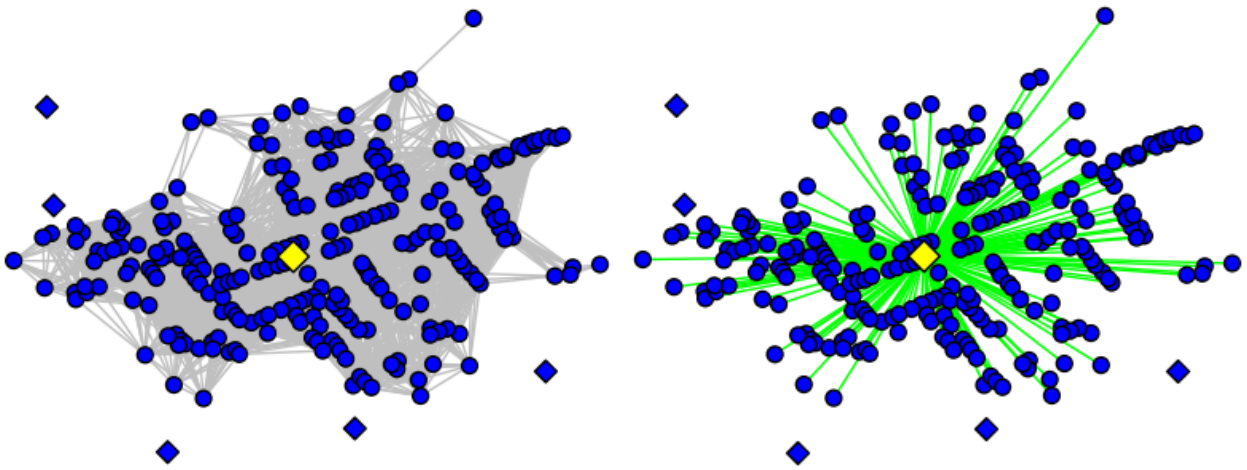

(a) $A^{(1)}$ from (6.14) (b) $A^{(3)}$ from (6.16)

Figure 6.7: Initial condition of simulations with graph structures: blue circles indicate healthy households and the yellow diamond indicates the infected pump. Note that $A^{(1)}$ and $A^{(3)}$ are portrayed, and that $A^{(2)}$ is the result of the union of the two sets of edges.

This initial condition is shown in Figure 6.7, where the contaminated pump is depicted as a yellow diamond. As a consequence of these assumptions, our tuning parameter for adjusting the learned δ_i parameters, and consequently the spread behavior, was the connectivity matrix A.

For the case that captures the general belief of the era, that cholera spreads through the air, we chose a graph structure that allows for local mixing. That is, we designed $A^{(1)}$ such that

$$a_{ij}^{(1)} = \begin{cases} 1, & \text{if } \|z_i - z_j\| < r, \\ 1, & \text{if } i = j, \\ 0, & \text{otherwise,} \end{cases} \tag{6.14}$$

where z_i is the location of household i and r was smallest number such that the graph was connected (shown in Figure 6.7a). Using the δ_i parameters derived from $A^{(1)}$, we simulated the system, using (2.10). To meet the constraints of Assumption 3, we had to set $h = \frac{1}{175}$. This simulation resulted in the distribution of deaths shown in Figure 6.8; this plot was created by multiplying the state of the system, i.e., the percentage of deaths in each household up to that point, by the household sizes (assumed to be 20), rounding to the nearest integer, taking the difference between the states of each time step (since the state represents cumulative number of deaths up to that point), and then summing every three time series points (due to the small h value), therefore assuming that each time series point corresponds to a third of a day. Note that for this simulation, and similarly for the subsequent simulations, zeros were added to the beginning of the simulation data to align the peaks of the simulations with the peak of the dataset. As would be expected, this graph structure does not capture the behavior of the system, as depicted in Figure 6.9.

For the case that is more realistic, since it is well known (now) that cholera spreads primarily through contaminated water, and that the Broad Street pump was the source of this epidemic, it was assumed that the pump affected everyone. This was done by setting

$$A^{(2)} = [\ A^{(1)}(1:n, 1:n-1)\ v\ ], \tag{6.15}$$

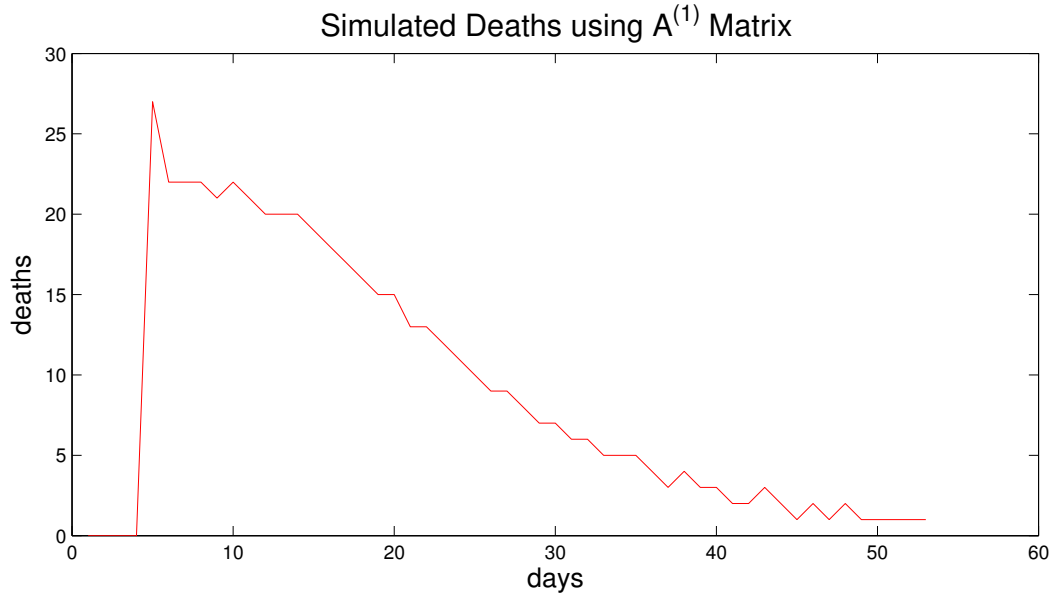

Figure 6.8: Simulated data using the learned parameters from the data in Figure 6.5, employing Corollary 8 and $A^{(1)}$ from (6.14).

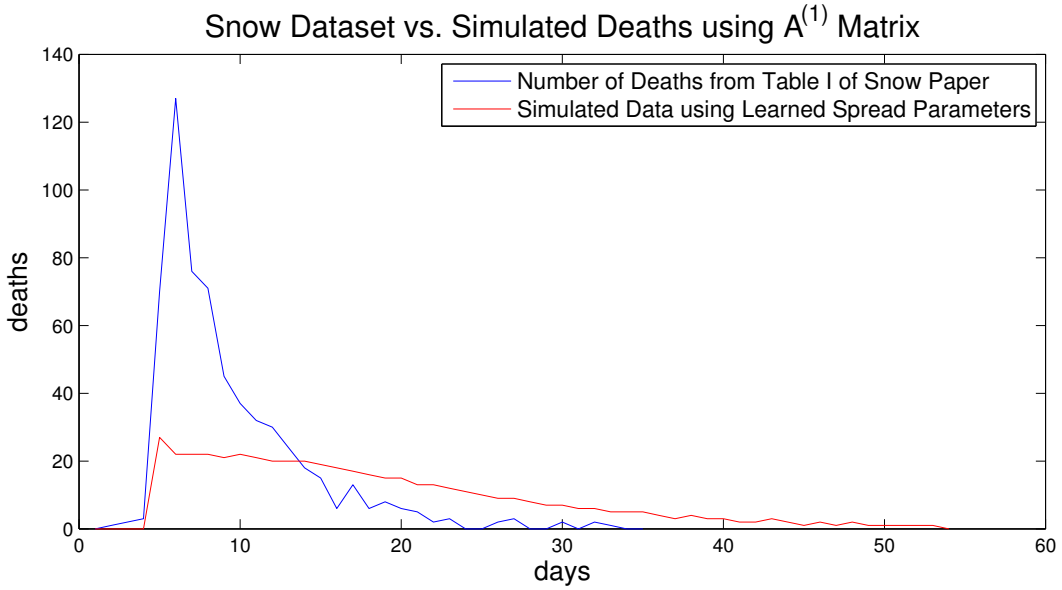

Figure 6.9: Comparison of Figures 6.6 and 6.8: Note that the model does not capture the behavior of the system well. The Euclidean distance between the two plots is 146.52, and the infinity norm is 105.

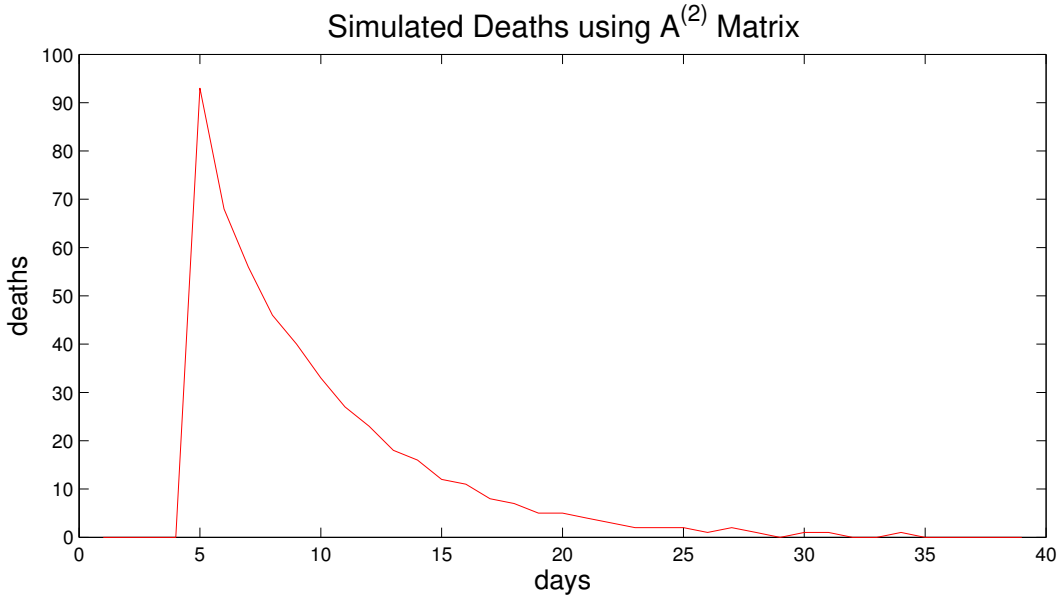

Figure 6.10: Simulated data using the learned parameters from the data in Figure 6.5, employing Corollary 8 and $A^{(2)}$ from (6.15).

Table 6.7: Estimates for household sizes from Figure 1 in [97] used in the simulation with $A^{(3)}$: * The workhouse population was set to 403.

Household Sizes	
Range in [97]	Estimate
0-4	4
5-9	7
10-14	12
15-24	20
24-403	25*

where $v = \mathbf{1} \in \mathbb{R}^n$ and the notation $A^{(1)}(1:n, 1:n-1)$ indicates all of the $A^{(1)}$ matrix except the last column. The system was simulated using the δ_i parameters derived from Corollary 8 using $A^{(2)}$, and again setting $h = \frac{1}{175}$. The resulting distribution of deaths is shown in Figure 6.10 (created similarly to Figure 6.8). Note that the shape is very similar to the original dataset from [96], shown in Figure 6.6, capturing the behavior of the true epidemic.

Plotting the distributions from Figures 6.6 and 6.10 on the same plot for comparison in Figure 6.11 shows that they are not identical. One of the reasons for the discrepancy is that, as noted in Section 6.4.1, the total number of deaths in the map (Figure 6.4), used to derive x^* and consequently the spread parameters and the simulation, is 489, and the total number of deaths in Table I of [96], used to create the distribution of deaths over days in Figure 6.6, is 616. Therefore, the lack of address information for the additional 127 deaths results in this inaccuracy. However, the largest discrepancy occurs near the peak of the epidemic, when people were arriving at hospitals too sick to provide their addresses [96]. Nevertheless, the results are very promising showing that the model in (2.10) captures the behavior of the cholera epidemic from John Snow's 1854 dataset quite well.

For the third attempt, we changed to heterogeneous household sizes, using Figure 1 in [97] to approximate

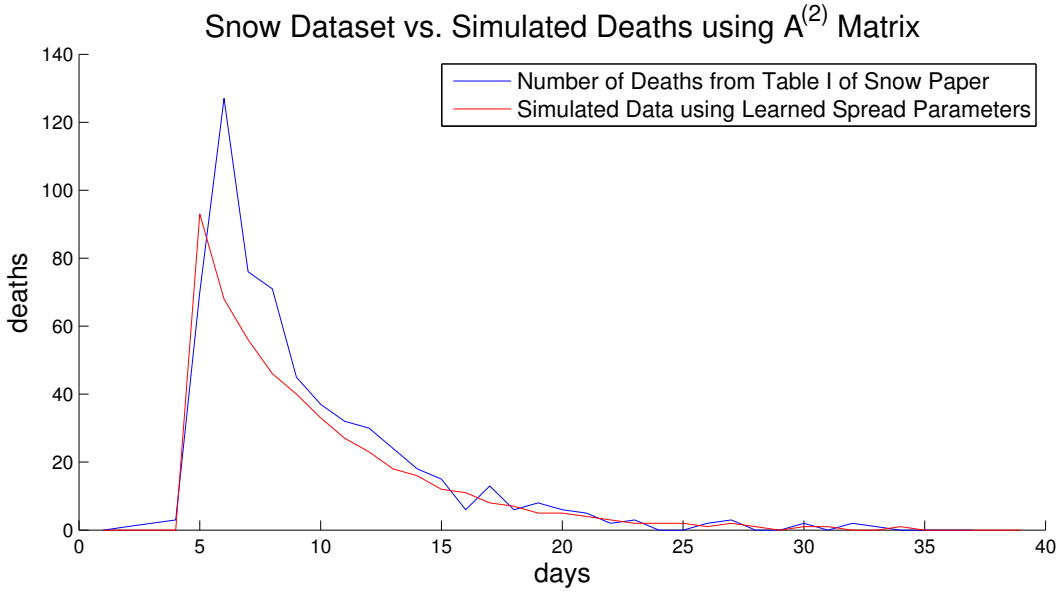

Figure 6.11: Comparison of Figures 6.6 and 6.10: Note that there is a difference in the magnitude, but the general shapes are very similar. The Euclidean distance between the two plots is 72.77, and the infinity norm is 59. One of the reasons for this discrepancy is due to the fact that we used the spatial dataset in Figures 6.4-6.5, which had only 489 documented deaths, while the cumulative data from Table I in [96], shown in Figure 6.6 and the blue line in Figure 6.13, has a total of 616 deaths. The difference of 127 has caused the discrepancy.

these values (see Table 6.7). We also removed all edges except the self loops and the binary directed edges from the pump to every household with at least one death. The connection from the pump to the workhouse was set to $\frac{1}{10}$ (corresponding to the 208th index) because they had their own well and only a small fraction of the 403 residents drank from the Broad Street pump [96] (by choosing $\frac{1}{10}$ we assume that approximately 10% of the residents drank water from the Broad Street pump). Therefore,

$$A^{(3)} = \begin{bmatrix} 1 & 0 & \dots & 0 & 1 \\ 0 & 1 & \dots & 0 & \vdots \\ 0 & 0 & \ddots & 0 & \frac{1}{10} \\ 0 & 0 & \dots & 1 & \vdots \\ 0 & 0 & \dots & 0 & 1 \end{bmatrix} \tag{6.16}$$

(shown in Figure 6.7b). Using the δ_i parameters derived from Corollary 8 using $A^{(3)}$, the system was simulated setting $h = \frac{1}{30}$. The distribution of the deaths is shown in Figure 6.12. As a result of the larger h value, no aggregation of the data was required; the plot shows the unedited simulated dataset (i.e. no summing of datapoints). For completeness, we include a link to a video of this simulation in the caption of Figure 6.12. We found via simulation that as long as the edge weight corresponding to the workhouse was less than or equal to 0.45 then the results were very similar.

Plotting the distributions from Figures 6.6 and 6.12 on the same plot for comparison in Figure 6.13 shows that we capture the behavior of the outbreak quite well. The lack of the address information for the additional 127 deaths is one of the reasons the plots are not identical. However, the discrepancy is distributed fairly

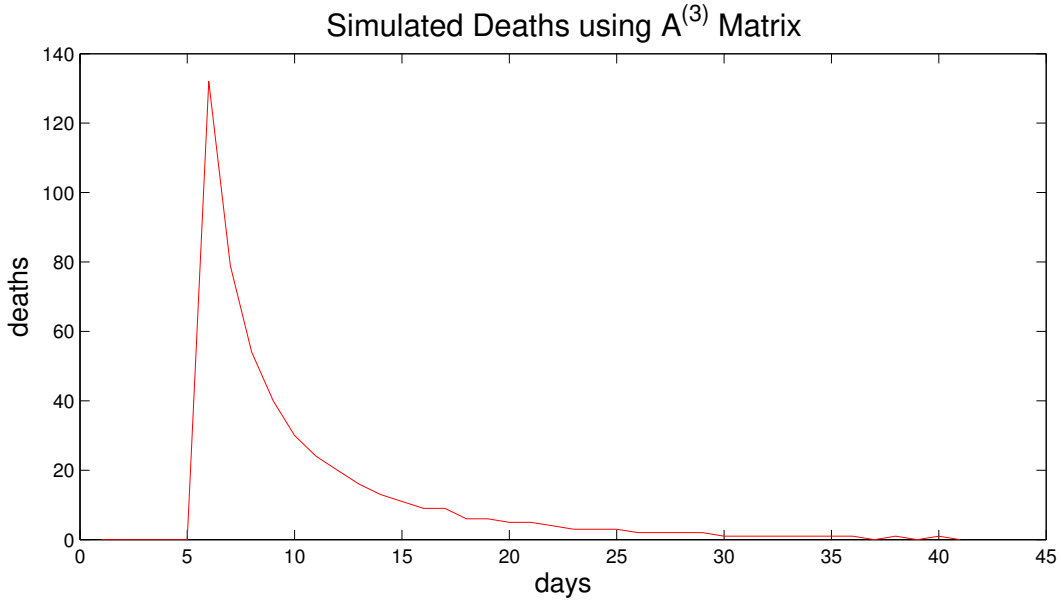

Figure 6.12: Simulated data using the learned parameters from the data in Figure 6.5, employing Corollary 8 and $A^{(3)}$ from (6.16). A video of the spread of the simulation can be found at youtu.be/PXqyce7zZFM

evenly across the whole sample time. Consequently, we have shown that the model in (2.10) captures the behavior of the cholera epidemic from John Snow's 1854 dataset very well. Note that by both error metrics the simulation from the second attempt in Figure 6.11 outperforms this last attempt, but recall it required summing every three data points. Therefore it can be argued that the last attempt captures the behavior of the dataset best since no summing was required. Also note that the fact that $A^{(3)}$ from (6.16) performs the best supports Snow's hypotheses that the Broad Street pump was the source of the cholera outbreak, and that cholera does not spread via the air, which is known to be true today.

6.5 Validation: USDA Dataset

The goal of this section is to study whether variation in the spatial pattern of farmers' enrollment in ACRE in 2009-2012 follows the spreading processes presented in Section 2.2. As we elaborate below, ACRE is a complex program, making the experience and knowledge of early adopters likely to spread by word of mouth through social and professional networks. For this dataset we assume homogeneous spread parameters, that is, β and δ are the same for all nodes. This work was done in collaboration with Barrett E. Kirwan of the ACES department at UIUC.

6.5.1 USDA Dataset

The characteristics of the ACRE program make it a good candidate to empirically test the model of spreading. Farmers rely on the experience of neighbors in the adoption of new or complex technologies [98, 99, 100]. As we elaborate below, ACRE is a complex program. Social and professional networks will likely facilitate the spread of information about the ACRE program from the experiences of early adopters.

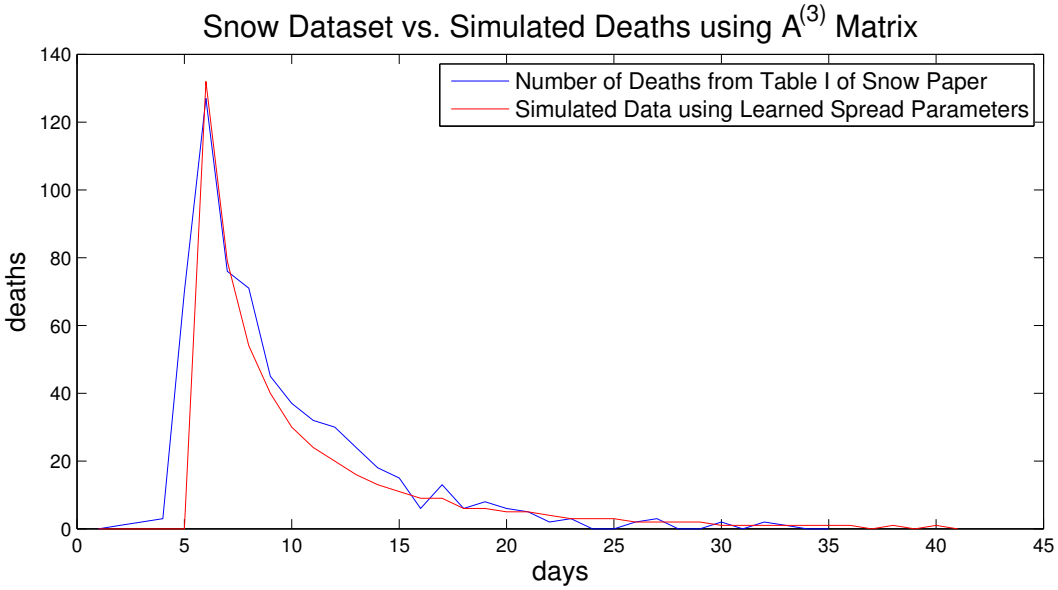

Figure 6.13: Comparison of Figures 6.6 and 6.10: Note that there is a difference in the magnitude, but the general shapes are very similar. The Euclidean distance between the two plots is 75.16, and the infinity norm is 70. One of the reasons for this discrepancy is due to the fact that we used the spatial dataset in Figures 6.4-6.5, which had only 489 documented deaths, while the cumulative data from Table I in [96], shown in Figure 6.6 and the blue in this plot, has a total of 616 deaths. The difference of 127 has caused the discrepancy.

The ACRE program was introduced by the Food, Conservation and Energy Act of 2008 (2008 Farm Bill). Initial enrollment was unexpectedly low, in part because of the program's complexity [101]. The ACRE payment a_{ij}^k for year k is calculated by the following formula:

$$a_{ij}^k = \phi \frac{\hat{\upsilon}_{ij}^k}{\hat{\upsilon}_{\sigma j}^k} \min\{(g_{\sigma j}^k - r_{\sigma j}^k), \frac{g_{\sigma j}^k}{4}\} \min\{\rho_{ij}^k, b_{ij}^k\} \mathbb{1}(r_{ij}^k < g_{ij}^k) \mathbb{1}(r_{\sigma j}^k < g_{\sigma j}^k), \tag{6.17}$$

where i is the farm index; j is the crop or commodity that subsidy corresponds to; ϕ is a constant scaling factor (equal to 0.85); σ indicates the state (e.g., Idaho); the benchmark yield (a.k.a. the Olympic yield) is

$$\hat{\upsilon}_{\iota j}^k = \frac{1}{3}\left[\sum_{l=1}^{5} \upsilon_{\iota j}^{k-l} - \max\{\Upsilon_{\iota j}\} - \min\{\Upsilon_{\iota j}\}\right],$$

where $\upsilon_{\iota j}^{k-l}$ is the crop yield in year $k-l$; the set $\Upsilon_{\iota j} = \{\upsilon_{\iota j}^{k-1}, \ldots, \upsilon_{\iota j}^{k-5}\}$, for $\iota \in \{i, \sigma\}$; the farm and state guaranteed revenues per acre are $g_{ij}^k = \hat{\upsilon}_{ij}^k \bar{\bar{p}}_j^k$ and $g_{\sigma j}^k = .9\hat{\upsilon}_{\sigma j}^k \bar{\bar{p}}_j^k$, respectively, with $\bar{\bar{p}}_j^k = \frac{1}{2}\sum_{l=1}^{2} \bar{p}_j^{k-l}$, where $\bar{p}_j^k$ is the National Average Market Price of crop j; actual revenue per acre is $r_{\iota j}^k = \upsilon_{\iota j}^k q_j^k$, with $q_j^k = \max\{0.7 l_j^k, \bar{p}_j^k\}$, where l_j^k is the National Loan Rate, which Congress sets in the farm bill; ρ_{ij}^k is the number of acres *planted* with crop j on farm i; b_{ij}^k is the number of acres of crop j on farm i qualifying for the Direct and Counter-cyclical Payment (DCP) subsidy, which are known as base acres; and $\mathbb{1}(\cdot)$ is the

indicator function [102].

The ACRE program benefits farmers by paying out when the farmers' *actual revenue* is low. In contrast, the Counter-cyclical Program (CCP), which ACRE replaces, takes into account current prices but the payout is determined by the subsidized land's productivity in the early 1980s.

The cost to participate in ACRE is not trivial. By choosing ACRE, farmers must forgo 20% of their annual unconditional subsidy, i.e., Direct Payment, and 30% of the production subsidy they would receive in the event of low crop prices. Another important consideration is that the decision to participate in ACRE is irreversible. Although farmers must re-enroll in ACRE every year, they cannot switch back to the CCP. Failure to enroll disqualifies farmers from the benefits of ACRE but not the costs. Since switching from ACRE back to CCP is not allowed, we should expect the healing rate δ to be small (or effectively zero) compared to the infection rate β, when we estimate the model parameters from the data.

The dataset includes the total annual payments received by each farm in the U.S. for each USDA-sponsored program from the year 2008 to 2012. Each datapoint has a program, payment amount, payment date, contract number, commodity (usually the crop), the farm number, and the customer's (farmer's) identification number and address. The dataset allows the opportunity to investigate the spread of the ACRE program through several different networks. Farmer-to-farmer networks could be created from the data by connecting farmer-nodes who receive payments on the same field or live nearby. Alternatively, farms can be aggregated to the county level. The USDA has an office in every county in the United States that distributes subsidies and administers farm programs locally. Farmers go to these offices (not necessarily their own county's office since an adjacent county's office could be closer) to learn how the subsidy programs work. Therefore, there are strong inner county dependencies, since, in addition to receiving the same information at their county offices, farmers meet each other at these offices as well. The approach of aggregating by county allows us to convert the binary decision to enroll in ACRE into a continuous measure of the proportion of eligible farms that enroll in ACRE in each county. The proportion of farms enrolled in ACRE corresponds exactly to the density of infection, facilitating our investigation of the spread of ACRE. For counties where no farms are enrolled in either, the infection state is set to zero. Alaska and Hawaii are omitted. The data for the four years considered can be found in Figure 6.14.

6.5.2 USDA Farm Subsidies as a Spread Process

In this section we use the learning techniques presented in Section 6.2 and tested in Section 6.3 for the model in (2.10) on the data presented in Section 6.5.1. We estimate the homogeneous model parameters using a subset of the dataset, the USDA data from Idaho, and then simulate the spread of ACRE over the whole contiguous United States using the estimated parameters. The adjacency matrices are calculated using the adjacency of counties, that is,

$$a_{ij} = \begin{cases} 1, & \text{if county } i \text{ and county } j \text{ share a border,} \\ 1, & \text{if } i = j, \\ 0, & \text{otherwise.} \end{cases} \tag{6.18}$$

To calculate the adjacency matrix for Idaho, adjacent counties from bordering states were ignored. Substituting the Idaho dataset into (6.2) with $h = 1$ and using the pseudo-inverse gives the following spread

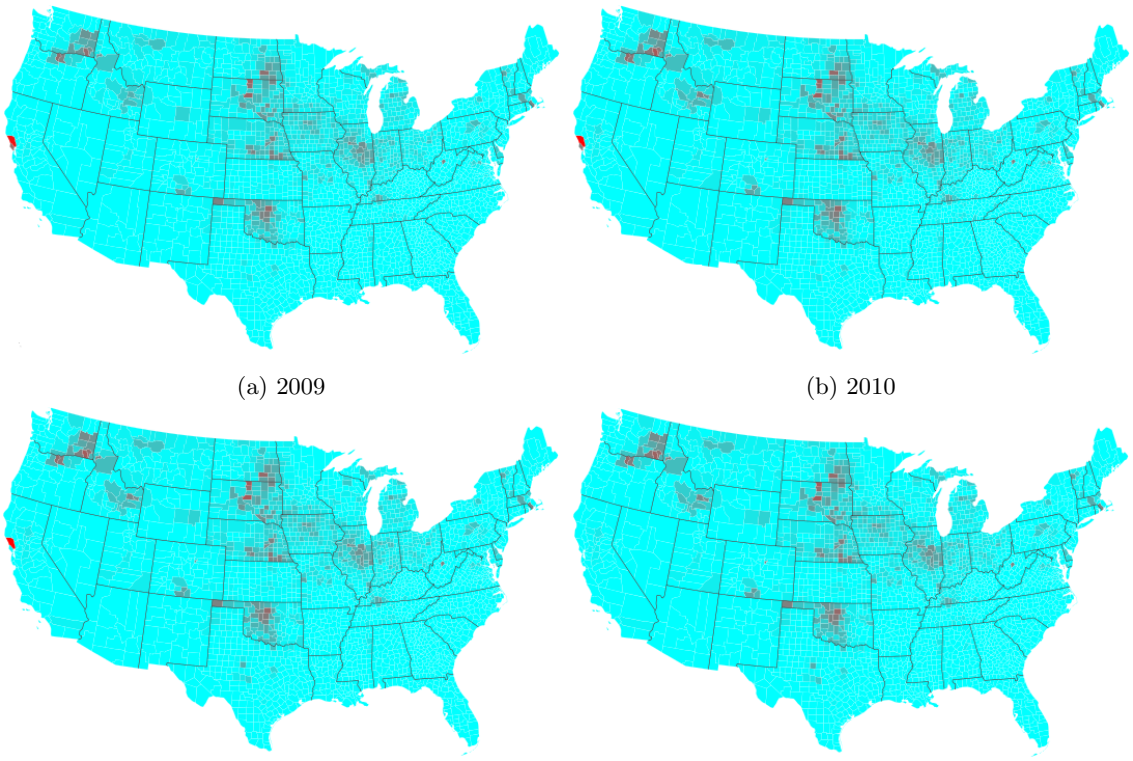

(a) 2009

(b) 2010

(c) 2011

(d) 2012

Figure 6.14: The percentage of farms enrolled in the ACRE Program that are enrolled in either ACRE or CCP calculated from the USDA dataset.

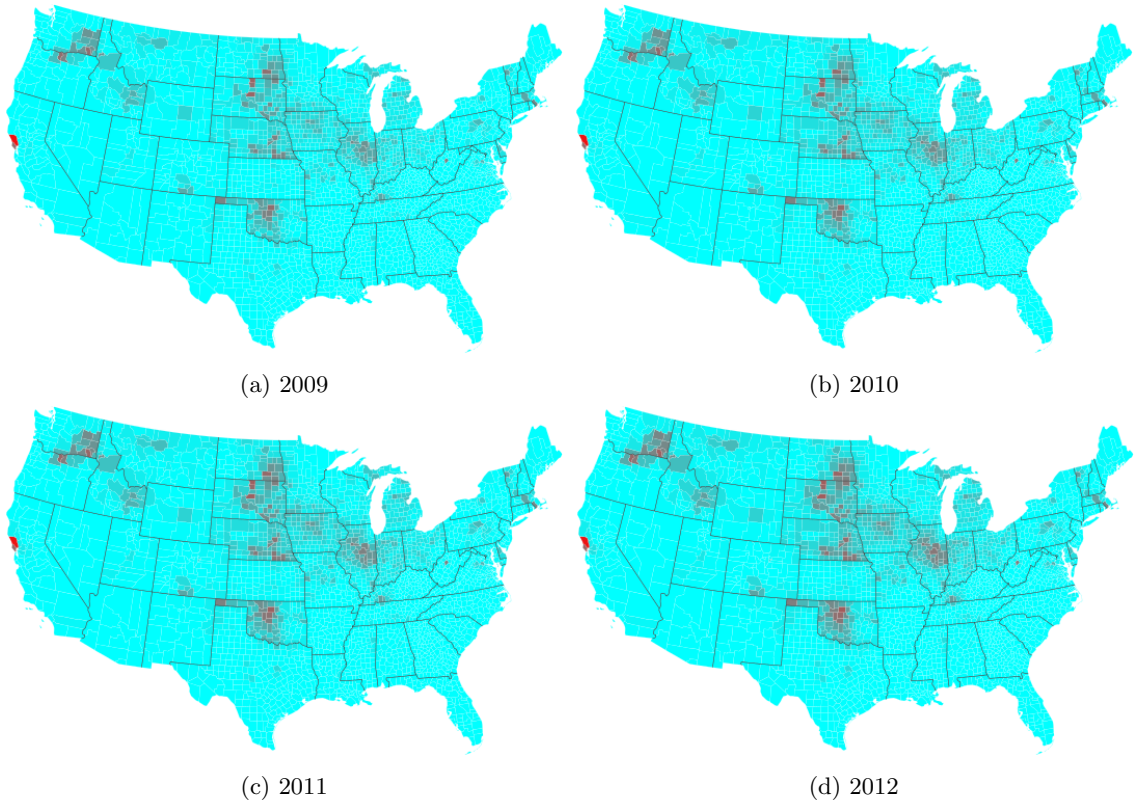

(a) 2009 (b) 2010

(c) 2011 (d) 2012

Figure 6.15: Simulated data using Figure 6.14a as the initial condition, simulating using the model in (2.10) with parameters calculated using the data from Idaho, given in (6.19).

parameters:

$$\begin{bmatrix} \hat{\delta} \\ \hat{\beta} \end{bmatrix} = \begin{bmatrix} 0.00909176 \\ 0.02237450 \end{bmatrix}. \tag{6.19}$$

As expected, switching h to the value 0.1 moves the decimal point one place to the right. We also tried to learn the spread parameters of (2.12) using (6.8) but the sampling of states we tried did not give sensible numbers; one of the spread parameters was always negative.

To validate the model, we simulate the spread over the contiguous United States using the model in (2.10) with parameters calculated using the data from Idaho, given in (6.19), with the data from Figure 6.14a being used as the initial condition. The simulation results are given in Figure 6.15. The scaled error between the dataset, $\mathbb{F}$, and the simulated data, $\hat{\mathbb{F}}$, using the Frobenius norm is

$$\frac{\left\|\mathbb{F} - \hat{\mathbb{F}}\right\|_{Fr}}{\|\mathbb{F}\|_{Fr}} = \frac{2.5331}{10.7872} = 0.2348,$$

showing that the system has approximately 23% error. For completeness, in Figure 6.16, we include a plot of $\|\mathbb{F}^k - \hat{\mathbb{F}}^k\|$ and $\frac{\left\|\mathbb{F}^k - \hat{\mathbb{F}}^k\right\|}{\|\mathbb{F}^k\|}$. While the model does not perfectly fit the data, it does seem to give some insight into the behavior of the system.

Therefore, if the USDA wanted to test a pilot program in a certain region of the country, for example Idaho, the resulting behavior could give some insight into how the whole country would react. The four time

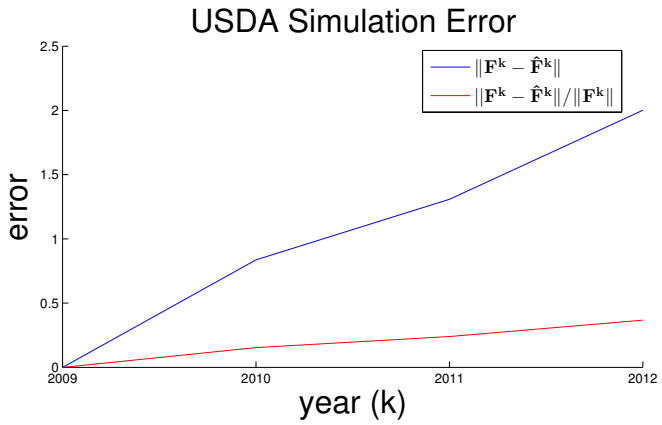

Figure 6.16: Error plots for Figures 6.14 and 6.15.

steps (years) do not allow the system to reach the equilibrium state, so the behavior depends significantly on the initial condition. Therefore, given the model learned from a pilot program, the USDA could determine the best counties to target for advertising of the new subsidy programs, assuming they wanted to maximize adoption of the new program.

Chapter 7

Future Research Directions

In this chapter ongoing and future investigations are described.

7.1 Ongoing Work

The work with the John Snow dataset has inspired another thread of research for modeling cholera. In [103], a SIWR (susceptible-infected-water-removed) model was proposed, similar to (1.1) in that there is no network structure:

$$\begin{aligned}
\dot{S}(t) &= \mu N - \beta_I S(t)I(t) - \beta_W S(t)W(t) - \mu S(t), \\
\dot{I}(t) &= \beta_I S(t)I(t) + \beta_W S(t)W(t) - \gamma I(t), \\
\dot{W}(t) &= \alpha I(t) - \xi W(t), \\
\dot{R}(t) &= \gamma I(t) - \mu R(t),
\end{aligned} \tag{7.1}$$

where N is the size of the population, μ is both the birth and death rates, β_I and β_W are the transmission rate parameters for person-to-person and water-to-person contact, respectively, W is the pathogen concentration in the water reservoir, γ is the recovery rate, α is the person-to-reservoir contamination rate, ξ is the water recovery rate from the pathogen, and $R(t)$ is the recovered proportion of the population. In [104], (7.1) is extended to include a death variable D and β_W is made a sinusoidal function of time to capture the seasonal effects of the disease. The model is compared via simulation to London's weekly mortality recorded in the Weekly Returns of the Registrar General's Office. In [105], the model has been extended to have two compartments (portions of the total population) that are connected to the same water source.

Since both human contact and water distribution occur via networks, we will incorporate ideas similar to those proposed in Chapter 4 on layered networks, except these networks will not be competing but propagating the virus spread. The first step of this work extends the SIS model to include a single contaminated water source, where the agents are networked but the water is not [106].

In this work we extend the model in (7.1) to include a graph structure, that is, n portions of the population that use the same water source and can possibly infect each other. We first add a human contact network to the spread of the virus through the population, and for future work we will also add network structure to the water portion of the model and couple the network to the human contact network. The rest of the work discussed here has been submitted to a conference [107] and is used here with permission.

In [108], Ruhi *et al.* examine the homogeneous discrete-time, networked SIR model: the full 3^n probabilistic model, the nonlinear mean-field model, and the linearized model. They examine the equilibria of the model and provide some stability results for the healthy state (the origin). In [109], Mei *et al.* examine the

homogeneous continuous-time, networked SIR nonlinear mean-field model, showing that the infection state will converge to zero for any initial condition, given that $\mu = 0$.

In Section 6.4, we assume the contaminated water pump is a node in the networked SIS model and that the infected state variable corresponds to the proportion of deceased household members. In this chapter, we introduce this new network-dependent model that includes polluted water as a separate variable and a removed state. Therefore we can model the pump as its own entity and allow household members to become infected and then die from the sickness, i.e. be removed.

7.1.1 Networked SIWR Model

We propose, analyze, and simulate a networked extension of (7.1). Consider a network of n nodes that can be interpreted as subpopulations or agents. Specifically, each agent can be infected if one of its neighbors is infected. The neighbor relationships among the n agents are described by an n-vertex directed graph. A directed edge from node j to node i means that agent i can be infected by agent j, i.e., agent j is a neighbor of agent i. Let S_i denote the number of susceptible individuals in subpopulation i, I_i denote the number of infected individuals in subpopulation i, W denote the pathogen concentration in the water source, and R_i denote the removed proportion of subpopulation i. We assume a constant subpopulation for each i, that is, $S_i(t) + I_i(t) + R_i(t) = N_i \ \forall i, t \geq 0$. The dynamics proceed similarly to (7.1):

$$\begin{aligned}
\dot{S}_i(t) &= \mu_i N_i - \sum_{j=1}^{n} \alpha_{ij} \frac{S_i(t)}{N_i} I_j(t) - \beta_{w,i} S_i(t) W(t) - \mu_i S_i(t), \\
\dot{I}_i(t) &= \sum_{j=1}^{n} \alpha_{ij} \frac{S_i(t)}{N_i} I_j(t) + \beta_{w,i} S_i(t) W(t) - \gamma_i I_i(t) - \mu_i I_i(t), \\
\dot{W}(t) &= \sum_{j=1}^{n} \phi_j I_j(t) - \xi W(t), \\
\dot{R}_i(t) &= \gamma_i I_i(t) - \mu_i R_i(t),
\end{aligned} \tag{7.2}$$

where, for each node i, μ_i is the birth rate and natural death rate, α_{ij} is the node-to-node infection rate (with the understanding that $\alpha_{ij} > 0$ whenever group j is a neighbor of group i and $\alpha_{ij} = 0$ otherwise), $\beta_{w,i}$ is the water-to-node infection rate, γ_i is the curing or death (from illness, depending on whether the state variable r is interpreted as recovered or removed, i.e. dead) rate, and ϕ_j is the node-to-water infection rate. Let p_i denote the proportion of the subpopulation i (or the probability of infection of agent i), w denote the pathogen concentration in the water source (we first assume a single water source), and r_i denote the removed proportion of subpopulation i (or the recovered/removed probability of agent i), that is,

$$\begin{aligned}
p_i &= \frac{I_i(t)}{N_i}, \\
r_i &= \frac{R_i(t)}{N_i}, \\
w &= W.
\end{aligned}$$

Therefore, the dynamics in (7.2) can be rewritten as follows:

$$\dot{p}_i = (1 - p_i - r_i) \left(\sum_{j=1}^{n} \beta_{ij} p_j + \beta_{w,i} w \right) - \delta_i p_i, \tag{7.3}$$

$$\dot{r}_i = \gamma_i p_i - \mu_i r_i, \tag{7.4}$$

$$\dot{w} = \sum_{j=1}^{n} \alpha_j p_j - \xi w, \tag{7.5}$$

where

$$\beta_{ij} = \alpha_{ij} \frac{N_j}{N_i}, \quad \alpha_j = \frac{\phi_j}{N_j}, \quad \delta_i = \gamma_i + \mu_i,$$

are the normalized node-to-node infection rates, normalized node-to-water infection rates, and the total decay rates on the normalized infection levels, respectively.

We can rewrite the system in (7.3)-(7.5) in matrix form:

$$\dot{p} = (I - P - R)(Bp + b_w w) - Dp, \tag{7.6}$$

$$\dot{r} = \gamma p - \mu r, \tag{7.7}$$

$$\dot{w} = \alpha^\top p - \xi w, \tag{7.8}$$

where $P = \text{diag}(p)$, $R = \text{diag}(r)$ (a slight abuse of notation given (7.1)), B is the matrix of β_{ij}'s, b_w is the vector of $\beta_{w,i}$'s, $D = \text{diag}(\delta_i)$, $\gamma = \text{diag}(\gamma_j)$, $\mu = \text{diag}(\mu_i)$, and α is the vector of α_i's.

Note that, for all $i, j \in [n]$, we can factor the β_{ij}'s in to $\beta_i a_{ij}$, where β_i is the susceptibility of node i, or the infection rate, and a_{ij} is the weight (intensity) attached to edge ij of the underlying graph. This transforms (7.6) into

$$\dot{p} = (I - P - R)(BAp + b_w w) - Dp, \tag{7.9}$$

where $B = \text{diag}(\beta_i)$ and A is the matrix of a_{ij}'s.

7.1.2 Analysis

In this section, we present the equilibria of the continuous time model, and provide some stability results on the equilibria. For this first attempt at analyzing the model, we take $\mu = 0$:

$$\dot{p} = (I - P - R)(Bp + b_w w) - Dp, \tag{7.10}$$

$$\dot{r} = \gamma p, \tag{7.11}$$

$$\dot{w} = \alpha^\top p - \xi w. \tag{7.12}$$

In Section 7.1.3, we explore the $\mu > 0$ case via simulations.

Equilibria:

The point $(\tilde{p}, \tilde{r}, \tilde{w}) = (\mathbf{0}, \mathbf{0}, 0)$ is clearly an equilibrium of the model, and we refer to it as the *trivial healthy state*. We refer to the set of states $(\tilde{p}, \tilde{r}, \tilde{w}) = (\mathbf{0}, \tilde{r}, 0)$ with $\tilde{r} > \mathbf{0}$, as the set of *healthy states*. Every healthy state is an equilibrium of the model.

In the case where $\mu > 0$, there may exist an endemic state; this behavior is illustrated via simulations in Section 7.1.3.

Stability:

For the analysis we need the following assumption on the model parameters.

Assumption 8. *Suppose that $\delta_i, \gamma_i > 0$ for all $i \in [n]$, $\xi > 0$, $\beta_{ij} \geq 0$ for all $i, j \in [n]$, $\beta_{ij} > 0$ whenever node j is a neighbor of node i, the matrix B is irreducible, $\beta_{w,i} > 0$ for all $i \in [n]$, and $\alpha_i > 0$ for all $i \in [n]$.*

Before providing the main results, we present the Jacobian of the model in (7.3)-(7.5). Let $(\tilde{p}, \tilde{r}, \tilde{w})$ be an equilibrium of (7.3)-(7.5). Then, the Jacobian matrix of the equilibrium, denoted by $J(\tilde{p}, \tilde{z}, \tilde{w})$, is

$$J(\tilde{p}, \tilde{z}, \tilde{w}) = \begin{bmatrix} \tilde{S}B - D - H_1 - H_2 & H_1 + H_2 & \tilde{S}b_w \\ \gamma & -\mu & \mathbf{0} \\ \alpha^\top & \mathbf{0}^\top & -\xi \end{bmatrix}, \tag{7.13}$$

where $\tilde{S}, H_1, H_2$ are diagonal matrices given by

$$\begin{aligned} \tilde{S} &= (I - \tilde{P} - \tilde{R}), \\ H_1 &= \operatorname{diag}\left\{ \sum_{j=1}^{n} \beta_{1j}\bar{p}_j, \sum_{j=1}^{n} \beta_{2j}\bar{p}_j, \cdots \sum_{j=1}^{n} \beta_{nj}\bar{p}_j \right\}, \\ H_2 &= \operatorname{diag}\left\{ \beta_{w,1}\bar{w}, \beta_{w,2}\bar{w}, \cdots, \beta_{w,n}\bar{w} \right\}, \end{aligned}$$

with $\tilde{P} = \operatorname{diag}(\tilde{p})$ and $\tilde{R} = \operatorname{diag}(\tilde{r})$.

For the healthy states, given $\tilde{R}$, we have the result stated in the next theorem. Toward that end, we first introduce the following two matrices:

$$\begin{aligned} D_w &= \begin{bmatrix} D & \mathbf{0} \\ \mathbf{0} & \xi \end{bmatrix}, \\ B_w &= \begin{bmatrix} (I - \tilde{R})B & (I - \tilde{R})b_w \\ \alpha^\top & 0 \end{bmatrix}. \end{aligned} \tag{7.14}$$

Theorem 21. *Let Assumption 8 hold for (7.10)-(7.12). If $\rho(D_w^{-1}B_w) < 1$, then the set of healthy states $(\mathbf{0}, \tilde{r}, 0)$ is locally exponentially stable.*

Proof. First suppose that $\tilde{r} \ll \mathbf{1}$. Using (7.13) and (7.14), we have

$$\begin{aligned} J(\mathbf{0}, \tilde{r}, 0) &= \begin{bmatrix} (I - \tilde{R})B - D & (I - \tilde{R})b_w \\ \alpha^\top & -\xi \end{bmatrix} \\ &= B_w - D_w. \end{aligned}$$

Note that under Assumption 8, D_w is an invertible matrix, since $\delta_i > 0 \ \forall i$, and B_w is an irreducible non-negative matrix, since $\tilde{r}_i < 1 \ \forall i$ implies $(1 - \tilde{r}_i) > 0 \ \forall i$. From Lemma 5, the condition $\rho(D_w^{-1}B_w) < 1$ is equivalent to $s(-D_w + B_w) < 0$, which implies that $J(\mathbf{0}, \tilde{r}, 0)$ is a continuous-time stable matrix.

Next suppose that $\tilde{r} = \mathbf{1}$. It is easy to see that

$$J(\mathbf{0}, \tilde{r}, 0) = \begin{bmatrix} -D & \mathbf{0} \\ \alpha^\top & -\xi \end{bmatrix},$$

which is a continuous-time stable matrix because of Assumption 8. From the continuity of the spectrum of a matrix with respect to its entries, we conclude that $J(\mathbf{0}, \tilde{r}, 0)$ is always stable for all possible $\tilde{r}$, which completes the proof. □

Now we consider the global stability of the healthy states. Using (7.10)-(7.12), since in the case when $\mu = 0$, $D = \gamma$, the system can be rewritten as

$$\dot{p} = S\left(Bp + b_w w\right) - Dp, \tag{7.15}$$

$$\dot{s} = -S\left(Bp + b_w w\right), \tag{7.16}$$

$$\dot{w} = \alpha^\top p - \xi w, \tag{7.17}$$

where $s(t)$ denotes the vector whose entries $s_i(t) = \frac{I_i(t)}{N_i}$, denoting the proportion of susceptible individuals in subpopulaton i, and $S = I - P - R = \mathrm{diag}(s)$. It is clear that $\dot{s} < \mathbf{0}$ and is lower bounded by $\mathbf{0}$. Then, $\lim_{t\to\infty} s(t)$ exists, and thus $\lim_{t\to\infty} \dot{s}(t) = \mathbf{0}$. Therefore, from (7.15), $\dot{p}(t)$ converges to $-Dp(t)$. Consequently, from Assumption 8, $p(t)$ converges to $\mathbf{0}$, and thus w converges to 0. We have thus proved the following result.

Theorem 22. *Suppose that Assumption 8 holds. Then, for any initial condition, the system (7.10) to (7.12) will asymptotically converge to a healthy state.*

7.1.3 Simulations

For nearly two centuries the Village of Richmond was the government center of Staten Island. The location now hosts an interactive museum/site called the Historic Richmond Town [110]. For the neighbor graph in our simulations in this section we have used a subset of the map of the current layout, given in Figure 7.1, with the nodes labelled by number. The water source is Richmond Creek. We made the simplifying assumption that the underlying interaction graph for each household is determined by its nearest proximity neighbors. We set the adjacency matrix A as a binary matrix corresponding to the edges in Figure 7.2, i.e., $\beta_{ij} = 1$ whenever j is a next-door (or across-the-street) neighbor of i. Note that we chose an undirected neighbor graph for convenience. The states of the system, p and r, are the proportions of the households that are infected with the disease and have died from the disease, respectively.

We use different node sizes and coloring for depicting the states of the model in (7.3)-(7.5). For all $i \in [n]$, the diameter of node i is given by

$$d_0 + p_i(t) r_0, \tag{7.18}$$

where d_0 is the default/smallest diameter and r_0 is the scaling factor depending on the infection proportion of node i. The removed/recovered variable, $r_i(t)$, is depicted by the color red (r) and the susceptible part of the system, $(1 - p_i(t) - r_i(t))$, is depicted by the color blue (b). For all $i \in [n]$, the color at each time t for node i is given by

$$r_i(t)\mathrm{r} + (1 - p_i(t) - r_i(t))\mathrm{b}. \tag{7.19}$$

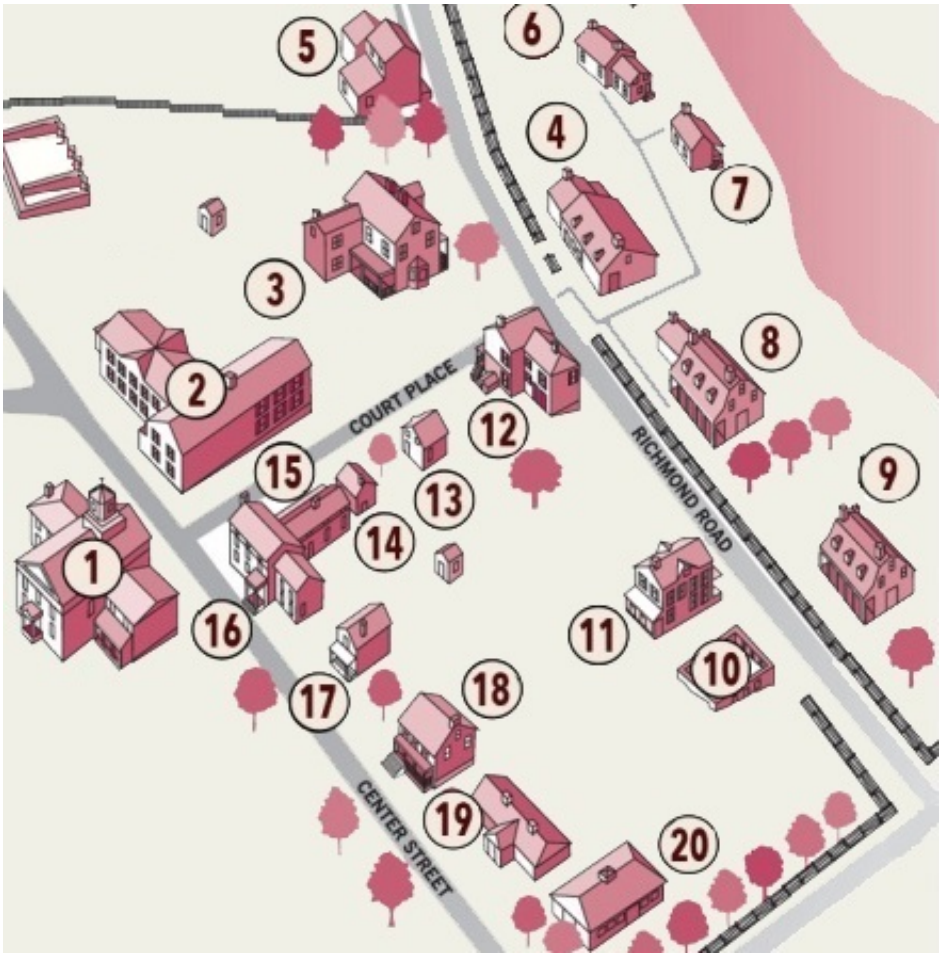

Figure 7.1: Map of Historic Richmond Town [110]

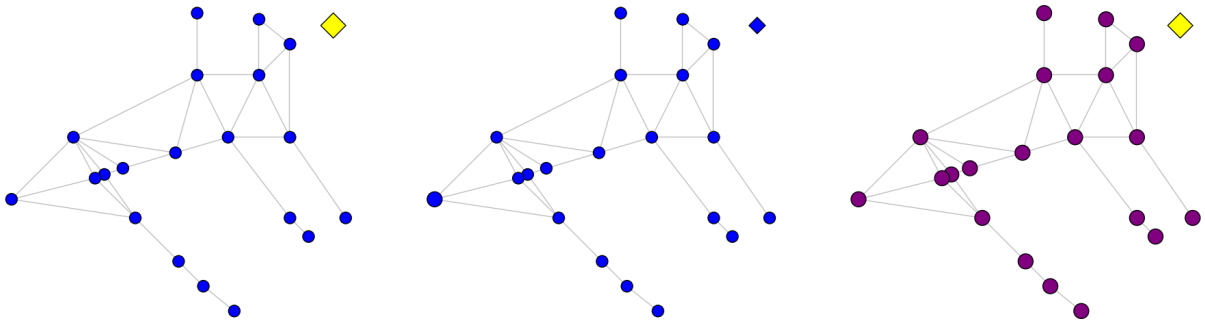

(a) Water polluted initially, $w(0) = 0.5$

(b) Node one initially infected, $p_1(0) = 0.5$

(c) $p(0) = r(0) = 0.5\mathbf{1}$ and $w(0) = 0.5$

Figure 7.2: These graphs show the graph topology and the different initial conditions used in the simulations. The diameters and colors follow (7.18) and (7.19).

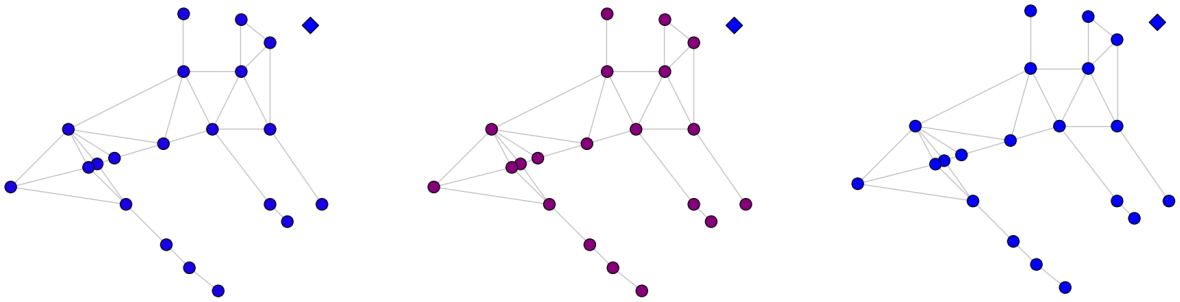

(a) Water polluted initially, $w(0) = 0.5$: $\tilde{p} = \mathbf{0}$ and the average of $\tilde{r}$ is 0.1002.

(b) Node one initially infected, $p_1(0) = 0.5$: $\tilde{p} = \mathbf{0}$ and the average of $\tilde{r}$ is 0.5259.

(c) $p(0) = r(0) = 0.5\mathbf{1}$ and $w(0) = 0.5$: $\tilde{p} = \mathbf{0}$ and the average of $\tilde{r}$ is 0.0126.

Figure 7.3: Endemic equilibria for the system with $\delta = 25$ and $\mu = \mathbf{0}$ using the three different initial conditions in Figure 7.2. The diameters and colors follow (7.18) and (7.19).

We depict the water variable w with a diamond, in yellow if $w > 0$ and in blue if $w = 0$. The size of the diamond is scaled linearly by $w(t)$, similar to (7.18).

For the simulations, we assume homogeneous virus spread with $\beta = 1$ and $\delta \in \{2, 10, 25\}$. We set $b_w = \mathbf{1}$, $\gamma_i = 0.5\ \forall i$, $\alpha = \mathbf{1}$, and $\xi = 1$. We explore the cases with $\mu_i = 0\ \forall i$ and $\mu_i = 1\ \forall i$. For $\delta \in \{2, 10\}$, the relevant spectral radii (using (7.14) for $\mu = \mathbf{0}$ and the analogous three-by-three version including μ for $\mu = \mathbf{1}$) are greater than one and for $\delta = 25$, they are less than one.

Case 1 $\mu_i = 0\ \forall i$:

For this case, consistent with Theorem 21, for $\delta = 25$, which has spectral radius less than one, the system converges to a healthy state. The $\tilde{r}$ values seem to be sensitive to initial condition, as shown in Figure 7.3.

The simulations show that as long as the water recovery rate $\xi > 0$, the system converges to a healthy state. This is clear from examining (7.11) and (7.12). If $p > \mathbf{0}$, then r increases. If r increases to the point that $r = \mathbf{1}$, then, from (7.10), $(I - P - R) = 0$ and p goes to $\mathbf{0}$, since by Assumption 8 the healing rates are all nonzero. Once $p = \mathbf{0}$, (7.12) reduces to $\dot{w} = -\xi w$, and therefore w goes to zero, since by Assumption 8 $\xi > 0$.

The simulations also show that the healing rates determine $\tilde{r}$. Since $\tilde{p} = \mathbf{0}$ for all systems with $\mu = \mathbf{0}$ (given that $\delta_i > 0\ \forall i$), the proportion of each node that is removed (or recovered) is the proportion of the population that is not healed (with perturbations due to initial condition). If we allow $\delta_i = 0\ \forall i$, violating Assumption 8, then $r > \mathbf{1}$ which makes $(I - P - R) < 0$, and drives p to $\mathbf{0}$. However, $r > \mathbf{1}$ is nonsensical in the interpretation of the states of the model and therefore we need Assumption 8.

Case 2 $\mu_i = 1\ \forall i$:

For the system with $\delta = 25$, the trivial healthy state appears to be the unique equilibrium of the system and asymptotically (inside the domain of interest) stable. The other two systems appear to have a unique endemic equilibrium (in addition to the trivial healthy state) with $\tilde{p} \gg \mathbf{0}$, $\tilde{r} \gg \mathbf{0}$, and $\tilde{w} > 0$ that is asymptotically stable, as long as the initial condition is not the origin (the trivial healthy state). Consequently, for these

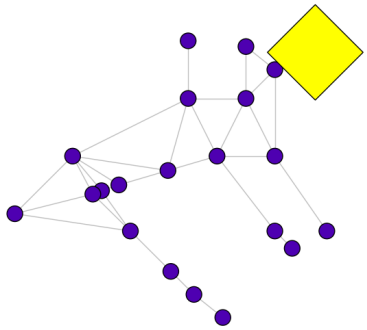

Figure 7.4: Endemic equilibrium for the system with $\delta = 2$ and $\mu = \mathbf{1}$, for all three initial conditions in Figure 7.2. The average of $\tilde{p}$, average of $\tilde{r}$, and $\tilde{w}$ values are 0.3898, 0.1949, and 7.7965, respectively.

Table 7.1: Estimates for household sizes from Figure 1 in [97] used in the simulation in Section 7.1.4: * The workhouse population was set to 403 [96].

Household Sizes	
Range in [97]	Estimate
0-4	2
5-9	5
10-14	10
15-24	15
24-403	24*

two systems, the trivial healthy state is an unstable equilibrium. See Figure 7.4 for a plot of the endemic state for the system with $\delta = 2$.

7.1.4 Validation

In this section we validate the model using Dr. John Snow's cholera dataset discussed in Section 6.4. We first provide the details of the dataset and introduce some assumptions on the parameters of the model. Then we simulate the model and compare to the dataset.

In [96], Dr. John Snow provides an intriguing disease spread dataset. Snow recorded the total number of deaths per household in a map, as discussed in the Introduction, which is shown in Figure 6.4. There are 250 households in the dataset ($n = 250$). He also recorded the number of fatal attacks, or cholera fatal infections, per day and the number of deaths from cholera per day in Table I of [96]. A plot of this data is in Figure 7.5.

In a similar way to as was done in Section 6.4, we approximated the heterogeneous household sizes using Figure 1 in [97]. These household size approximations are shown in Table 7.1.

For this dataset we treat the total number of cholera-related deaths per household as r_i, interpreting it as the removed (deceased from sickness) proportion of the ith household; therefore, r_i is a cumulative sum of the number of deaths per day up until that point in household i, divided by the household size. The state p_i is the infected proportion of household i. Therefore, the data in Figure 6.6, for each point $k > 0$, is

$$\sum_{i=1}^{n} p_i^k \text{ and } \sum_{i=1}^{n} r_i^k - r_i^{k-1}. \tag{7.20}$$

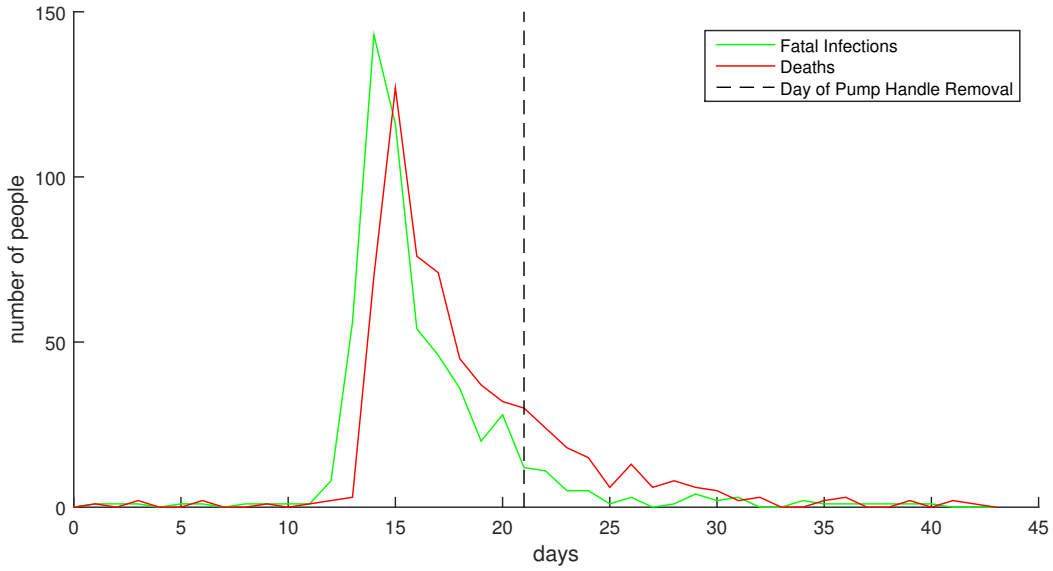

Figure 7.5: Numbers of cholera fatal infections (green) and deaths (red) per day in the Soho District of London in 1854 compiled by John Snow [96]. Day 1 corresponds to August 19th and Day 43 corresponds to September 30th. The vertical black dashed line indicates the day ($t = 21$) the pump handle was removed (September 8th).

Since we know the Broad Street water pump was the source of the epidemic, we set the initial conditions of the model to

$$p^0 = \mathbf{0},\ r^0 = \mathbf{0},\ w^0 = 20.$$

Since the dataset only spans 45 days, we ignore the natural death rate; therefore, for all $i \in [250]$,

$$\mu_i = 0.$$

Therefore, from Sections 7.1.2 and 7.1.3, we have that

$$\tilde{p} = \mathbf{0}, \tag{7.21}$$

which is consistent with how cholera behaves; a sick individual either heals or dies. Since the outbreak does not start spreading rapidly until day 13 (August 30th), that is when we begin the simulation of the model. Since the pump handle was removed on September 7th (see vertical black dashed line in Figure 6.6), we have two sets of b_w and α values. Also, as Snow noted, the workhouse had its own water pump and many of the residents there drank beer [96]; so we have different values for the workhouse. For $t < 9$ (day 21), since the workhouse corresponds to the 208th index in the ordering, we let

$$\beta_{w,208} = 0.01 \text{ and } \alpha_{w,208} = 0.01,$$

and we assume that the rest of the households are affected identically by, and identically affect, the polluted

water pump, that is, for all $i \in [n] \setminus \{208\}$,

$$\beta_{w,i} = 0.25 \text{ and } \alpha_i = 0.5.$$

For $t \geq 9$, we set

$$b_w = 0.5 b_{w_{t<9}} \text{ and } \alpha = 0.5 \alpha_{t<9}.$$

In modern times, the cholera fatality rate can be under 1% [111], but can also be up to 50% [112]. In the 19th century, cholera fatality rates were much higher [96], thus we assume that, for all $i \in [n]$,

$$\gamma_i = 0.75.$$

We also assume that $\xi = 0.5$. For the graph topology we use the binary structure referred to as $A^{(1)}$ in (6.14), which we call A, defined as

$$a_{ij} = \begin{cases} 1, & \text{if } \|z_i - z_j\| < r, \\ 1, & \text{if } i = j, \\ 0, & \text{otherwise,} \end{cases} \tag{7.22}$$

where z_i is the location of household i and r is the smallest number such that the graph remains connected. Note that we do not include the final row and column of $A^{(1)}$ in (6.14) since the water pump is not included in the same way.

Given the limited amount of data and the large number of parameters in the model, learning the model parameters from the data is difficult. Note that, by (7.21), we have $\tilde{p} = \mathbf{0}$, and thus we cannot use the same technique used for this dataset in Section 6.4 of exploiting the uniqueness of the endemic equilibrium since, as we saw in Section 7.1.3, with $\mu = \mathbf{0}$, the equilibrium $\tilde{r}$ is not unique. Also, the times series data available (Figure 6.6) is aggregated, not node-level data. Therefore, estimating the network spread parameters is quite difficult.

Therefore, we simulate the model using the above assumptions, choosing homogeneous virus spreading parameters:

$$\beta = 1 \text{ and } \delta = 125.$$

Consequently, the model is, for $i \in [n] \setminus \{208\}$ and $t < 9$,

$$\dot{p}_i = (1 - p_i - r_i) \left(\sum_{j=1}^{n} a_{ij} p_j + 0.25 w \right) - 125 p_i, \tag{7.23}$$

$$\dot{r}_i = 0.8 p_i, \tag{7.24}$$

$$\dot{w} = \sum_{j=1}^{n} 0.5 p_j - 0.5 w, \tag{7.25}$$

with the a_{ij}'s defined in (7.22).

The results were quite good, as we can see by comparing the simulation to the data in Figure 6.6. See

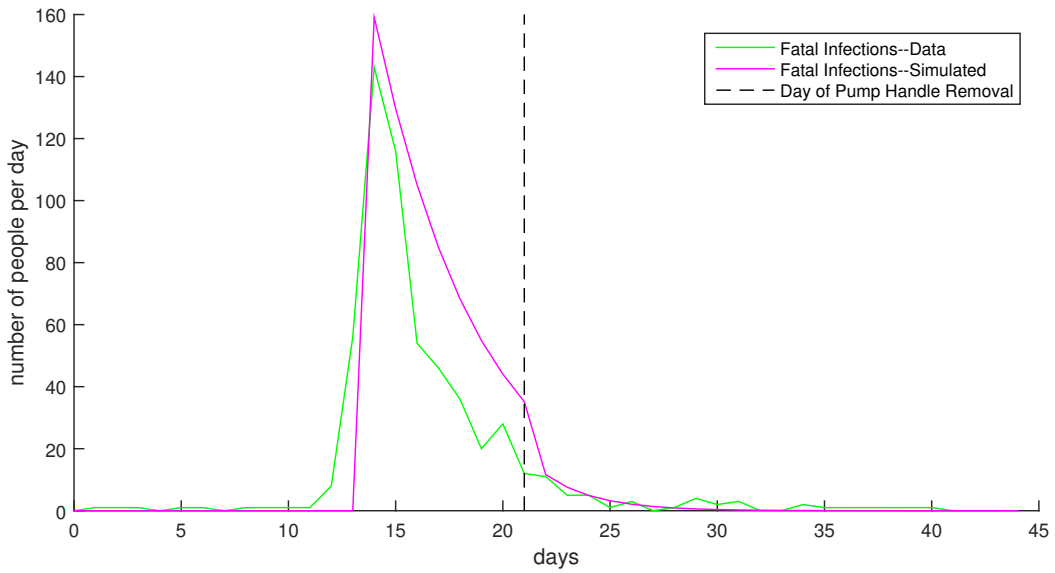

Figure 7.6: Numbers of cholera fatal infections from the data (green) and the simulation (magenta) per day. The vertical black dashed line indicates the day ($t = 21$) the pump handle was removed (September 8th).

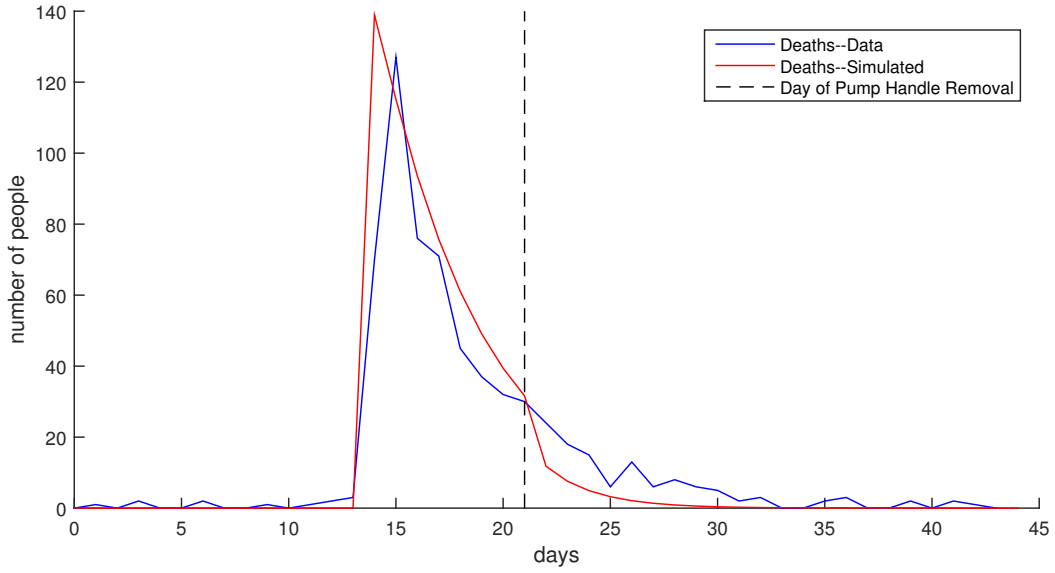

Figure 7.7: Numbers of cholera-related deaths from the data (blue) and the simulation (red) per day. The vertical black dashed line indicates the day ($t = 21$) the pump handle was removed (September 8th).

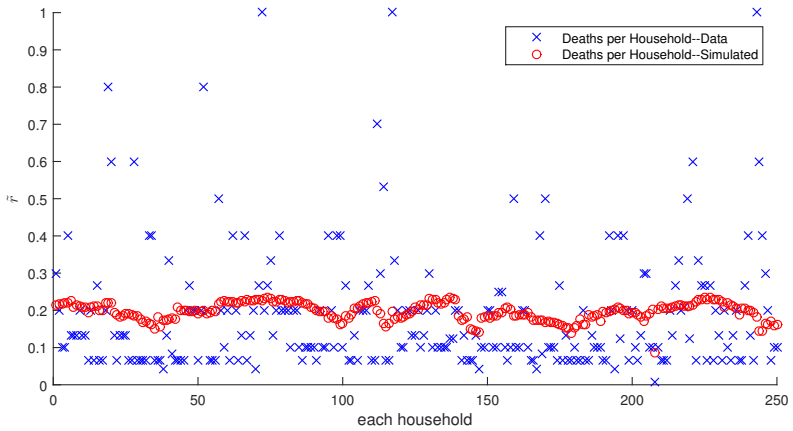

Figure 7.8: Final proportion of cholera-related deaths per household from the data (blue) and the simulation (red).

Figure 7.6 for a comparison of the data and the total infection levels from the simulation for each time t,

$$\sum_{i=1}^{n} p_i(t).$$

See Figure 7.7 for a comparison of the data and the total number of simulated deaths for each time t,

$$\sum_{i=1}^{n} r_i(t) - r_i(t-1).$$

The total number of deaths in the simulation is 638, which is greater than the 616 in Snow's Table 1 [96]. However, this is reasonable because not all deaths were recorded by Snow. In Figure 7.8, the proportion of deaths for each household i,

$$\tilde{r}_i$$

is given, as well as the data from Figure 6.4 for comparison.

7.1.5 Conclusion

We have proposed a novel network-dependent SIWR model, deriving it from a proportion of subpopulation interpretation of the state. We have presented the equilibria of the model, and have provided local and global analysis of the healthy states, and a number of illustrative simulations. Finally, we have shown via simulation that the proposed model can capture real cholera spread by comparing to John Snow's cholera dataset.

For future work we would like to extend the model to have a networked water system. We would also like to design control techniques for mitigating the spread of the epidemic. Finally, we would like to develop a game-theoretic framework that allows an adversary to attack the water source and has a designer tasked with protecting the network from actions of such an adversary.

7.2 Future Work

In this section we discuss various future directions for research.

7.2.1 Model Reduction of Spread Models

On small scales, as we saw in Chapter 6, the models seem to be effective. However as these systems grow in scale, such as online social networks, they will be limited in functionality by computational power. Model reduction for linear systems is a well-studied area [113, 114, 115]. However, the majority of these techniques do not preserve network structure; some work has been done in this direction [116, 117, 118, 119]. For nonlinear systems there are practically no model reduction results that include error bounds [120]. It would be interesting to look into nonlinear model reduction with error bounds; however, it is difficult to even formulate this problem since previous results have appealed to bounded operator theory on transfer functions, but for nonlinear systems we do not have analogous representations. It would also be interesting to look at preserving network structure during model reduction for both linear and nonlinear systems. This work could first be explored for specific model classes, such as nonlinear, networked spread models, and then expanded to more generalize models.

7.2.2 Observability of Spread Models

One avenue of interest for the future is exploring the observability and controllability of these virus spread systems. Observability poses an interesting direction since theoretically one can recover ground zero, or the initial condition, of the virus, which is of great interest in the area of epidemiology. The only relevant work we have found to date is [121]; however, it seems to be a limited approach.

Consider the model in (2.8) but suppose that at each time instant we only see the state of a subset of the nodes, i.e.,

$$y(t) = C(t)p(t),$$

where $C(t) = [I \;\; 0]$.

We first linearize the system in (2.8) as

$$\dot{p} = (BA - D)p \tag{7.26}$$

$$y = Cp. \tag{7.27}$$

This is an LTI system to which classical observability tests can be applied. The first most natural formulation of interest is to employ the observability gramian

$$W_o(A, C) = \int_0^\infty e^{A^*\tau} C^* C e^{A\tau}, \tag{7.28}$$

in the following way:

$$
\begin{aligned}
\text{minimize} \quad & k \\
\text{subject to} \quad & W_o(\tilde{B}\tilde{A} - \tilde{D}, \tilde{C}) \text{ is full rank}, \\
& \dot{\tilde{p}} = (\tilde{B}\tilde{A} - \tilde{D})\tilde{p}, \\
& \tilde{y} = \tilde{C}\tilde{p}, \\
& \tilde{C} = [I_k \;\; 0], \quad I_k \in \mathbb{R}^{k \times k}, \\
& \tilde{p} = Tp, \quad T \text{ is a permutation matrix.}
\end{aligned}
$$

This could clearly be extended to use different approaches for nonlinear observability gramians [122, 123], and time-varying observability gramians [124].

Appendix A

Select Proofs

To prove Proposition 1 and some of the subsequent theorems we need the following results.

Lemma 14. (Proposition 2 in [30]) *Suppose that M is a Metzler matrix such that $s(M) < 0$. Then, there exists a positive diagonal matrix P such that $M'P + PM$ is negative definite.*

Lemma 15. (Lemma 2.3 in [31]) *Suppose that M is an irreducible Metzler matrix. Then, $s(M)$ is a simple eigenvalue of M and there exists a unique (up to scalar multiple) vector $x \gg \mathbf{0}$ such that $Mx = s(M)x$.*

Lemma 16. (Section 2.1 in [31]) *Suppose that M is an irreducible Metzler matrix in $\mathbb{R}^{n\times n}$ and $x > \mathbf{0}$ is a vector in $\mathbb{R}^n$. If $Mx < \lambda x$, then $s(M) < \lambda$. If $Mx = \lambda x$, then $s(M) = \lambda$. If $Mx > \lambda x$, then $s(M) > \lambda$.*

Lemma 17. (Lemma A.1 in [16]) *Suppose that M is an irreducible Metzler matrix such that $s(M) = 0$. Then, there exists a positive diagonal matrix P such that $M'P + PM$ is negative semi-definite.*

The following proposition is Proposition 1 in [22].

Proposition 5. *Suppose that Λ is a negative diagonal matrix in $\mathbb{R}^{n\times n}$ and N is an irreducible non-negative matrix in $\mathbb{R}^{n\times n}$. Let $M = \Lambda + N$. Then, $s(M) < 0$ if and only if $\rho(-\Lambda^{-1}N) < 1$, $s(M) = 0$ if and only if $\rho(-\Lambda^{-1}N) = 1$, and $s(M) > 0$ if and only if $\rho(-\Lambda^{-1}N) > 1$.*

Proof: Suppose that Λ is a negative diagonal matrix in $\mathbb{R}^{n\times n}$ and N is an irreducible non-negative matrix in $\mathbb{R}^{n\times n}$. Let $M = \Lambda + N$. By Theorem 3.29 in [31], $s(M) < 0$ if and only if $\rho(-\Lambda^{-1}N) < 1$. To prove the proposition, it suffices to show that $s(M) = 0$ if and only if $\rho(-\Lambda^{-1}N) = 1$.

First suppose that $s(M) = 0$. Set $\Lambda_\varepsilon = \Lambda - \varepsilon I$ with $\varepsilon > 0$. Let $M_\varepsilon = \Lambda_\varepsilon + N = \Lambda - \varepsilon I + N$. Then, $\lim_{\varepsilon\to 0^+} \rho(-\Lambda_\varepsilon^{-1}N) = \rho(-\Lambda^{-1}N)$. Since $\varepsilon > 0$, $s(M_\varepsilon) < 0$. Then, $\rho(-\Lambda_\varepsilon^{-1}N) < 1$ and, therefore, $\lim_{\varepsilon\to 0^+} \rho(-\Lambda_\varepsilon^{-1}N) \leq 1$. Thus, $\rho(-\Lambda^{-1}N) \leq 1$. To prove that $\rho(-\Lambda^{-1}N) = 1$, suppose that, to the contrary, $\rho(-\Lambda^{-1}N) < 1$. Then, $s(M) < 0$, which is a contradiction. Therefore, $\rho(-\Lambda^{-1}N) = 1$.

Now suppose that $\rho(-\Lambda^{-1}N) = 1$. Again set $\Lambda_\varepsilon = \Lambda - \varepsilon I$ with $\varepsilon > 0$ and $M_\varepsilon = \Lambda_\varepsilon + N$. Then, $\lim_{\varepsilon\to 0^+} s(M_\varepsilon) = s(M)$. Since $\varepsilon > 0$, $-\Lambda_\varepsilon^{-1}N$ is a non-negative matrix. Since N is irreducible and non-negative, so is $-\Lambda_\varepsilon^{-1}N$. Note that the ith diagonal entry of $-\Lambda_\varepsilon$ is strictly larger than the ith diagonal entry of $-\Lambda$ since $\varepsilon > 0$. Thus, $-\Lambda^{-1}N > -\Lambda_\varepsilon^{-1}N$. By Lemma 15, $\rho(-\Lambda_\varepsilon^{-1}N) < 1$. Then, $s(M_\varepsilon) < 0$ and, thus, $\lim_{\varepsilon\to 0^+} s(M_\varepsilon) \leq 0$. Thus, $s(M) \leq 0$. To prove that $s(M) = 0$, suppose that, to the contrary, $s(M) < 0$. Then, $\rho(-\Lambda^{-1}N) < 1$, which is a contradiction. Therefore, $s(M) = 0$. □

Lemma 18. *Suppose that $\delta_i \geq 0$ for all $i \in [n]$ and that matrix BA is non-negative and irreducible. If p^* is a nonzero equilibrium of system (2.9), then $p^* \gg \mathbf{0}$.*

Proof: Suppose that p^* is a nonzero equilibrium of (2.9). By Lemma 9, it must be true that $p^* \geq \mathbf{0}$. To prove $p^* \gg \mathbf{0}$, suppose that, to the contrary, p^* has at least one zero entry. Without loss of generality, set $p_1^* = 0$. Since p^* is an equilibrium of (2.9), from (2.8),

$$-\delta_1 p_1^* + (1 - p_1^*) \sum_{j=1}^{n} \beta_{1j} p_j^* = \sum_{j=1}^{n} \beta_1 a1j p_j^* = 0.$$

It then follows that for any $j \in [n]$ such that $\beta_{1j} > 0$, $p_j^* = 0$. By repeating this argument, since BA is irreducible, we have $p_i^* = 0$ for all $i \in [n]$. This contradicts the assumption that $p^* \geq 0$. Thus, $p^* \gg \mathbf{0}$. □

The following corollary is a direct consequence of Lyapunov's stability theorem (see Theorem 4.1 in [43]) and the definition of domain of attraction.

Corollary 9. *Let z be an equilibrium of (2.15) and $\mathcal{E} \subset \mathcal{X}$ be a domain containing z. Let $V : \mathcal{E} \to \mathbb{R}$ be a continuously differentiable function such that $V(z) = 0$, $V(x) > 0$ in $\mathcal{E} \setminus \{z\}$, $\dot{V}(z) = 0$, and $\dot{V}(x) < 0$ in $\mathcal{E} \setminus \{z\}$. If $\mathcal{E}$ is a positively invariant set, then the equilibrium z is asymptotically stable with a domain of attraction $\mathcal{E}$.*

Proof of Proposition 1. We prove this proposition through several cases: 1) $s(BA - D) \leq 0$ and 2) $s(BA - D) > 0$.

1) Case $s(BA - D) \leq 0$:

We first consider the case when $s(BA - D) < 0$. Since $(BA - D)$ is an irreducible Metzler matrix, by Lemma 14, there exists a positive diagonal matrix Q such that $(BA-D)'Q+Q(BA-D)$ is negative definite. Consider the Lyapunov function candidate $V(p(t)) = p(t)'Qp(t)$. From (2.9), when $p(t) \neq \mathbf{0}$,

$$\begin{aligned}
\dot{V}(p(t)) &= 2p(t)'Q\left(-D + BA - P(t)BA\right)p(t) \\
&< -2p(t)'QP(t)BAp(t) \\
&\leq 0.
\end{aligned}$$

Thus, in this case, $\dot{V}(p(t)) < 0$ if $p(t) \neq \mathbf{0}$. By Lemma 9 and Corollary 9, $x = \mathbf{0}$ is asymptotically stable with domain of attraction $[0, 1]^n$.

Next we consider the case when $s(BA - D) = 0$. Since $(BA - D)$ is an irreducible Metzler matrix, by Lemma 17, there exists a positive diagonal matrix Q such that $(BA - D)'Q + Q(BA - D)$ is negative semi-definite. Consider the Lyapunov function candidate $V(p(t)) = p(t)'Qp(t)$. From (2.9), we have

$$\begin{aligned}
\dot{V}(p(t)) &= 2p(t)'Q\left(-D + BA - P(t)BA\right)p(t) \\
&= p(t)'\left((BA - D)'Q + Q(BA - D)\right)p(t) - 2p(t)'QP(t)BAp(t) \\
&\leq 0.
\end{aligned}$$

We claim that $\dot{V}(p(t)) < 0$ if $p(t) \neq \mathbf{0}$. To establish this claim, we first consider the case when $p(t) \gg \mathbf{0}$. Since BA is non-negative and irreducible, $BAp(t) \gg \mathbf{0}$. Since Q is a positive diagonal matrix, it follows

that $p(t)'QP(t)BAp(t) > 0$, so $\dot{V}(p(t)) < 0$. Next we consider the case when $p(t) > \mathbf{0}$ and $p(t)$ has at least one zero entry. Since $(BA - D)$ is an irreducible Metzler matrix and Q is a positive diagonal matrix, $(BA - D)'Q + Q(BA - D)$ is a symmetric irreducible Metzler matrix. Since $(BA - D)'Q + Q(BA - D)$ is negative semi-definite, it follows that $s((BA - D)'Q + Q(BA - D)) = 0$. By Lemma 15, 0 is a simple eigenvalue of $(BA - D)'Q + Q(BA - D)$ and it has a unique (up to scalar multiple) strictly positive eigenvector corresponding to the eigenvalue 0. That is, there exists $\tilde{x} \gg 0$ such that $A\tilde{x} = 0\tilde{x}$. Thus, $p(t)' \left((BA - D)'Q + Q(BA - D)\right) p(t) < 0$ when $p(t) > \mathbf{0}$ and $p(t)$ has at least one zero entry. Therefore, $\dot{V}(p(t)) < 0$ if $p(t) \neq \mathbf{0}$. By Lemma 9 and Corollary 9, $x = \mathbf{0}$ is asymptotically stable with domain of attraction $[0, 1]^n$.

2) Case $s(BA - D) > 0$:

It will suffice to show that if $s(BA - D) > 0$, then there exists a unique strictly positive equilibrium. We first show that there exists an $p^* \gg \mathbf{0}$ which is an equilibrium of (2.9).

Let $c > 0$ be any positive constant such that

$$s(BA - D) - c > 0. \tag{A.1}$$

Such a constant c always exists since $s(BA - D) > 0$. Set $\bar{D} = D + cI$. Since $\delta_i \geq 0$ for all $i \in [n]$, D is a non-negative diagonal matrix. Thus, $\bar{D}$ is nonsingular and $\bar{D}^{-1}$ is also a positive diagonal matrix.

Consider the above equation and define a continuous map $f : (0, 1]^n \to [0, 1]^n$ given by

$$f(p) = \left(I - c\bar{D}^{-1} + \mathrm{diag}(\bar{D}^{-1}BAp)\right)^{-1} \bar{D}^{-1}BAp.$$

Since the domain of f is $(0, 1]^n$, p as the argument of f satisfies $p \gg \mathbf{0}$. Therefore $\mathrm{diag}(\bar{D}^{-1}BAp)$ is a positive diagonal matrix, and we have that $(I - c\bar{D}^{-1} + \mathrm{diag}(\bar{D}^{-1}BAp))$ is invertible. Therefore f is well-defined. Note that the ith entry of $f(p)$, denoted by $f_i(p)$, is given by

$$f_i(p) = \frac{\left(\bar{D}^{-1}BAp\right)_i}{1 - \frac{c}{c+\delta_i} + \left(\bar{D}^{-1}BAp\right)_i}.$$

Since $\bar{D}^{-1}$ and BA are both non-negative, for any $y \geq z$ in $(0, 1]^n$, $f_i(y) \geq f_i(z)$, so $f(y) \geq f(z)$.

Since $\bar{D}^{-1}BA$ is an irreducible non-negative matrix, by Lemma 15, there exists $v \gg \mathbf{0}$ such that

$$\bar{D}^{-1}BAv = rv, \tag{A.2}$$

where $r = \rho(\bar{D}^{-1}BA)$. Since $s(BA - \bar{D}) = s(BA - D) - c$, from (A.1), $s(BA - \bar{D}) > 0$. By Proposition 5, it follows that $r > 1$. Then, we can always find an $\varepsilon > 0$ such that for each $i \in [n]$,

$$\varepsilon v_i \leq \frac{r - 1}{r}. \tag{A.3}$$

From this, it follows that $1 \leq \frac{r}{1+\varepsilon r v_i}$, and thus, $\varepsilon v_i \leq \frac{\varepsilon r v_i}{1+\varepsilon r v_i}$. From (A.2), we have

$$\varepsilon v_i \leq \frac{\left(\bar{D}^{-1}BA\varepsilon v\right)_i}{1 + \left(\bar{D}^{-1}BA\varepsilon v\right)_i} \leq \frac{\left(\bar{D}^{-1}BA\varepsilon v\right)_i}{1 - \frac{c}{c+\delta_i} + \left(\bar{D}^{-1}BA\varepsilon v\right)_i},$$

which implies that $\varepsilon v \leq f(\varepsilon v)$. It follows from (A.3) that $\varepsilon v \ll \mathbf{1}$. Since we have already shown that for any

$y \geq z$ in $(0,1]^n$, $f(y) \geq f(z)$, f maps the compact, convex set $\mathcal{C} = \{x \mid \varepsilon v \leq x \leq \mathbf{1}\}$ to itself. By Brouwer's fixed-point theorem, f has a fixed point in $\mathcal{C}$, which must be strictly positive. Let $p^* \gg \mathbf{0}$ denote this fixed point. Then $f(p^*) = p^*$, i.e.,

$$p^* = \left(I - c\bar{D}^{-1} + \operatorname{diag}(\bar{D}^{-1}BAp^*)\right)^{-1} \bar{D}^{-1}BAp^*.$$

Therefore we have

$$\begin{aligned}
\bar{D}^{-1}BAp^* &= \left(I - c\bar{D}^{-1} + \operatorname{diag}(\bar{D}^{-1}BAp^*)\right) p^* \\
&= p^* + \operatorname{diag}(\bar{D}^{-1}BAp^*)p^* - c\bar{D}^{-1}p^* \\
&= p^* + P^*\bar{D}^{-1}BAp^* - c\bar{D}^{-1}p^* \\
&= p^* + \bar{D}^{-1}P^*BAp^* - c\bar{D}^{-1}p^*.
\end{aligned}$$

Therefore, $BAp^* = \bar{D}p^* + P^*BAp^* - cp^* = Dp^* + P^*BAp^*$, by definition of $\bar{D}$. Thus, we have $((BA - D) - P^*BA)p^* = \mathbf{0}$, and therefore $p^* \gg \mathbf{0}$ is an equilibrium of (2.9).

It remains to show that the strictly positive equilibrium is unique. Suppose that x and y are both nonzero equilibria of (2.9), and let ε from (A.3) be sufficiently small such that $x, y \in \mathcal{C}$. From Lemma 18, it follows that $x, y \gg \mathbf{0}$. Set

$$\kappa = \max_{i \in [n]} \frac{x_i}{y_i}.$$

Then, $x \leq \kappa y$, and there exists $j \in [n]$ for which $x_j = \kappa y_j$. We claim that $\kappa \leq 1$. To establish this claim, suppose that, to the contrary, $\kappa > 1$. Since x is a fixed point of f and for any $u \geq v$ in $(0,1]^n$, $f_j(u) \geq f_j(v)$ for all $j \in [n]$, it follows that

$$\begin{aligned}
x_j &= \frac{\left(\bar{D}^{-1}BAx\right)_j}{1 - \frac{c}{c+\delta_j} + \left(\bar{D}^{-1}BAx\right)_j} \\
&\leq \frac{\left(\bar{D}^{-1}BA\kappa y\right)_j}{1 - \frac{c}{c+\delta_j} + \left(\bar{D}^{-1}BA\kappa y\right)_j} \\
&= \frac{\kappa\left(\bar{D}^{-1}BAy\right)_j}{1 - \frac{c}{c+\delta_j} + \kappa\left(\bar{D}^{-1}BAy\right)_j}.
\end{aligned}$$

From the assumption that $\kappa > 1$, we have

$$\frac{\kappa\left(\bar{D}^{-1}BAy\right)_j}{1 - \frac{c}{c+\delta_j} + \kappa\left(\bar{D}^{-1}BAy\right)_j} < \frac{\kappa\left(\bar{D}^{-1}BAy\right)_j}{1 - \frac{c}{c+\delta_j} + \left(\bar{D}^{-1}BAy\right)_j}.$$

Since y is a fixed point of f,

$$\frac{\left(\bar{D}^{-1}BAy\right)_j}{1 - \frac{c}{c+\delta_j} + \left(\bar{D}^{-1}BAy\right)_j} = y_j.$$

Then, it follows that

$$x_j < \frac{\kappa\left(\bar{D}^{-1}By\right)_j}{1 - \frac{c}{c+\delta_j} + \left(\bar{D}^{-1}BAy\right)_j} = \kappa y_j = x_j,$$

which is a contradiction. Therefore, $\kappa \leq 1$, which implies that $x \leq y$. Using the same arguments and by

exchanging the roles of x and y, it also can be shown that $y \leq x$. Thus, $x = y$, which establishes the uniqueness of the strictly positive equilibrium. This completes the proof. □

Proof of Theorem 1.

To simplify notation, let $M = I + hB - hD$ and $\hat{M} = I + h((I - P^k)B - D)$. By Assumptions 2-5, M is an irreducible non-negative matrix. First we evaluate the case where $\rho(I - hD + hB) < 1$. Therefore, by Lemma 3, there exists a positive diagonal matrix P_1 such that $M^\top P_1 M - P_1$ is negative definite. Consider the Lyapunov function $V_1(p^k) = (p^k)^\top P_1 p^k$. Using (2.14) with $p^k \neq 0$, gives

$$\begin{aligned}
\Delta V_1^k &= (p^k)^\top \hat{M}^\top P_1 \hat{M} p^k - (p^k)^\top P_1 p^k \\
&= (p^k)^\top (M^\top P_1 M - P_1) p^k - 2h(p^k)^\top B^\top P^k P_1 M p^k + h^2 (p^k)^\top B^\top P^k P_1 P^k B p^k \\
&< h^2 (p^k)^\top B^\top P^k P_1 P^k B p^k - 2h(p^k)^\top B^\top P^k P_1 M p^k \qquad \text{(A.4)} \\
&= h^2 (p^k)^\top B^\top P^k P_1 P^k B p^k - 2h^2 (p^k)^\top B^\top P^k P_1 B p^k - 2h(p^k)^\top B^\top P^k P_1 (I - hD) p^k \\
&\leq h^2 ((p^k)^\top B^\top P^k P_1 P^k B p^k - 2(p^k)^\top B^\top P^k P_1 B p^k) \qquad \text{(A.5)} \\
&\leq -h^2 (p^k)^\top B^\top P^k P_1 (I - P^k) B p^k \\
&\leq 0, \qquad \text{(A.6)}
\end{aligned}$$

where (A.4) holds by Lemma 3, (A.5) holds by Assumptions 2 and 3, and (A.6) holds by Lemma 2. Therefore, by Proposition 3, the system converges asymptotically to the healthy state for this case.

For the case where $\rho(I - hD + hB) = 1$, we have, by Lemma 4, that there exists a positive diagonal matrix P_2 such that $M^\top P_2 M - P_2$ is negative semi-definite. Consider the Lyapunov function $V_2(p^k) = (p^k)^\top P_2 p^k$. Using (2.14) with $p^k \neq 0$, gives

$$\begin{aligned}
\Delta V_2^k &= (p^k)^\top \hat{M}^\top P_2 \hat{M} p^k - (p^k)^\top P_2 p^k \\
&= (p^k)^\top (M^\top P_2 M - P_2) p^k - 2h(p^k)^\top B^\top P^k P_2 M p^k + h^2 (p^k)^\top B^\top P^k P_2 P^k B p^k \\
&< h^2 (p^k)^\top B^\top P^k P_2 P^k B p^k - 2h(p^k)^\top B^\top P^k P_2 M p^k \\
&= h^2 (p^k)^\top B^\top P^k P_2 P^k B p^k - h(p^k)^\top B^\top P^k P_2 M p^k - h^2 (p^k)^\top B^\top P^k P_2 B p^k - h(p^k)^\top B^\top P^k P_2 (I - hD) p^k \\
&\leq h^2 (p^k)^\top B^\top P^k P_2 P^k B p^k - h(p^k)^\top B^\top P^k P_2 M p^k - h^2 (p^k)^\top B^\top P^k P_2 B p^k \\
&\leq -h^2 (p^k)^\top B^\top P^k P_2 (I - P^k) B p^k - h(p^k)^\top B^\top P^k P_2 M p^k \\
&\leq -h(p^k)^\top B^\top P^k P_2 M p^k \\
&\leq 0.
\end{aligned}$$

Clearly if $p^k = \mathbf{0}$, then $-h(p^k)^\top B^\top P^k P_2 M p^k = 0$. Since, by Assumptions 2 and 4, B, P_2, M are nonzero, non-negative matrices, if $-h(p^k)^\top B^\top P^k P_2 M p^k = 0$, then $p^k = \mathbf{0}$. Therefore, by Proposition 3, the healthy state is asymptotically stable with domain of attraction $[0, 1]^n$. □

Proof of Theorem 4: Note that since $(P(t)BA(t))_{ij} \geq 0 \ \forall i, j$, by construction and Lemma 1,

$$\begin{aligned}
\dot{p} &= (BA(t) - P(t)BA(t) - D)p \\
&\leq (BA(t) - D)p. \qquad \text{(A.7)}
\end{aligned}$$

Therefore, by Grönwall's Inequality ([46]), the solution of the original system will be bounded above by the solution of the linear system. Stability of the linear time–varying model follows from [125, 44]; for completeness we include a clarified version for the virus case.

Since $\sup_{t\geq 0} s_1(BA(t)-D) < 0$, we have $BA(t)-D$ is Hurwitz for all $t \geq 0$ and therefore, for any given $t \geq 0$, (A.7) is exponentially stable. This also implies that for any given t, there exists a symmetric, positive definite $Q(t)$ (by Theorem 4.6 of [43]) such that

$$Q(t)(BA(t)-D) + (BA(t)-D)^\top Q(t) = -I. \tag{A.8}$$

Note that the solution to this equation is given by

$$Q(t) = \int_0^\infty e^{(BA(t)-D)^\top \tau} e^{(BA(t)-D)\tau} d\tau. \tag{A.9}$$

By our assumption, there exists an $L > 0$ such that $\|BA(t)-D\| \leq L \ \forall t$, which implies for any $\tau > 0$

$$\|p\| \leq e^{L\tau} \left\| e^{(BA(t)-D)\tau} p \right\|.$$

Therefore $\|e^{(BA(t)-D)\tau} p\| \geq e^{-L\tau}\|p\|$, so from (A.9) we have

$$p^\top Q(t) p \geq \gamma_0 \|p\|^2, \tag{A.10}$$

where $\gamma_0 := \int_0^\infty e^{-2L\tau} d\tau = \frac{1}{2L}$.

Let $V(p,t) = p^\top Q(t) p$. By (A.10), (3.4) and (A.9) we have

$$\gamma_0 \|p\|^2 \leq p^\top Q(t) p \leq \gamma_1 \|p\|^2, \tag{A.11}$$

where γ_1 is well-defined and finite by assumption. Taking the time derivative of $V(p,t)$ gives

$$\dot{V} = p^\top (Q(t)(BA(t)-D) + (BA(t)-D)^\top Q(t) + \dot{Q}(t)) p = -\|p\|^2 + p^\top \dot{Q}(t) p, \tag{A.12}$$

where the second equality follows from (A.8). Taking the time derivative of (A.8) and rearranging terms gives

$$\dot{Q}(t)(BA(t)-D) + (BA(t)-D)^\top \dot{Q}(t) = -Q(t)(B\dot{A}(t)-D) - (B\dot{A}(t)-D)^\top Q(t) =: R(t). \tag{A.13}$$

Note

$$\|R(t)\| \leq 2\|Q(t)(B\dot{A}(t)-D)\| \leq 2\|Q(t)\|\|B\dot{A}(t)-D\|. \tag{A.14}$$

The solution to (A.13) is

$$\dot{Q}(t) = \int_0^\infty e^{(BA(t)-D)^\top \tau} R(t) e^{(BA(t)-D)\tau} d\tau.$$

Therefore

$$\|\dot{Q}(t)\| \leq 2\gamma_1^2 \|B\dot{A}(t)-D\|. \tag{A.15}$$

Substituting (A.15) into (A.12) and using (A.8) gives

$$\dot{V}(p,t) \leq -(1 - 2\gamma_1^2 \|B\dot{A}(t) - D\|)\|p\|^2. \tag{A.16}$$

Thus for $\sup_{t>0} \|B\dot{A}(t) - D\| < \frac{1}{2\gamma_1^2}$, the origin is GES.

Otherwise, using (A.11), we can rewrite (A.16) as

$$\dot{V}(p,t) \leq -\left(\frac{1}{\gamma_1} - 2\frac{\gamma_1^2}{\gamma_0}\|B\dot{A}(t) - D\|\right) V(p,t).$$

By the Comparison Lemma (e.g. Section 3.4 in [43]), we have

$$V(p,t) \leq e^{2\frac{\gamma_1^2}{\gamma_0}\alpha} e^{-(\frac{1}{\gamma_1} - 2\frac{\gamma_1^2}{\gamma_0}\mu)(t-t_0)} V(p(t_0), t_0).$$

Therefore, since $\int_t^{t+T} \|B\dot{A}(s) - D\|ds \leq \mu T + \alpha$ by our assumption, if $\mu < \frac{\gamma_0}{2\gamma_1^3}$ then, with $\bar{c} = e^{2\frac{\gamma_1^2}{\gamma_0}\alpha}$ and $\bar{\lambda} = \frac{1}{\gamma_1} - 2\frac{\gamma_1^2}{\gamma_0}\mu$,

$$\|p(t)\| \leq \bar{c}e^{-\bar{\lambda}(t-t_0)}\|p(t_0)\|,$$

that is, the origin is globally exponentially stable.

Therefore by (A.7), the DFE is GES (in the latter case, for small enough μ) for the system in (3.1). □

Proof of Theorem 7: Consider the Lyapunov function candidate $V(p) = \frac{1}{2}p^\top p$. Clearly V is positive definite uniformly in t. Since $\sup_{t\geq 0} \lambda_1(BA(t) - D) < 0$, there exists $\varepsilon > 0$ such that for all $t \geq 0$, $\sup_{t\geq 0} \lambda_1(BA(t) - D) \leq -\varepsilon$. Therefore, for $p \geq 0$,

$$\begin{aligned}
\frac{d^0V}{dt} &= p^\top(BA(t) - P(t)BA(t) - D)p \\
&\leq p^\top(BA(t) - D)p \qquad (A.17) \\
&\leq \left(\sup_{t\geq 0} \lambda_1(BA(t) - D)\right)\|p\|^2 \leq -\varepsilon p^\top p = -2\varepsilon V,
\end{aligned}$$

where (A.17) follows from our assumption that $p_i(0) \geq 0$ for all $i = 1, ..., n$ and by Lemma 6.

By our assumption $\|g_i(t,p)\| \leq k_i|p_i|^2$ we have that

$$\begin{aligned}
\|g(t,p)\|^2 &\leq \sum_{i=1}^n \|g_i(t,p)\|^2 \qquad (A.18) \\
&\leq \sum_{i=1}^n (k_i|p_i|^2)^2 \leq c\sum_{i=1}^n (|p_i|^2)^2 \\
&\leq c\left(\sum_{i=1}^n |p_i|^2\right)^2 \qquad (A.19) \\
&\leq c\|p\|^4, \qquad (A.20)
\end{aligned}$$

for all $t \geq 0$, where $c = \max_i k_i^2$. Note (A.18) holds by the relationship between the 2-induced norm and the Frobenius norm and (A.19) holds because the cross terms $|p_i|^2|p_j|^2 \geq 0$. Therefore $\|g(t,p)\| \leq \sqrt{c}V$;

so (3.16) is satisfied. Also, since $\xi(t,\omega)$ is i.i.d. it satisfies the strong law of large numbers and (3.15) is satisfied by the zero mean assumption. Therefore by Lemma 7, the origin is almost surely asymptotically stable. □

Proof of Theorem 14: The homogeneity assumption on the infection rates allows us to factor $B^k = \beta^k A$, for each virus $k \in [m]$. For the state $(\tilde{p}^1, \dots, \tilde{p}^m)$ to be an equilibrium of (4.2) the following must hold for all $k \in [m]$

$$(I - \tilde{P}^1 - \cdots - \tilde{P}^m)A\tilde{p}^k = \frac{\delta^k}{\beta^k}\tilde{p}^k, \tag{A.21}$$

in which $(I - \tilde{P}^1 - \cdots - \tilde{P}^m)A$ is an irreducible Metzler matrix, since $\tilde{P}^1 + \cdots + \tilde{P}^m$ is diagonal and $[\tilde{P}^1 + \cdots + \tilde{P}^m]_{ii} < 1$ for all $i \in [n]$, by Lemma 9. From Lemma 15, it must be true that $\tilde{p}^k \gg \mathbf{0}$ $\forall k \in [m]$ and $\tilde{p}^i = \alpha^{ik}\tilde{p}^k$ $\forall i,k \in [m]$, for some constant $\alpha^{ik} > 0$. □

Proof of Theorem 15: From (4.3) and the assumption that $\delta_i^1 = \cdots = \delta_i^m > 0$, $\forall i \in [n]$ and $\beta_{ij}^1 = \cdots = \beta_{ij}^m$ $\forall \beta_{ij}^k \neq 0,\ k \in [m]$,

$$\dot{p}^1(t) + \cdots + \dot{p}^m(t) = (-D + B - (P^1(t) + \cdots + P^m(t))B)(p^1(t) + \cdots + p^2(t)).$$

Thus, the dynamics of $p^1(t) + \cdots + p^m(t)$ is equivalent to that of the single-virus model (2.8). From Proposition 1, $p^1 + \cdots + \tilde{p}^m(t)$ has a unique nonzero equilibrium in $[0,1]^n$. Thus, $\tilde{p}^1 + \cdots + \tilde{p}^m$ is unique.

We will now show that $\tilde{p}^1 + \cdots + \tilde{p}^m \ll \mathbf{1}$. Suppose, to the contrary, that there exists an i such that $\tilde{p}_i^1 + \cdots + \tilde{p}_i^m = 1$. Therefore, there exists a $k \in [m]$ such that, by (4.2),

$$\dot{p}_i^k = -\delta_i \tilde{p}_i^k < 0,$$

by the assumption that $\delta_i > 0$. Thus, $\tilde{p}^1 + \cdots + \tilde{p}^m$ is not an equilibrium, which is a contradiction. Therefore, $\tilde{p}^1 + \cdots + \tilde{p}^m \ll \mathbf{1}$. Thus, $-D + (I - (\tilde{P}^1 + \cdots + \tilde{P}^m))B$ is an irreducible Metzler matrix. By Lemma 16, since

$$(-D + B - (\tilde{P}^1 + \cdots + \tilde{P}^m)B)(\tilde{p}^1 + \cdots + \tilde{p}^m) = \mathbf{0},$$

and $p^1(t) + \cdots + p^2(t) \gg \mathbf{0}$,

$$s(-D + B - (\tilde{P}^1 + \cdots + \tilde{P}^m)B) = 0. \tag{A.22}$$

From (4.3),

$$\begin{aligned}
\dot{p}^1(t) - \cdots - \dot{p}^m(t) &= (-D + B - (P^1(t) + \cdots + P^m(t))B)(p^1(t) - p^2(t) - \cdots - p^m(t)),\\
&\vdots\\
\dot{p}^1(t) + \cdots - \dot{p}^m(t) &= (-D + B - (P^1(t) + \cdots + P^m(t))B)(p^1(t) + \cdots + p^{m-1}(t) - p^m(t)).
\end{aligned}$$

Then,

$$\begin{aligned}(-D+B-(\tilde{P}^1+\cdots+\tilde{P}^m)B)(\tilde{p}^1-\tilde{p}^2-\cdots-\tilde{p}^m)&=\mathbf{0},\\ &\vdots\\ (-D+B-(\tilde{P}^1+\cdots+\tilde{P}^m)B)(\tilde{p}^1+\cdots+\tilde{p}^{m-1}-\tilde{p}^m)&=\mathbf{0}.\end{aligned} \tag{A.23}$$

From Lemma 15, the eigenvector corresponding to $s(-D+B-(\tilde{P}^1+\cdots+\tilde{P}^m)B)$ is unique up to a constant and strictly greater than zero. Therefore, by (A.22), either

$$\begin{aligned}\tilde{p}^1+\cdots+\tilde{p}^m&=\gamma_1(\tilde{p}^1+\cdots+\tilde{p}^{m-1}-\tilde{p}^m)\\ &\vdots\\ &=\gamma_{m-1}(\tilde{p}^1-\tilde{p}^2-\cdots-\tilde{p}^m),\end{aligned} \tag{A.24}$$

for some constants $\gamma_i > 0$, or the vectors equal zero. Without loss of generality, if the first equation of (A.23) has the vector equal zero then $\tilde{p}^1 = \tilde{p}^2 + \cdots + \tilde{p}^m$. Using these expressions and/or the expressions from (A.24), for any i, $\tilde{p}^i = \alpha^{ik}\tilde{p}^k$ for some constant $\alpha^{ik} > 0$, and thus $\tilde{p}^1, \ldots, \tilde{p}^m \gg \mathbf{0}$. □

References

[1] D. Bernoulli, "Essai d'une nouvelle analyse de la mortalité causée par la petite vérole et des avantages de l'inoculation pour la prévenir," *Histoire de l'Acad. Roy. Sci.(Paris) avec Mém. des Math. et Phys. and Mém*, pp. 1–45, 1760.

[2] W. O. Kermack and A. G. McKendrick, "Contributions to the mathematical theory of epidemics. II. The problem of endemicity," *Proceedings of the Royal society of London. Series A*, vol. 138, no. 834, pp. 55–83, 1932.

[3] A. Fall, A. Iggidr, G. Sallet, J.-J. Tewa et al., "Epidemiological models and Lyapunov functions," *Math. Model. Nat. Phenom*, vol. 2, no. 1, pp. 62–68, 2007.

[4] Y. Wan, S. Roy, and A. Saberi, "Network design problems for controlling virus spread," in *Proceedings of the 46th IEEE Conference on Decision and Control (CDC)*. IEEE, 2007, pp. 3925–3932.

[5] Y. Wan, S. Roy, and A. Saberi, "Designing spatially heterogeneous strategies for control of virus spread," *IET Systems Biology*, vol. 2, no. 4, pp. 184–201, 2008.

[6] P. Van Mieghem, J. Omic, and R. Kooij, "Virus spread in networks," *IEEE/ACM Transactions on Networking*, vol. 17, no. 1, pp. 1–14, 2009.

[7] P. E. Paré, C. L. Beck, and A. Nedić, "Stability analysis and control of virus spread over time–varying networks," in *Proceedings of the 54th IEEE Conference on Decision and Control (CDC)*. IEEE, 2015.

[8] H. J. Ahn and B. Hassibi, "Global dynamics of epidemic spread over complex networks," in *Proceedings of the 52nd IEEE Conference on Decision and Control (CDC)*. IEEE, 2013, pp. 4579–4585.

[9] Y. Wang, D. Chakrabarti, C. Wang, and C. Faloutsos, "Epidemic spreading in real networks: An eigenvalue viewpoint," in *Proceedings of the 22nd International Symposium on Reliable Distributed Systems*. IEEE, 2003, pp. 25–34.

[10] C. Peng, X. Jin, and M. Shi, "Epidemic threshold and immunization on generalized networks," *Physica A: Statistical Mechanics and its Applications*, vol. 389, no. 3, pp. 549–560, 2010.

[11] S. Boyd, S.-J. Kim, L. Vandenberghe, and A. Hassibi, "A tutorial on geometric programming," *Optimization and Engineering*, vol. 8, no. 1, pp. 67–127, 2007.

[12] V. M. Preciado, M. Zargham, C. Enyioha, A. Jadbabaie, and G. J. Pappas, "Optimal vaccine allocation to control epidemic outbreaks in arbitrary networks," in *Proceedings of the 52nd IEEE Conference on Decision and Control (CDC)*. IEEE, 2013, pp. 7486–7491.

[13] V. M. Preciado, M. Zargham, C. Enyioha, A. Jadbabaie, and G. J. Pappas, "Optimal resource allocation for network protection against spreading processes," *IEEE Transactions on Control of Network Systems*, vol. 1, no. 1, pp. 99–108, March 2014.

[14] F. Pasqualetti, S. Zampieri, and F. Bullo, "Controllability metrics, limitations and algorithms for complex networks," *IEEE Transactions on Control of Network Systems*, vol. 1, no. 1, pp. 40–52, March 2014.

[15] A. Khanafer, T. Basar, and B. Gharesifard, "Stability properties of infected networks with low curing rates," in *Proceedings of the American Control Conference (ACC)*. IEEE, 2014, pp. 3579–3584.

[16] A. Khanafer, T. Başar, and B. Gharesifard, "Stability of epidemic models over directed graphs: a positive systems approach," *Automatica*, vol. 74, pp. 126–134, 2016.

[17] R. Pastor-Satorras, C. Castellano, P. Van Mieghem, and A. Vespignani, "Epidemic processes in complex networks," *Reviews of Modern Physics*, vol. 87, no. 3, p. 925, 2015.

[18] C. Nowzari, V. M. Preciado, and G. J. Pappas, "Analysis and control of epidemics: A survey of spreading processes on complex networks," *IEEE Control Systems Magazine*, vol. 36, no. 1, pp. 26–46, 2016.

[19] P. E. Paré, C. L. Beck, and A. Nedić, "Epidemic processes over time–varying networks," *IEEE Transactions on Control of Network Systems*, vol. 5, no. 3, pp. 1322–1334, 2018.

[20] J. R. Norris, *Markov chains*. Cambridge university press, 1998, no. 2.

[21] S. Chatterjee and R. Durrett, "Contact processes on random graphs with power law degree distributions have critical value 0," *The Annals of Probability*, vol. 37, no. 6, pp. 2332–2356, 2009.

[22] J. Liu, P. E. Paré, A. Nedić, C. T. Tang, C. L. Beck, and T. Başar, "Analysis and control of a continuous-time bi-virus model," conditionally accepted to *IEEE Transactions on Automatic Control*, 2018.

[23] J. Liu, P. E. Paré, A. Nedić, C. T. Tang, C. L. Beck, and T. Başar, "On the analysis of a continuous-time bi-virus model," *arXiv*, 2016, arXiv:1603.04098v2 [math.OC].

[24] C. Li, R. van de Bovenkamp, and P. Van Mieghem, "Susceptible-infected-susceptible model: A comparison of N-intertwined and heterogeneous mean-field approximations," *Physical Review E*, vol. 86, no. 2, p. 026116, 2012.

[25] R. Pastor-Satorras and A. Vespignani, "Epidemic dynamics and endemic states in complex networks," *Physical Review E*, vol. 63, no. 6, p. 066117, 2001.

[26] A. L. Hill, D. G. Rand, M. A. Nowak, and N. A. Christakis, "Emotions as infectious diseases in a large social network: the SISa model," *Proceedings of the Royal Society of London B: Biological Sciences*, vol. 277, no. 1701, pp. 3827–3835, 2010.

[27] P. Van Mieghem and R. van de Bovenkamp, "Accuracy criterion for the mean-field approximation in susceptible-infected-susceptible epidemics on networks," *Physical Review E*, vol. 91, no. 3, p. 032812, 2015.

[28] P. E. Paré, J. Liu, C. L. Beck, B. E. Kirwan, and T. Başar, "Analysis, estimation, and validation of discrete-time epidemic processes," *IEEE Transactions on Control Systems Technology*, pp. 1–15, 2018.

[29] K. E. Atkinson, *An introduction to numerical analysis*. John Wiley & Sons, 2008.

[30] A. Rantzer, "Distributed control of positive systems," in *Proceedings of the 50th IEEE Conference on Decision and Control (CDC)*, 2011, pp. 6608–6611.

[31] R. Varga, *Matrix Iterative Analysis*. Springer-Verlag, 2000.

[32] R. A. Horn and C. R. Johnson, *Matrix analysis*. Cambridge University Press, 2012.

[33] J. Liu, P. E. Paré, A. Nedić, C. Y. Tang, C. L. Beck, and T. Başar, "On the analysis of a continuous-time bi-virus model," in *Proceedings of the 55th IEEE Conference on Decision and Control (CDC)*. IEEE, 2016.

[34] B. A. Prakash, H. Tong, N. Valler, M. Faloutsos, and C. Faloutsos, "Virus propagation on time-varying networks: Theory and immunization algorithms," in *Machine Learning and Knowledge Discovery in Databases*. Springer, 2010, pp. 99–114.

[35] V. S. Bokharaie, O. Mason, and F. R. Wirth, "Spread of epidemics in time-dependent networks," in *Proceedings of the 19th International Symposium on Math. Theory of Networks and Systems–MTNS*, vol. 5, no. 9, 2010.

[36] M. A. Rami, V. S. Bokharaie, O. Mason, and F. R. Wirth, "Stability criteria for SIS epidemiological models under switching policies," *Discrete and Continuous Dynamical Systems Series*, vol. 19, no. 9, pp. 2865–2887, 2014.

[37] M. R. Sanatkar, W. N. White, B. Natarajan, C. M. Scoglio, and K. A. Garrett, "Epidemic threshold of an SIS model in dynamic switching networks," *IEEE Transactions on Systems, Man, and Cybernetics: Systems*, vol. 46, no. 3, pp. 345–355, 2016.

[38] Q. Liu, "The threshold of a stochastic susceptible–infective epidemic model under regime switching," *Nonlinear Analysis: Hybrid Systems*, vol. 21, pp. 49–58, 2016.

[39] M. Ogura and V. M. Preciado, "Stability of spreading processes over time-varying large-scale networks," *IEEE Transactions on Network Science and Engineering*, vol. 3, no. 1, pp. 44–57, 2016.

[40] S. Liu, N. Perra, M. Karsai, and A. Vespignani, "Controlling contagion processes in activity driven networks," *Physical Review Letters*, vol. 112, no. 11, p. 118702, 2014.

[41] P. Holme, "Modern temporal network theory: a colloquium," *The European Physical Journal B*, vol. 88, no. 9, pp. 1–30, 2015.

[42] E. Valdano, L. Ferreri, C. Poletto, and V. Colizza, "Analytical computation of the epidemic threshold on temporal networks," *Physical Review X*, vol. 5, no. 2, pp. 021 005–1–9, 2015.

[43] H. K. Khalil, *Nonlinear systems*. Prentice Hall New Jersey, 1996, vol. 3.

[44] P. A. Ioannou and J. Sun, *Robust adaptive control*. Dover, 2012, originally published in 1996 by Prentice Hall.

[45] V. Solo, "On the stability of slowly time-varying linear systems," *Math. of Control, Signals and Systems*, vol. 7, no. 4, pp. 331–350, 1994.

[46] T. H. Gronwall, "Note on the derivatives with respect to a parameter of the solutions of a system of differential equations," *Annals of Mathematics*, vol. 20, no. 4, pp. 292–296, 1919.

[47] R. Khasminskii, *Stochastic stability of differential equations*. Springer Science & Business Media, 2011, vol. 66.

[48] J. Shi and J. Malik, "Normalized cuts and image segmentation," *IEEE Transactions on Pattern Analysis and Machine Intelligence*, vol. 22, no. 8, pp. 888–905, 2000.

[49] P. E. Paré, J. Liu, C. L. Beck, A. Nedić, and T. Başar, "Multi-competitive viruses over static and time–varying networks," in *Proceedings of the American Control Conference (ACC)*, 2017.

[50] P. E. Paré, J. Liu, C. L. Beck, A. Nedić, and T. Başar, "Multi-competitive viruses over static and time–varying networks," *arXiv*, 2017, arXiv:1702.07754v2 [math.OC].

[51] P. E. Paré, J. Liu, C. L. Beck, A. Nedić, and T. Başar, "Multiple competing viruses over time–varying networks with mutations and human awareness," to be submitted to *Automatica*, 2018.

[52] M. Nowak, "The evolution of viruses: Competition between horizontal and vertical transmission of mobile genes," *Journal of Theoretical Biology*, vol. 150, no. 3, pp. 339–347, 1991.

[53] B. A. Prakash, A. Beutel, R. Rosenfeld, and C. Faloutsos, "Winner takes all: Competing viruses or ideas on fair-play networks," in *Proceedings of the 21st International Conference on World Wide Web*, 2012, pp. 1037–1046.

[54] F. D. Sahneh and C. Scoglio, "Competitive epidemic spreading over arbitrary multilayer networks," *Physical Review E*, vol. 89, no. 6, p. 062817, 2014.

[55] A. Santos, J. Moura, and J. Xavier, "Bi-virus SIS epidemics over networks: Qualitative analysis," *IEEE Transactions on Network Science and Engineering*, vol. 2, no. 1, pp. 17–29, Jan 2015.

[56] X. Wei, N. C. Valler, B. A. Prakash, I. Neamtiu, M. Faloutsos, and C. Faloutsos, "Competing memes propagation on networks: A network science perspective," *IEEE Journal on Selected Areas in Communications*, vol. 31, no. 6, pp. 1049–1060, 2013.

[57] N. J. Watkins, C. Nowzari, V. M. Preciado, and G. J. Pappas, "Optimal resource allocation for competitive spreading processes on bilayer networks," *IEEE Transactions on Control of Network Systems*, vol. 5, no. 1, pp. 298–307, March 2018.

[58] O. Yagan, D. Qian, J. Zhang, and D. Cochran, "Conjoining speeds up information diffusion in overlaying social-physical networks," *IEEE Journal on Selected Areas in Communications*, vol. 31, no. 6, pp. 1038–1048, 2013.

[59] S. Xu, W. Lu, and Z. Zhan, "A stochastic model of multivirus dynamics," *IEEE Transactions on Dependable and Secure Computing*, vol. 9, no. 1, pp. 30–45, 2012.

[60] J. J. Kutch and P. Gurfil, "Optimal control of HIV infection with a continuously-mutating viral population," in *Proceedings of the American Control Conference (ACC)*, 2002.

[61] N. Singh, "Epidemiological models for mutating pathogens with temporary immunity," 2006.

[62] E. Gubar and Q. Zhu, "Optimal control of influenza epidemic model with virus mutations," in *Proceedings of the European Control Conference (ECC)*, 2013.

[63] S. Funk, E. Gilad, C. Watkins, and V. A. A. Jansen, "The spread of awareness and its impact on epidemic outbreaks," *Proceedings of The National Academy of Sciences*, vol. 106, pp. 6872–6877, 2009.

[64] F. D. Sahneh and C. Scoglio, "Epidemic spread in human networks," in *Proceedings of the 50th IEEE Conference on Decision and Control (CDC)*, 2011, pp. 3008–3013.

[65] F. D. Sahneh and C. Scoglio, "Optimal information dissemination in epidemic networks," in *Proceedings of the 51st IEEE Conference on Decision and Control (CDC)*, 2012, pp. 1657–1662.

[66] H. Shakeri, F. D. Sahneh, C. Scoglio, P. Poggi-Corradini, and V. M. Preciado, "Optimal information dissemination strategy to promote preventive behaviors in multilayer epidemic networks," *Mathematical Biosciences and Engineering*, vol. 12, no. 3, pp. 609–623, 2015.

[67] C. Granell, S. Gómez, and A. Arenas, "Dynamical interplay between awareness and epidemic spreading in multiplex networks," *Physical Review Letters*, vol. 111, p. 128701, Sep 2013. [Online]. Available: http://link.aps.org/doi/10.1103/PhysRevLett.111.128701

[68] M. Ogura and V. M. Preciado, "Epidemic processes over adaptive state-dependent networks," *Physical Review E*, vol. 93, p. 062316, Jun 2016. [Online]. Available: http://link.aps.org/doi/10.1103/PhysRevE.93.062316

[69] K. Paarporn, C. Eksin, J. S. Weitz, and J. S. Shamma, "Networked SIS epidemics with awareness," *IEEE Transactions on Computational Social Systems*, vol. 4, no. 3, pp. 93–103, 2017.

[70] J. Liu, P. E. Paré, A. Nedić, C. L. Beck, and T. Başar, "On a continuous-time multi-group bi-virus model with human awareness," in *Proceedings of the 56th IEEE Conference on Decision and Control (CDC)*. IEEE, 2017, pp. 4124–4129.

[71] A. Beutel, B. A. Prakash, R. Rosenfeld, and C. Faloutsos, "Interacting viruses in networks: can both survive?" in *Proceedings of the 18th ACM SIGKDD International Conference on Knowledge Discovery and Data Mining*. ACM, 2012, pp. 426–434.

[72] P. E. Paré, C. L. Beck, and A. Nedić, "Epidemic processes over time–varying networks," *arXiv*, 2016, arXiv:1609.05128v1 [math.OC].

[73] S. Shane and V. Goel, "Fake Russian Facebook accounts bought $100,000 in political ads," https://www.nytimes.com/2017/09/06/technology/facebook-russian-political-ads.html, accessed: 2017-09-13.

[74] D. Dasgupta and F. González, "An immunity-based technique to characterize intrusions in computer networks," *IEEE Transactions on Evolutionary Computation*, vol. 6, no. 3, pp. 281–291, 2002.

[75] G. Wang, J. Yu, and Q. Xie, "Security analysis of a single sign-on mechanism for distributed computer networks," *IEEE Transactions on Industrial Informatics*, vol. 9, no. 1, pp. 294–302, 2013.

[76] M. H. Manshaei, Q. Zhu, T. Alpcan, T. Başar, and J.-P. Hubaux, "Game theory meets network security and privacy," *ACM Computing Survey*, vol. 45, no. 3, 2013, article No. 25.

[77] M. E. J. Newman, S. Forrest, and J. Balthrop, "Email networks and the spread of computer viruses," *Physical Review E*, vol. 66, no. 3, p. 035101, 2002.

[78] J. Balthrop, S. Forrest, M. E. J. Newman, and M. M. Williamson, "Technological networks and the spread of computer viruses," *Science*, vol. 304, no. 5670, pp. 527–529, 2004.

[79] D. Acemoglu, A. Malekian, and A. Ozdaglar, "Network security and contagion," *Journal of Economic Theory*, vol. 166, pp. 536–586, 2016.

[80] B. K. Mishra and D. Saini, "Mathematical models on computer viruses," *Applied Mathematics and Computation*, vol. 187, no. 2, pp. 929–936, 2007.

[81] J. Ren, X. Yang, Q. Zhu, L.-X. Yang, and C. Zhang, "A novel computer virus model and its dynamics," *Nonlinear Analysis: Real World Applications*, vol. 13, no. 1, pp. 376–384, 2012.

[82] J. Liu, P. E. Paré, C. L. Beck, and T. Başar, "A coupled bi-virus spread model in networked systems," in proceedings of the *American Control Conference*, 2018.

[83] S. Goyal, H. Heidari, and M. Kearns, "Competitive contagion in networks," *Games and Economic Behavior*, 2014.

[84] A. Vijayshankar and S. Roy, "Cost of fairness in disease spread control," in *51st IEEE Conference on Decision and Control (CDC)*. IEEE, 2012, pp. 4930–4935.

[85] V. S. Mai, A. Battou, and K. Mills, "Distributed algorithm for suppressing epidemic spread in networks," *IEEE Control Systems Letters*, vol. 2, no. 3, pp. 555–560, 2018.

[86] E. A. Enns, J. J. Mounzer, and M. L. Brandeau, "Optimal link removal for epidemic mitigation: A two-way partitioning approach," *Mathematical Biosciences*, vol. 235, no. 2, pp. 138–147, 2012.

[87] J. Hanna and A. Fantz, "Maine nurse won't submit to Ebola quarantine, lawyer says," http://www.cnn.com/2014/10/29/health/us-ebola/, accessed: 2015-03-19.

[88] J. Wright, A. Ganesh, S. Rao, Y. Peng, and Y. Ma, "Robust principal component analysis: Exact recovery of corrupted low-rank matrices via convex optimization," in *Advances in Neural Information Processing Systems*, 2009, pp. 2080–2088.

[89] E. J. Candes, M. B. Wakin, and S. P. Boyd, "Enhancing sparsity by reweighted ℓ_1 minimization," *Journal of Fourier Analysis and Applications*, vol. 14, no. 5-6, pp. 877–905, 2008.

[90] P. E. Paré, B. E. Kirwan, J. Liu, T. Başar, and C. L. Beck, "Discrete-time spread processes: Analysis, identification, and validation," in *Proceedings of the American Control Conference (ACC)*, 2018.

[91] M. J. Keeling *et al.*, "Dynamics of the 2001 UK foot and mouth epidemic: stochastic dispersal in a heterogeneous landscape," *Science*, vol. 294, no. 5543, pp. 813–817, 2001.

[92] H. Miao, X. Xia, A. S. Perelson, and H. Wu, "On identifiability of nonlinear ODE models and applications in viral dynamics," *SIAM Review*, vol. 53, no. 1, pp. 3–39, 2011.

[93] L. Xue, H. M. Scott, L. W. Cohnstaedt, and C. Scoglio, "A network-based meta-population approach to model Rift Valley fever epidemics," *Journal of Theoretical Biology*, vol. 306, pp. 129–144, 2012.

[94] A. Kolesnichenko, B. Haverkort, A. Remke, and P.-T. de Boer, "Fitting a code-red virus spread model: An account of putting theory into practice," in *Proceedings of the 12th International Conference on the Design of Reliable Communication Networks (DRCN)*, 3 2016, pp. 39–46.

[95] D. Chakrabarti, Y. Wang, C. Wang, J. Leskovec, and C. Faloutsos, "Epidemic thresholds in real networks," *ACM Transactions on Information and System Security (TISSEC)*, vol. 10, no. 4, p. 1, 2008.

[96] J. Snow, *On the mode of communication of cholera.* John Churchill, 1855.

[97] N. Shiode, S. Shiode, E. Rod-Thatcher, S. Rana, and P. Vinten-Johansen, "The mortality rates and the space-time patterns of John Snow's cholera epidemic map," *International Journal of Health Geographics*, vol. 14, no. 1, p. 21, 2015.

[98] A. D. Foster and M. R. Rosenzweig, "Learning by doing and learning from others: Human capital and technical change in agriculture," *Journal of Political Economy*, pp. 1176–1209, 1995.

[99] T. G. Conley and C. R. Udry, "Learning about a new technology: Pineapple in Ghana," *American Economic Review*, vol. 100, no. 1, pp. 35–69, 2010.

[100] E. Duflo, M. Kremer, and J. Robinson, "Nudging farmers to use fertilizer: Theory and experimental evidence from Kenya," *American Economic Review*, vol. 101, no. October, pp. 2350–2390, 2011.

[101] P. D. Mitchell, R. M. Rejesus, K. H. Coble, and T. O. Knight, "Analyzing farmer participation intentions and county enrollment rates for the average crop revenue election program," *Applied Economic Perspectives and Policy*, vol. 34, no. 4, pp. 615–636, 2012.

[102] USDA, "2009 average crop revenue election (acre) program: Fact sheet," https://www.fsa.usda.gov/Internet/FSA_File/acre.pdf, accessed: 2016-07.

[103] J. H. Tien and D. J. Earn, "Multiple transmission pathways and disease dynamics in a waterborne pathogen model," *Bulletin of Mathematical Biology*, vol. 72, no. 6, pp. 1506–1533, 2010.

[104] J. H. Tien, H. N. Poinar, D. N. Fisman, and D. J. Earn, "Herald waves of cholera in nineteenth century london," *Journal of the Royal Society Interface*, vol. 8, no. 58, pp. 756–760, 2011.

[105] S. L. Robertson, M. C. Eisenberg, and J. H. Tien, "Heterogeneity in multiple transmission pathways: modelling the spread of cholera and other waterborne disease in networks with a common water source," *Journal of Biological Dynamics*, vol. 7, no. 1, pp. 254–275, 2013.

[106] J. Liu, P. E. Paré, E. Du, and Z. Sun, "A networked SIS disease dynamics model with a waterborne pathogen," in submission to *the American Control Conference (ACC)*, 2019.

[107] P. E. Paré, J. Liu, C. L. Beck, A. Nedić, and T. Başar, "Contaminated water and network-dependent infectious disease spread model," in submission to *the European Control Conference (ECC)*, 2019.

[108] N. A. Ruhi, H. J. Ahn, and B. Hassibi, "Analysis of exact and approximated epidemic models over complex networks," *arXiv preprint arXiv:1609.09565*, 2016.

[109] W. Mei, S. Mohagheghi, S. Zampieri, and F. Bullo, "On the dynamics of deterministic epidemic propagation over networks," *Annual Reviews in Control*, vol. 44, pp. 116 – 128, 2017. [Online]. Available: http://www.sciencedirect.com/science/article/pii/S1367578817300810

[110] "Main village - Richmond town site," https://www.historicrichmondtown.org/collections/main-village, accessed: 2018-09-24.

[111] W. H. Organization, "Cholera–Fact Sheet," 2018, http://www.who.int/news-room/fact-sheets/detail/cholera.

[112] A. K. Siddique, K. Akram, K. Zaman, S. Laston, A. Salam, R. N. Majumdar, M. S. Islam, and N. Fronczak, "Why treatment centres failed to prevent cholera deaths among Rwandan refugees in Goma, Zaire," *The Lancet*, vol. 345, no. 8946, pp. 359–361, 1995.

[113] G. E. Dullerud and F. Paganini, *A Course in Robust Control Theory: A Convex Approach*. Springer, 2013.

[114] W. H. A. Schilders, H. A. Van der Vorst, and J. Rommes, *Model order reduction: theory, research aspects and applications*. Springer, 2008, vol. 13.

[115] P. E. Paré, A. T. Wilson, M. K. Transtrum, and S. C. Warnick, "A unified view of balanced truncation and singular perturbation approximations," in *American Control Conference (ACC), 2015*. IEEE, 2015, pp. 1989–1994.

[116] L. Li and F. Paganini, "Structured coprime factor model reduction based on LMIs," *Automatica*, vol. 41, no. 1, pp. 145–151, 2005.

[117] C. Beck, "Coprime factors reduction methods for linear parameter varying and uncertain systems," *Systems & Control Letters*, vol. 55, no. 3, pp. 199–213, 2006.

[118] H. Sandberg and R. M. Murray, "Model reduction of interconnected linear systems," *Optimal Control Applications and Methods*, vol. 30, no. 3, pp. 225–245, 2009.

[119] D. A. Jaoude and M. Farhood, "Coprime factors model reduction of spatially distributed LTV systems over arbitrary graphs," *IEEE Transactions on Automatic Control*, vol. 62, no. 10, pp. 5254–5261, 2017.

[120] S. Lall, J. E. Marsden, and S. Glavaški, "A subspace approach to balanced truncation for model reduction of nonlinear control systems," *International Journal of Robust and Nonlinear Control: IFAC-Affiliated Journal*, vol. 12, no. 6, pp. 519–535, 2002.

[121] A. Alaeddini and K. A. Morgansen, "Optimal disease outbreak detection in a community using network observability," in *Proceedings of the American Control Conference (ACC)*. IEEE, 2016, pp. 7352–7357.

[122] R. Hermann and A. Krener, "Nonlinear controllability and observability," *IEEE Transactions on Automatic Control*, vol. 22, no. 5, pp. 728–740, 1977.

[123] K. Kowalski and W.-H. Steeb, *Nonlinear dynamical systems and Carleman linearization*. World Scientific, 1991.

[124] G. Bastin and M. R. Gevers, "Stable adaptive observers for nonlinear time-varying systems," *IEEE Transactions on Automatic Control*, vol. 33, no. 7, pp. 650–658, 1988.

[125] C. Desoer, "Slowly varying system $\dot{x} = A(t)x$," *IEEE Transactions on Automatic Control*, vol. 14, no. 6, pp. 780–781, Dec 1969.